12-30-2020

Assessing Airborne Radar to Map Glacier Elevations in Alpine Terrain Including Estimated Glacier Volume Change

Bryce Allen Glenn
Portland State University

Assessing Airborne Radar to Map Glacier Elevations in Alpine Terrain Including Estimated Glacier Volume Change

by

Bryce Allen Glenn

A thesis submitted in partial fulfillment of the
requirements for degree of

Master of Science
in
Geography

Thesis Committee:
Andrew G. Fountain, Chair
Martin Lafrenz
Geoffrey Duh

Portland State University
2020

Abstract

Alpine glaciers and perennial snowfields (G&PS) are important hydrologically and ecologically, providing meltwater during the hottest and driest summer periods. Climate warming shrinks these natural reservoirs while temporarily providing increased streamflow. To assess regional changes in glacier volume, from which contribution to streamflow can be estimated, I used NASA's Airborne Glacier and Ice Surface Topography Interferometer (GLISTIN). This instrument mapped the surface topography of alpine glaciers; differencing these elevations from historic elevations derived from topographic maps, volume change is calculated. GLISTIN was flown over the glacier-populated mountain ranges of the western U.S. Of the 3289 glaciers and perennial snowfields with at least 1 pixel of GLISTIN coverage, 1770 had coverage ≥ 80%. Modeling shows that about half of the missing data is due to terrain shadowing of the radar and the remainder is likely caused by layover effects due to the steep terrain. Data coverage is increased with more passes of the GLISTIN aircraft. For a single pass about 55% of the data (all terrain) was missing, and for two and four pass mosaics, it was reduced to 30% and 11%, respectively. GLISTIN elevations (3-meter resolution) were compared to lidar elevations over non-glaciated control zones for four regions in the Cascade Range. The mean GLISTIN height-precision, a self-reported value from data processing, over bedrock control zones was between 0.69 ± 0.57 m (standard deviation) and 1.34 ± 1.23 m. The mean elevation difference (GLISTIN minus lidar) for control zones ranged from -0.14 ± 1.78 m to +0.38 ± 1.83 m. Differencing GLISTIN elevations from elevations of the historical National Elevation Dataset for glaciers shows a thinning

(and volume loss) over the last ~60 years. The thinning for individual G&PS ranged from -1.28 ± 0.25 m yr-^{1} to +0.80 ± 0.33 m yr^{-1} with a median of -0.24 ± 0.20 m yr^{-1}. Results show GLISTIN potential to be a valuable tool for rapidly mapping ice surfaces in the alpine environment.

Acknowledgments

I would like to thank my advisor Andrew G. Fountain for taking me on as a student and for his support over the last several years. I'm also appreciative of Martin Lafrenz and Geoffrey Duh for taking the time to serve on my committee. A special thank you to Delwyn Moller and Yang Zhen for answering all of my radar questions. Thank you to all of my friends and family, especially all of those who encouraged me to go back to graduate school. I would also like to thank all of my coworkers in the Glacier Research Group, especially Julian Cross, Luna Brett, Christina Gray, Felix Zamora, and Allison Trcka. They were a great sounding board for all of my ideas. I would also like to thank all of the Geography and Geology graduate students. Lastly, I would like to acknowledge all of the hard work of the GLISTIN-A and UAVSAR teams, who collected and processed the radar data. This project was funded by NASA and relied on GLISTIN-A data courtesy of NASA/JPL-Caltech.

Table of Contents

List of Tables

List of Figures

I Introduction

Glacier melt is important to runoff in high alpine landscapes. At a local scale, alpine glaciers maintain streamflow during the dry, late summer months after the seasonal snow has melted (Fountain and Tangborn, 1985; Moore et al., 2009). As they shrink, their ability to buffer seasonal runoff is reduced, making watersheds more vulnerable to drought (Hall and Fagre, 2003; Moore et al., 2009). At a global scale, this loss of water, stored as ice, increases global sea-levels (Meier 1984; Radić and Hock, 2010; Pfeffer et al., 2014; Zemp et al., 2019). Over the last century, glaciers have significantly decreased in size due to an increase in global temperature (Oerlemans, 2005; Zemp, 2009; Zemp et al., 2019). To define glacier change and to predict future changes, regional-scale glacier monitoring is needed.

A variety of methods are employed to measure glacier change. Field measurements of ablation and accumulation, at points over the glacier surface is the most direct method (Meier et al., 1971; Østrem and Haakensen, 1999; Kaser et al., 2003). Point measurements are then interpolated/extrapolated over the whole glacier and the mass change is calculated. This method provides detailed data of mass change over seasonal and annual time scales; however, it is time consuming, costly, and requires extensive fieldwork. Therefore, only a small number of glaciers can be monitored directly. Remote methods provide a more rapid way to monitor glaciers across broad regions, sacrificing a detailed understanding for more general metrics (Cogley, 2009). Change in glacier area can be measured by outlining the extent of ice using aerial photographs or satellite imagery (Lambrecht and Kuhn, 2007; Pfeffer et al., 2014;

Selkowitz and Forster 2016). This method utilizes the vast amount of available imagery, including historical photographs, but manual outlining can be labor-intensive and automated techniques can perform poorly, misclassifying ice as water or debris-covered ice as non-ice (Paul et al., 2002; Racoviteanu et al., 2009; Selkowitz and Forster, 2016). Although, area change is a good visual measure of glacier change~~s~~, it is a poor proxy for volume change, which is important for assessing contributions to streamflow and sea level (Huss and Farinotti, 2012).

To estimate volume change, elevations of a glacier surface between two times are differenced. Various methods are used to measure surface elevation, including photogrammetry, lidar, and radar interferometry, carried on either aerial or satellite platforms. Photogrammetry (aerial and satellite) can be used to estimate the elevation of glacier surfaces by measuring the displacement between the same object found in two images, taken from different angles (Bakker et al., 2009). Historically, photogrammetry was limited to aerial surveys and was labor-intensive due to the measuring the displacement by hand. Advances in computer software have led to automation, reducing the time required to create digital elevation models (DEMs) from aerial and satellite imagery (Shean et al., 2016; Menounos et al., 2018). However, photogrammetry operates in the optical range of the electromagnetic spectrum, limiting its use to day-light and cloud-free conditions. In addition, low contrast snow, typically found on glaciers, presents challenges to remotely define the surface (McNabb et al., 2018).

Another method for mapping glacier elevations is light detection and ranging (lidar; Sapiano et al., 1998; Nuth et al., 2010). A laser pulse, commonly in the near-

infrared, is emitted, and its reflection from the surface is detected, and the time interval between the two is measured. The distance between the sensor and the surface is determined from the speed of light and travel time. Accurately knowing the position of the sensor in space, the height of the surface is determined (Bakker et al., 2009). Airborne lidar accuracy on glacier surfaces is ~ 0.10 to 0.30 m (Garvin and Williams, 1993; Thomas et al., 1995; Sapiano et al., 1998; Kohler et al., 2007). The accuracy of satellite lidar on glacier surfaces is < 0.10 m (Fricker et al., 2005; Brunt et al., 2019). This method provides a distinct advantage, particularly in the low contrast snow-covered portion of glaciers. However, it, too, operates in the optical spectrum and is limited to cloud-free conditions.

Another method for measuring surface elevations is satellite synthetic aperture radar interferometry (InSAR). InSAR is a technique that utilizes data from synthetic aperture radar (SAR), a type of imagining radar. Like other imaging radar, SAR emits an electromagnetic pulse in the microwave range towards the Earth's surface; the pulses bounce off the Earth's surface and are backscattered to the sensor. The time interval between when the energy is emitted and the backscattered energy is received, along with the speed of light, yields the distance from the satellite to the surface. However, unlike other imaging radar, the satellite's forward movement is utilized to create a synthetic aperture by combining the backscattered pulses from the same object. The synthetic aperture allows for higher spatial resolution than other imaging radar systems. InSAR infers elevation by differencing the phase of the wavelength of corresponding pixels from multiple radar images. Radar images represent the intensity of the backscattered signal.

The difference in phase is due to the change in position of the corresponding pixels in each image. Satellite InSAR captures these two images by flying multiple passes over the same surface from different angles (Bakker et al., 2009). Since radar is an active system, it can collect data regardless of the amount of available light. InSAR can also collect data regardless of cloud cover, making it a strong alternative to optical methods. Penetration of the radar wave into snow or ice is reduced by selecting appropriate wavelengths, typically a meter or less (Hensley et al., 2016). The all-weather, day/night capabilities, and the large swath coverage of radar saves time and reduces the cost of region-wide glacier surveys.

We test a novel approach for determining elevations over glacier surfaces using airborne InSAR, NASA's Glacier, and Ice Surface Topography Interferometer (GLISTIN; Moller et al., 2011). Unlike satellite InSAR, GLISTIN collects two radar images simultaneously using two antennas, allowing elevation to be derived from a single flight pass. Mounted on a jet aircraft, GLISTIN can cover a broad area in a short time. GLISTIN has been used to map ice sheets (Hensley et al., 2016), but it has not been used to extensively map alpine glaciers where complex terrain and warm ice and snow pose challenges for radar backscatter. The purpose of my thesis is to assess the accuracy and coverage of GLISTIN for glaciers and perennial snowfields in the western U.S. and to estimate their volume change.

II Study Region & Previous Work

The study region is the American West, defined as the states west of the 100th meridian, exclusive of Alaska and Hawaii, and includes an area of about $2x10^6$ km^2 (Figure **1**). The region is made up of three large mountain ranges, the Rocky Mountains, the Cascade Range, and the Sierra Nevada. The Rocky Mountains span 4800 km and from Canada to New Mexico (Montana, Idaho, Wyoming, and Colorado) and are nearly 500 km in width. Many peaks exceed 4000 m in elevation. The Cascade Range extends 1100 km from Canada, through Washington and Oregon, to Northern California, with peaks > 3000 m. The Sierra Nevada are located along the eastern edge of California, 640 km in length, with peaks > 4000 m, and includes the highest peak in the continental U.S., Mount Whitney (4421 m; NGS, 2006). About 5036 glaciers and perennial snowfields (G&PS), total area ~ 672 km^2 (average 0.13 km^2), with a volume of ~14 km^3, populate the mountain ranges (Fountain et al., 2017; Figure 1). Of these G&PS, 1276 (554 km^2) are estimated to be glaciers. The glaciers are found in two distinct regions. The relatively low elevation G&PS, 2000 m - 3000 m, of the Pacific Northwest (north-west Montana, Oregon, and Washington), account for half the total number and 73% of total G&PS area in the American West. The regional climate is maritime, characterized by warmer wetter winters (2100 mm ± 630 mm; mean ± standard deviation) and warm summers (9 ± 2 C°). The other population are continental glaciers at relatively high elevations, > ~3000m, with a climate characterized, by colder drier winters (880 ± 330 mm) and cooler summers (7 ± 1 C°; Fountain et al., 2017).

Regional studies of glaciers have shown drastic decreases in area over the last century. In the North Cascades, WA, glacier area decreased by -56% from ~1900 to 2014

(Dick, 2013), -55% in the Sierra Nevada, CA (1903 to 2004, Basagic and Fountain, 2011), -66% in the Lewis Range of Glacier National Park (1850 to 1979, Hall and Fagre, 2003), and -47% in the Wind River Range, WY (~1900 to 2006, DeVisser and Fountain, 2015). Since the mid-20th century, glaciers in the American West have lost -39% of their area (Fountain et al., 2017). However, the change has not been constant or uniform. Glaciers retreated in the early 1900s, maintained a period of stability/advance mid-century, and by the end of the 20th-century, glaciers were again retreating (Hoffman et al., 2007; Zemp et al., 2009; Basagic and Fountain 2011).

Glacier volume losses in the western U.S. have been estimated by differencing elevation surfaces from recent lidar and the historic National Elevation Dataset (NED; Gesch, 2007). Glaciers on Mount Rainier, WA, lost -0.65 km^3 from 1970 to 2007/2008 (Sisson et al., 2011). Between 1957 and 2010, 15 glaciers on the Three Sisters, OR lost -0.072 km^3 (Ohlschlager, 2015). In the Lewis Range, MT, nine glaciers lost -0.14 km^3 between 1966 and 2015 (Brett, 2017). Using satellite DEMs, Menounos et al. (2018) estimated a mass loss of -6.5 ± 2.3 Gt yr^{-1} between 2000 and 2018 for most of the glaciated terrain in Western North America. Their results show a drastic increase in loss between the period 2000-2009 and 2009-2018. Using extrapolated field measurements from a small number of glaciers, change for all western North American glaciers was estimated between 2003 and 2009 to be -14 ± 3 Gt yr^{-1} (Gardner et al., 2013). A greater loss than the -2.9 ± 3.1 Gt yr^{-1} reported from 2000 to 2009 by Menounos et al. (2018). Menounos et al. (2018) attribute the difference to the small sample size used in Gardner et at. (2013).

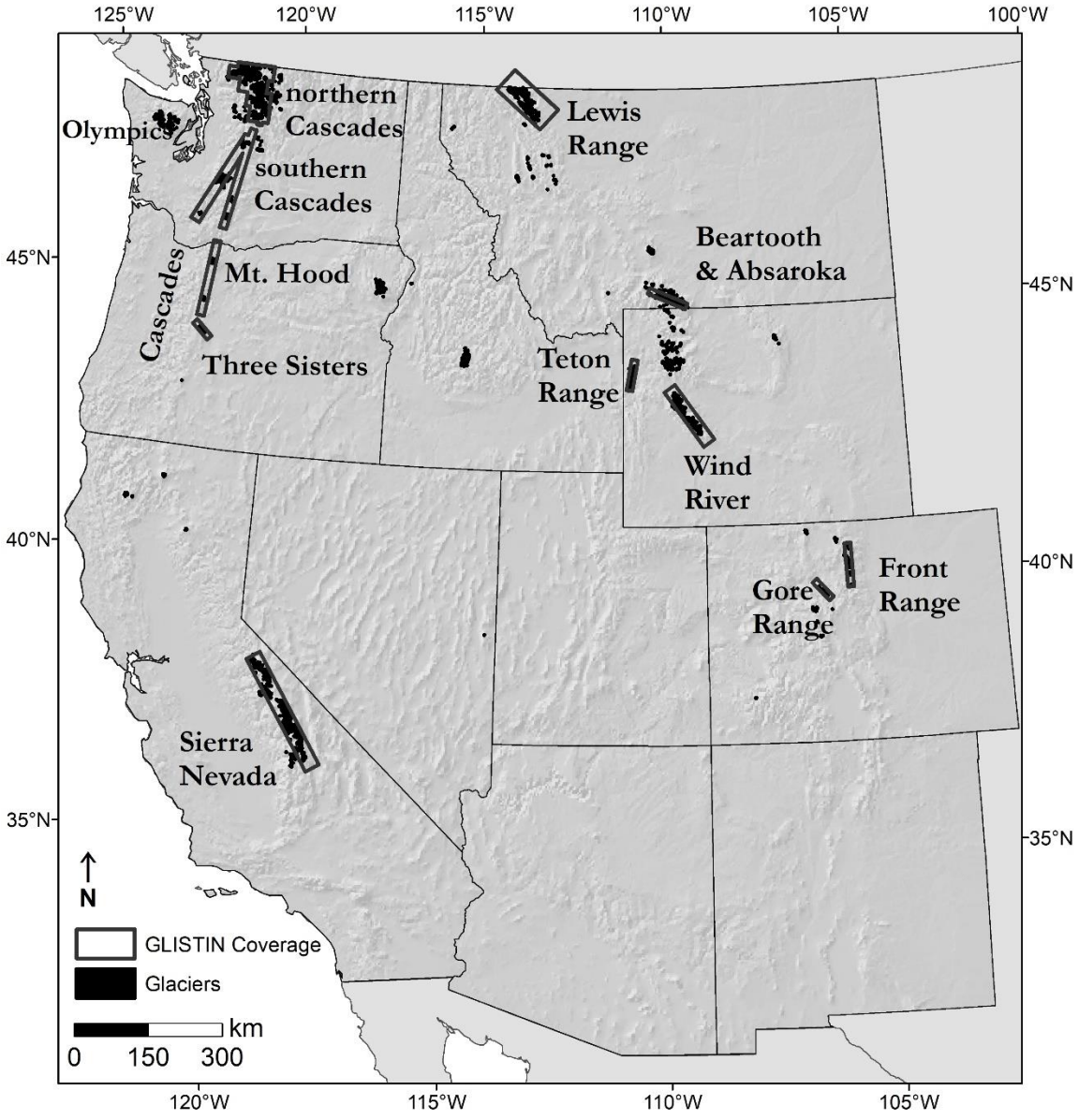

Figure 1. Map of glaciers and perennial snowfields (black dots) in the Western U.S. The boxes show regions surveyed by GLISTIN.

III Methods

To measure the elevation of glacier surfaces, NASA's GLISTIN instrument was flown across the western U.S. GLISTIN is an active InSAR remote sensing system, utilizing the Ka-band (8.4 mm, 35.66 GHz; Moller et al., 2011). GLISTIN emits a microwave pulse from the transmitter towards the earth's surface, and a portion of that pulse is backscattered to the receiving antenna. Water, such as lakes or rivers, absorb the radiation yielding no backscatter. On glaciers, some of the pulse may penetrate almost 30 cm in dry snow or firn or be partially absorbed by wet ice and snow (Hensley et al., 2016; Rignot et al., 2001; Ulaby and Dobson, 1989).

GLISTIN is a left looking instrument mounted in an external pod on NASA's G-III aircraft with a look angles of 15-50°, measured from nadir. The pod includes two differential GPS (DGPS) for measuring instrument location and an inertial navigation system (INU)/GPS system that measures aircraft pitch, roll, and azimuth, together fixing aircraft position with a 3-5 cm accuracy (Moller et al., 2011). The flight altitude was about 12,500 m with a speed of 720 km hr^{-1}. The radar swath width is nominally 12 km. The system utilizes two horizontal antennas (horizontal polarization). Both antennas are capable of transmitting and receiving, which improves the vertical accuracy compared to using only one antenna to transmit (Moller et al., 2019). Like satellite-borne InSAR, travel time and the backscattered energy of the pulses is measured, along with instrument position. Unlike satellite InSAR, GLISTIN uses two antennas (rather than one) separated by 25 cm, in the cross-track direction, collecting two radar images from two different positions simultaneously, rather than from repeat passes as in the satellite application.

The travel time to each antenna from the same point on the Earth's surface is slightly different due to their separation. An interferogram is created when the images are differenced. This difference is expressed in terms of the phase of the wavelengths, which repeat after 2π, so the phase must be "unwrapped" to determine its unique location (Rosen et al., 2000; Moller et al., 2011). Finally, the elevation data is referenced to the Shuttle Radar Topography Mission (Farr et al., 2007) DEM, which uses the WGS84 ellipsoid as its vertical datum.

An issue for SAR in the alpine regions is the complex topographic relief (Eineder and Holzner, 2000; Rees, 2000). Steep terrain can block the radar beam resulting in radar shadows. Steep terrain can also cause phase decorrelation when backscatter from two different points arrives at the antenna at or close to the same moment, as might occur on a steep slope. In addition, steep slopes can cause geometric distortions of foreshortening and layover due to the relative location of the instrument, and the base and peak of a slope. Foreshortening occurs when the return from the base of a steep slope arrives shortly before the return from the peak, yielding a slope steeper than in reality. Layover occurs when the return from the peak arrives before the base.

To minimize missing data from radar shadow and error from layover and foreshortening, GLISTIN typically flew multiple flight passes in opposite directions across each region. For some regions perpendicular flight passes were also flown. The DEMs from each pass were mosaicked into a 3-meter pixel-size DEM and projected into the Universal Transverse Mercator (UTM) coordinate system. Elevation precision is inferred from the height-precision, which is the statistical precision estimate for each 3 m

pixel. It is derived from the interferometric correlation of each radar pixels making up the 3 m pixel (Moller et al., 2011). Low height-precision values indicate high elevation precision and vice versa. In the final mosaicked DEM, each pixel is the weighted sum of elevations from individual passes. The weight is inversely proportional to the height-precision (Hensley et al., 2016). The vertical uncertainty of GLISTIN is about ± 30 cm, estimated from the root mean square error (RMSE) of elevation differences between GLISTIN and high-resolution lidar over non-glaciated, unvegetated surfaces in the Central Valley, CA (Schumann et al., 2015). Data collection and processing for this project was done by the Jet Propulsion Laboratory at California Institute of Technology, Pasadena, CA.

Several methods were used to determine the accuracy of GLISTIN. One is height-precision, a relative measure of the interferometric correlation within a 3 m pixel for each radar return used to create the pixel. For an absolute estimate, GLISTIN elevations were compared to four lidar datasets on the Cascade Range (Oregon and Washington; Table 1). This provided error assessment of GLISTEN over a variety of slopes and aspects, including bedrock and snow/ice surfaces. Only the Mount Adams, WA, lidar was flown the same year as GLISTIN; it is the only lidar compared to the glacier surfaces. The lidar on Mount Adams was flown 28 days prior to the GLISTIN flights, such that we would expect an elevation difference on the snow/ice surfaces due to melting and compaction. All lidar was converted from its native coordinate system to WGS84 to match GLISTIN's coordinate system, using Vdatum (Version 3.8, 2017, National Oceanic and Atmospheric Administration, Washington, DC), inducing an error of 0.076 m. The lidar

data were resampled to 3 m to match the GLISTIN resolution, using bilinear interpolation.

Table 1. List of lidar datasets used for the absolute error assessment. The datasets came from three sources, the National Map, maintained by the U.S. Geological Survey (USGS; https://viewer.nationalmap.gov/basic/), Washington Department of Natural Resources (WA DNR; https://lidarportal.dnr.wa.gov/), and Oregon Department of Geology and Mineral Industries (DOGAMI; https://gis.dogami.oregon.gov/maps/lidarviewer/). 'Uncertainty' refers to the reported absolute vertical uncertainty of the lidar. For the location of regions, see Figures 1 and A1.

Region	Year	Source	Uncertainty
Mount Adams, WA	2016	USGS	0.07
northern Cascade Range, WA	2009	WA DNR	0.04
Mount Rainier, WA	2007/2008	WA DNR	0.04
Three Sisters, OR	2010	DOGAMI	0.04

The location and footprint of the G&PS in the American West were derived from Fountain et al. (2007, 2017). G&PS were separated into glaciers and perennial snowfields to be used separately in the analysis. The G&PS outlines are based on the U.S. Geological Survey (USGS) 1:24000 topographic maps. The USGS maps were compiled over a number of years. Mapping photography used for the 1:24000 maps for the regions surveyed by GLISTIN was flown during the period 1943 to 1998, with 30 G&PS surveyed prior to 1950 (all in Oregon) and 330 G&PS after 1990 (Oregon, Washington, and Wyoming; Figure 2).

The elevations of the glacier surfaces, against which GLISTIN elevations will be compared for volume change estimates, are from the National Elevation Dataset (NED), which is derived from various sources, including aerial photogrammetry and lidar (Gresch, 2007). The resolution of the NED is ⅓ arc-second (~10 m). The horizontal coordinate system is the North American Datum of 1983 (NAD83), and the vertical coordinate system is the North American Vertical Datum of 1988 (NAVD88). The NED

is continually being updated. The USGS does not maintain an original version. The original version is of interest for this project due to its historical surface elevations of G&PS. For this project, a 'historical' version of the NED was compiled from several sources (Table A1). However, elevations were unavailable for 3 G&PS in the Front Range; they are excluded from the volume change analysis. To identify the date of each G&PS DEM, the G&PS outlines were combined with a shapefile of the NED metadata (https://viewer.nationalmap.gov/basic) in ArcGIS (Version 10.6, 2016, Esri, Redlands, CA). The NED from non-USGS sources (Table A1) did not include metadata for the imagery date. In those cases, I used the dates listed on the map collars of the USGS 1:24000 topographic maps. Often the same aerial photographs used to create the topographic maps were also used to derive the NED. Photography used to create the portion of the NED overlapping the GLISTIN surveys were flown between 1950-1993, with only two G&PS surveyed in 1950 (Wind River Range, WY) and nine G&PS after 1990 (Sierra Nevada, CA). There were 108 G&PS outlines where the NED was derived from imagery spanning multiple years, of which 23 had USGS metadata, clearly identifying which portion of the outline corresponds with which year. The DEMs covering the remaining 85 G&PS were from non-USGS sources, and it is unclear what portion of the G&PS were covered by imagery from which year. For G&PS, where multiple images were used to create the NED, if >80% of the G&PS area was imaged within a single year (21 G&PS), that year defined the date. For the remaining 64 G&PS, the date is defined as the average of all years listed. The reported RMSE of the NED (1999 version) is 3.74 m, but that RMSE under samples high elevation and slopes, fewer

than ten samples for slope > 30°, and ~20 samples for elevations > 3000 m (Gesch, 2007). Therefore, the error over glaciers and the surrounding alpine environment is probably much higher.

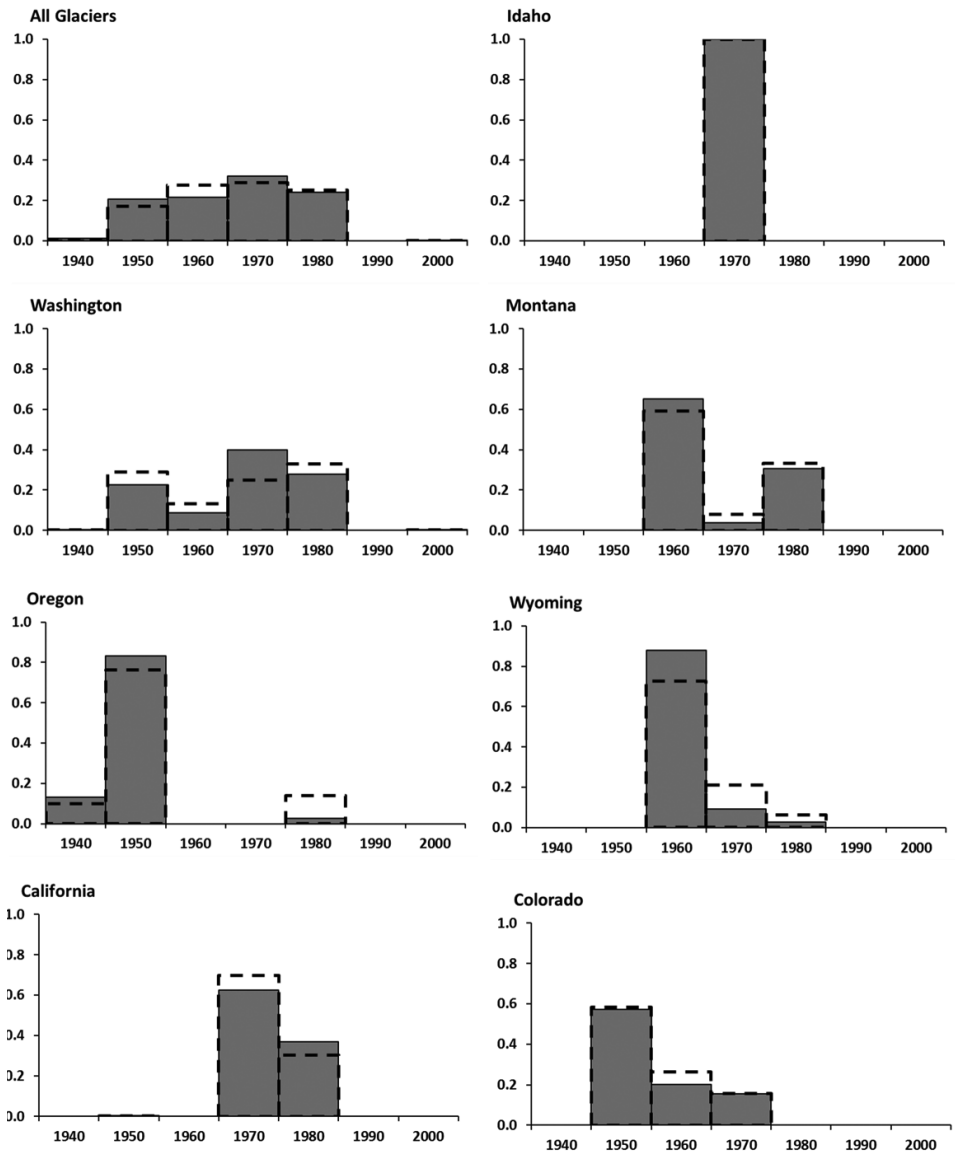

Figure 2. Acquisition dates for imagery used to create the U.S. Geological Survey 1:24000 topographic maps for areas with glaciers and perennial snowfields (G&PS). The date on the x-axis represents the full decade (e.g., 1960 = 1960 to 1969). The y-axis is the fraction of the total. The solid grey bars are the fraction of area, and the dashed outline is the fraction of the number of G&PS. The top left depicts the imagery for all G&PS in the western U.S. The other graphs show the acquisition date for each state. Reprinted from Fountain et al. (2017).

The NED was split into regions corresponding to the mountain ranges covered by GLISTIN. In some cases, regions were split into smaller sub-regions to reduce processing time. Each was converted to the same vertical reference system as GLISTIN (WGS84) using Vdatum then projected into the UTM coordinate system and resampled to 10 m using bilinear interpolation. Before resampling, the pixel resolution of the NED differed by region, ranging from 8.5 m (northern Cascades, WA) to 9.4 m (Sierra Nevada, CA). pixel -size was resampled to 10 m so that it was standard across all regions. GLISTIN was also resampled to 10 m and co-registered to the NED using the methods of Berthier et al. (2007). The co-registration process reduces the horizontal and vertical offsets between the DEMs by first minimizing the standard deviation of differences over control zones and then applying that shift to the whole DEM. Offsets between DEMs can significantly influence estimates of elevation change, particularly on steep slopes (Berthier et al., 2007).

Topographic variables, including slope and aspect and elevation, were derived from the co-registered NED using ArcGIS. ArcGIS calculates the slope for each pixel in the input DEM by determining the maximum rate of change in elevation between the input pixel and the eight neighboring pixels. Aspect is calculated by taking the arctangent of the rate of change in the x and y directions. Rate of change is determined using the eight neighboring pixels. The mean slope and elevation for individual G&PS were determined using the zonal statistic tool (ArcGIS). The zonal statics tool assigns each pixel to a specific zone, in this case individual G&PS. The arithmetic mean is than calculated using the values of each pixel in the zone. Because aspect is based on compass

scale with a discontinuity at 360° aspect was calculated using a python script (Beyerhelm 2018, https://community.esri.com/thread/47864). The script calculates the mean aspect by separating each raster pixel 's aspect within the glacier or perennial snowfield outline into a north and east component using cosine and sine, respectively. The mean cosine and sine for each G&PS are then calculated and converted into a single mean aspect using the arctangent.

Volume change was estimated by multiplying the mean elevation change (GLISTIN elevation minus NED elevation) within the perimeter of individual G&PS by the area of the individual glacier or perennial snowfield included in the GLISTIN DEM. Because changes in volume occur over different periods of time, due to variations in the NED mapping date, a specific volume rate over time (m yr^{-1}) was calculated by dividing the volume change by time span and the G&PS area covered by GLISTIN.

To estimate the uncertainty of the volume change, previous volume change studies in the western U.S. applied a slope dependent method, whereby change was calculated for surfaces at different slopes to account for higher uncertainty at higher slopes (Ohlschlager, 2015; Brett 2017). For example, for the North and Middle Sisters of the Cascade Range in Oregon, RMSEs were between 4.7 m (0° to 10°) and 12.3 m (50° to 60°) for slopes < 60°. For slopes ≥ 60°, the RMSEs ranged from 15.8 m (60° to 70°) and 21.6 m (70° to 80°; Ohlschlager, 2015). I chose not to use this method because few G&PS have slopes greater than 60°, and uncertainty becomes more pronounced at slopes above 60°. Volume change uncertainty ($\sigma_{\Delta V}$) is calculated for each individual glacier or perennial snowfield, using the vertical and area uncertainties (Menounos et al., 2018),

$$\sigma_{\Delta V} = \sqrt{\left(\sigma_{\Delta z}\, A_g\right)^2 + \left(\sigma_A \Delta z\right)^2}\,, \qquad (1)$$

where $\sigma_{\Delta Z}$ is the RMSE of elevation differences between GLISTIN and the NED for all control zones, for the region in which the glacier or perennial snowfield is located, A_g is the area included in the GLISTIN DEM for the glacier or perennial snowfield, Δz is the average elevation change of the glacier or perennial snowfield, and σ_A is area uncertainty. Uncertainty of the G&PS area from the 1:24000 topographic maps is considered 9% based on comparisons of manually derived outlines for G&PS in the Sierra Nevada, CA (Fountain et al., 2017).

IV GLISTIN Results and Analysis

GLISTIN was flown across the glaciated regions of the American West between September 12 and 28, 2016, covering about 41,000 km^2 (Figure **1**; A1-3). Due to an unexpected reassignment of GLISTIN, several mountain ranges were not included, most notably the Olympic Mountains, WA, and the Absaroka Range, WY. Table A2 lists all glaciated mountain ranges not covered. The radar data for each flight pass were mosaiced to create a DEM for each region (Figure 1). Mosaics typically consisted of data from two to six flight passes. However, as few as one or as many as 14 flight passes were used for some regions. Not every pixel in the DEMs has a value due to radar shadow, layover/foreshortening, or low correlation, and are considered missing data.

The surveyed regions included 3889 G&PS (586 km^2), of which 3289 (85%) had at least one pixel of elevation from the GLISTIN flights (Table 2). The total area of GLISTIN-measured elevations on G&PS was 441 km^2: 619 G&PS (33 km^2) had 100% coverage and 1770 G&PS (309 km^2) $\geq$ 80% coverage (Figure 3).

Table 2. List of glaciated regions surveyed by GLISTIN, including the number of glaciers and perennial snowfields (G&PS) in each region. 'Total G&PS' is the number of G&PS in the surveyed region, including those with no measured elevations. 'Total Area' is the area of all glaciers within the surveyed region. 'Measured' refers to G&PS with at least one pixel of GLISTIN measured elevation. 'Measured Area' is the total area of measured G&PS elevations.

State/Range	Total G&PS	Total Area (km^2)	Measured G&PS	Measured G&PS Area (km2)
California				
Sierra Nevada	804	32	661	19
Colorado				
Front	44	2	35	1
Gore	34	1	32	1
Montana				
Beartooth-Absaroka	226	19	128	11
Lewis	401	39	315	26
Oregon				
Cascade	260	40	243	37
Washington				
northern Cascades	1183	268	1059	199
southern Cascades	297	124	240	100
Wyoming				
Teton	159	6	118	4
Wind River	481	55	458	44
Total	3889	586	3289	441

The demographic of GLISTIN coverage showed that all large G&PS (> 5 km^2), totaling 10 (72.23 km^2), had coverage greater than 80% (Figure 4). Coverage of small G&PS (< 0.10 km^2) totaling 3091 G&PS (97.70 km^2), which make up 79% of the G&PS covered by GLISTIN flights, ranged from 0% (550 G&PS, 15.48 km^2) to 100% (391 G&PS, 9.92 km^2), with a median of 80%. G&PS were grouped into quartiles based on the initial area (Figure 5). Grouping the surveyed G&PS areas into quartiles of nearly equal numbers of G&PS showed that the majority of G&PS in each area range had >75% coverage.

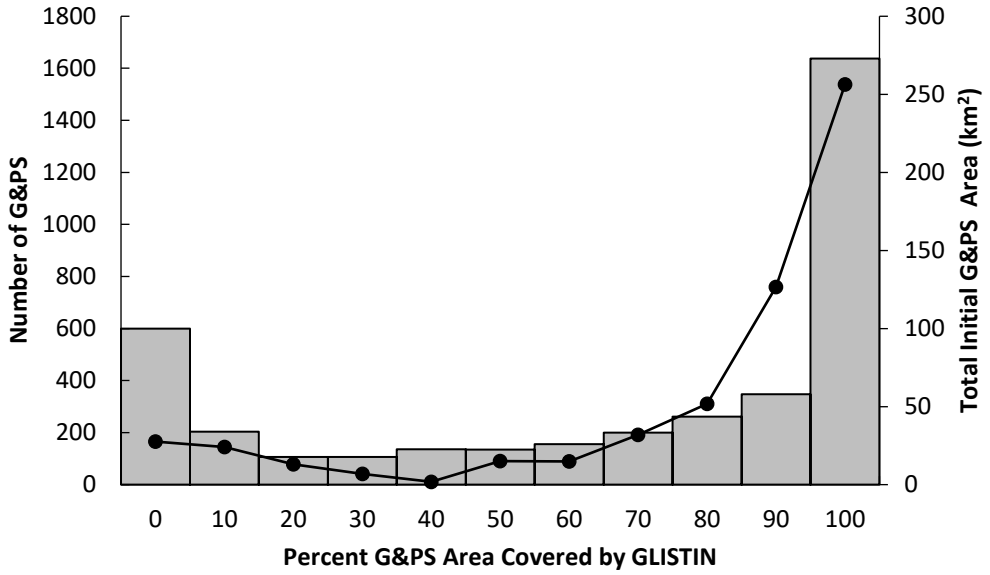

Figure 3. Histogram of GLISTIN coverage as a percentage of the individual glacier or perennial snowfield (G&PS) areas. The black line and circles represent the total initial G&PS area of each bin. G&PS area is derived from outlines on the U.S. Geological Survey 1:24000 map series. The x-axis value is the maximum for each bin, except for the first bin (0), which are G&PS with no coverage.

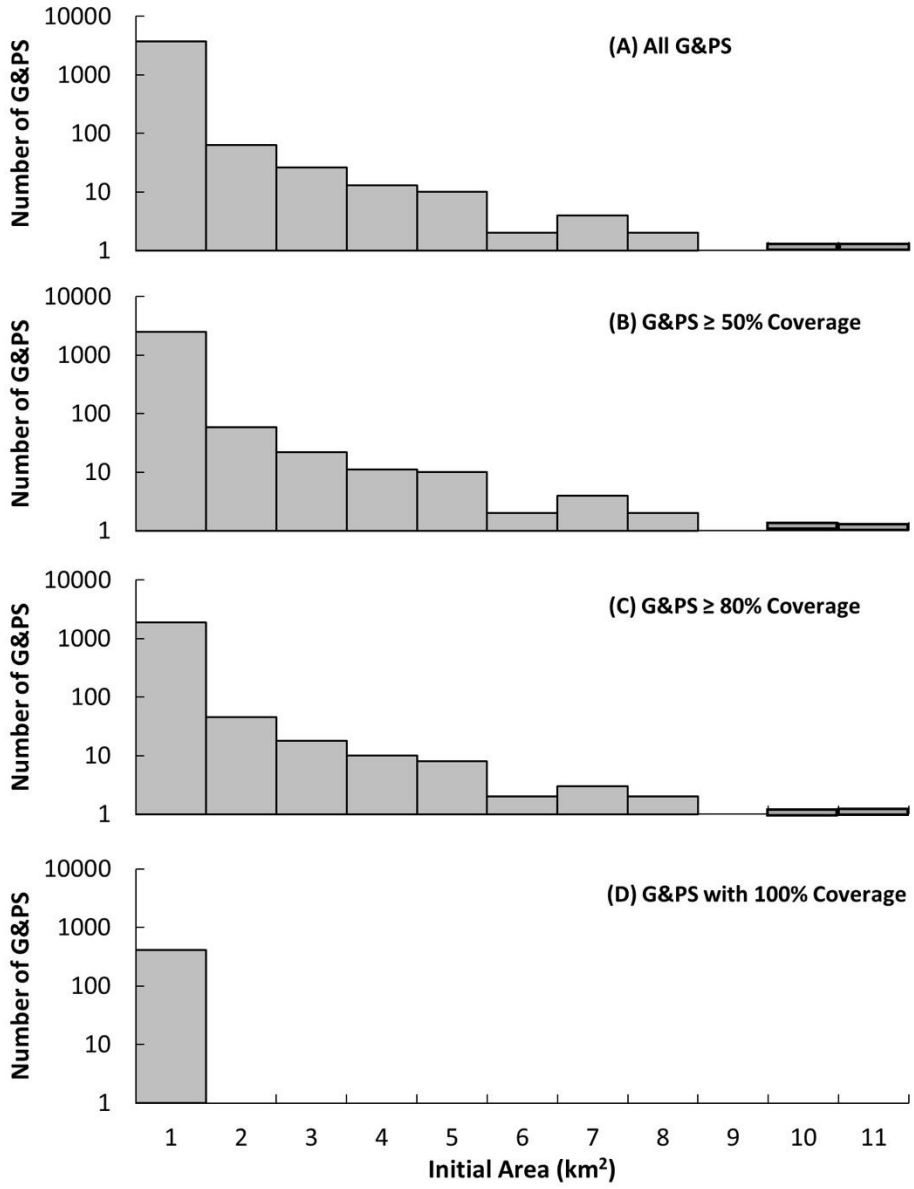

Figure 4. Histogram of the initial area of glacier or perennial snowfield (G&PS) for G&PS with ≥ 50% (A), ≥ 80% (B), and 100% (C) GLISTIN coverage. The black line represents the cumulative % number of G&PS. G&PS area is derived from outlines on the U.S. Geological Survey 1:24000 map series. The x-axis value is the maximum for each bin.

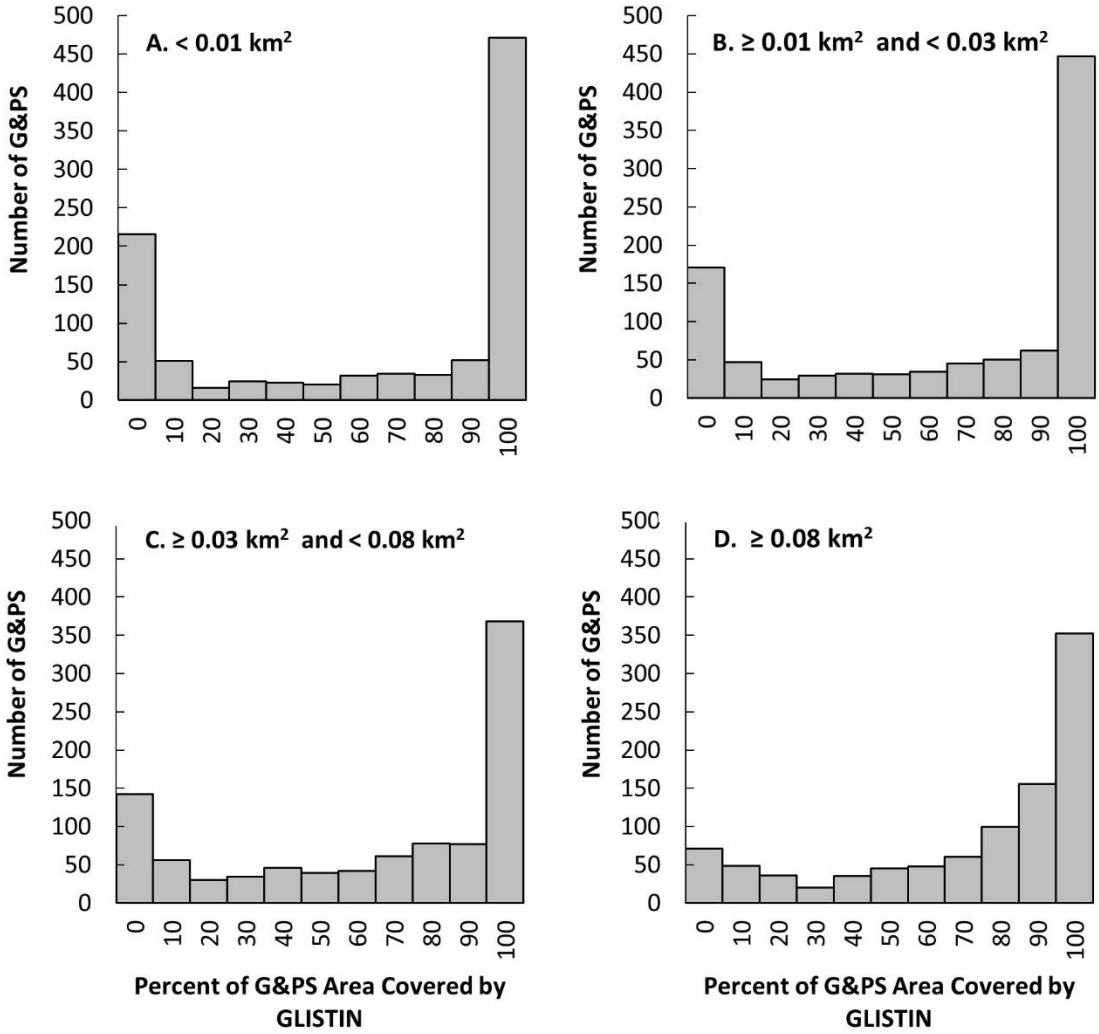

Figure 5. Histograms showing GLISTIN coverage as a percentage of the individual glacier or perennial snowfield (G&PS) grouped by area quartiles, for all G&PS covered by GLISTIN flights. Quartiles are defined as having nearly equal number of G&PS (972, 972, 793, 972, respectively). The x-axis value is the maximum for each bin, except for the first bin (0), which are G&PS with no coverage.

To understand whether surface conditions, snow versus ice, and slope, may affect missing data I divided individual G&PS, with at least 1 pixel of GLISTIN coverage into accumulation and ablation zones. The accumulation zone is the perennially snow-covered portion that is annually gaining mass; the ablation zone is ice-exposed during the late summer and annually loses mass (Cuffey and Patterson, 2011). The boundary between the two zones was estimated using the mean elevation of each G&PS, a rough estimate of

the equilibrium of a glacier (Leonard and Fountain 2003; Le Bris and Paul, 2011). Slightly more than half of the missing data (58%) were located in the accumulation zone (Table 3). More data were missing from the accumulation zones than the ablation zone in all mountain ranges surveyed. For slope, missing data was significantly correlated with steeper slopes ($p < 0.05$, Mann-Whitney U test) regardless of mountain range or location in the accumulation or ablation zone. It should be noted that the average slope of accumulation zones was significantly steeper ($p < 0.05$, Mann-Whitney U test) than the average slope of ablation zones.

Table 3. The area of collected and missing data (pixels) for glaciers and perennial snowfields for each region grouped by accumulation and ablation zones. 'Collected' refers to GLISTIN DEM pixels with elevation values. The area is in km^2, '%' is the percentage of the missing data compared to the total glaciated area for that zone. 'Acc' refers to the accumulation zone, and 'Abl' refers to the ablation zone.

	Collected			Missing		
Region	**Total Area**	**Acc %**	**Abl %**	**Total Area**	**Acc %**	**Abl %**
northern Cascades, WA	199.08	48	52	60.43	27	19
southern Cascades, WA	100.29	45	55	19.55	19	14
Mount Hood, OR	25.64	46	54	1.82	9	5
Three Sisters, OR	11.09	47	53	1.20	12	8
Sierra Nevada, CA	18.75	42	58	8.33	40	22
Lewis, MT	25.87	42	58	9.51	35	20
Beartooth-Absaroka, MT	10.52	46	54	4.59	35	26
Teton, WY	3.56	45	55	1.07	27	19
Wind River, WY	43.80	47	53	10.42	22	16
Front, CO	1.18	37	63	0.65	50	23
Gore, CO	1.14	45	55	0.23	26	8
Total	440.93	46	54	117.79	25	17

To understand the relationship between topography and missing data, missing data within G&PS outlines were compared to slope, aspect and elevation using probability density functions (pdfs). For each topographic variable, the pdf for all terrain

within the G&PS outlines were plotted with the pdf for missing data as well as the ratio of the two. If missing data were uniformly distributed over the terrain, then the pdf for the missing data would match that of the terrain data and the ratio would be constant at one. Any variability in the distribution of missing data would result in a pdf different from the terrain pdf. The pdf ratio was > 1 for terrain slopes >30^{o} (Figure 6) and for relatively high elevations. No pattern was obvious with aspect due to variability in orientation of flight lines and mosaics that used multiple passes. See Appendix B for more details (Figures B1-B17).

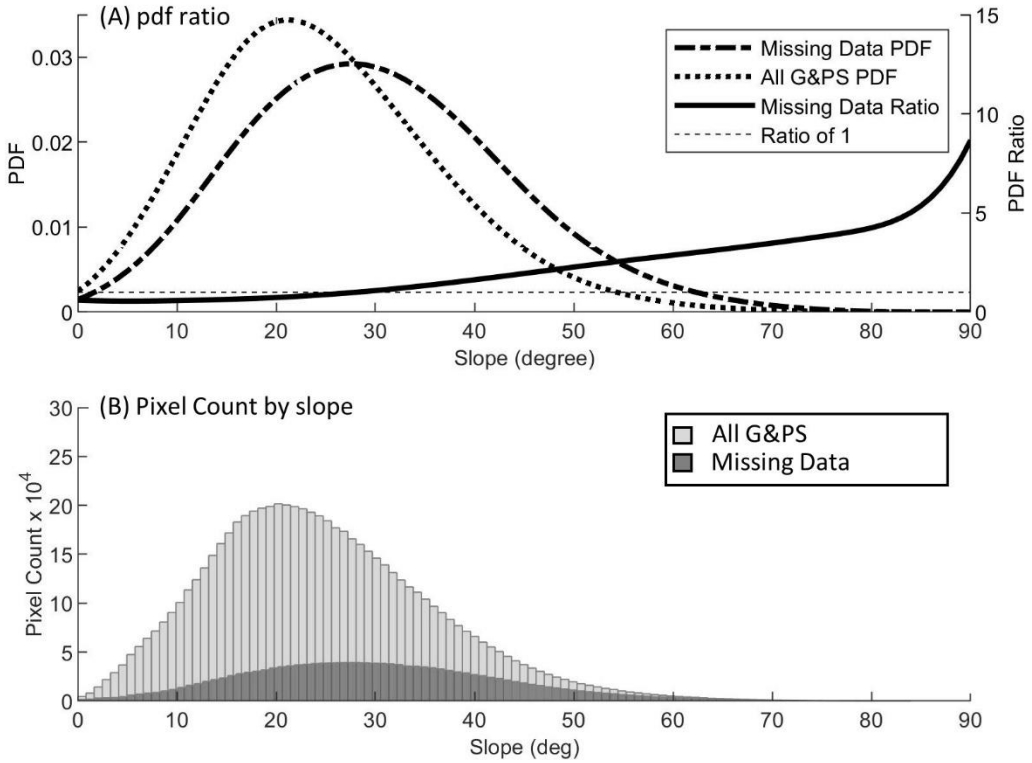

Figure 6. Plots of probability density functions (pdf) and pdf ratios (A) and histograms of slope for all glacier and perennial snowfield (G&PS) surfaces and the missing data on G&PS (B).

To understand how the mosaicking process improves data coverage, individual flight surveys in the Cascade Range, Washington were compared to the mosaics. (Figure 7). Each flight direction roughly followed one of the cardinal directions yielding two sets of parallel and overlapping flight paths (but in opposite directions) and a mosaic of all four flights. The data from each parallel set were mosaiced together, creating two mosaics (east-west and north-south). The overlapping area of all four flights were mosaiced. Considering only the area overlapped by all four flights, missing data ranged 53% - 55%, for two-flight mosaics, 30% - 43%, and for the four-flight mosaic 11% (Table 4). Results for the G&PS shows a similar trend of fewer missing data with increasing number of flights, but with a higher fraction of missing data.

Table 4. Missing and measured data for individual and mosaiced flight passes in the Cascade Range, WA. 'Mosaic' refers to the two-flight mosaic of the two previous flights listed, and 'All Mosaic' refers to the four-flight mosaic. 'All' refers to the area of entire terrain and 'G&PS' to the area of all glaciers and perennial snowfields within the area overlapped by all four flights (see Figure 7), '%' is the ratio of the missing or measured area divided by the total area within that category.

	Missing				**Measured**			
	All		**G&PS**		**All**		**G&PS**	
Flight Direction (°)	**Area (km^2)**	**%**	**Area (km^2)**	**%**	**Area (km^2)**	**%**	**Area (km^2)**	**%**
77	100.57	55	6.35	67	80.94	45	3.08	33
257	96.28	53	5.37	57	85.23	47	4.05	43
Mosaic	54.03	30	3.71	39	127.48	70	5.72	61
161	100.57	55	6.35	67	80.94	45	3.08	33
341	99.87	55	6.52	69	81.64	45	2.90	31
Mosaic	77.45	43	5.51	58	104.06	57	3.92	42
All Mosaic	19.60	11	1.12	12	161.91	89	8.31	88

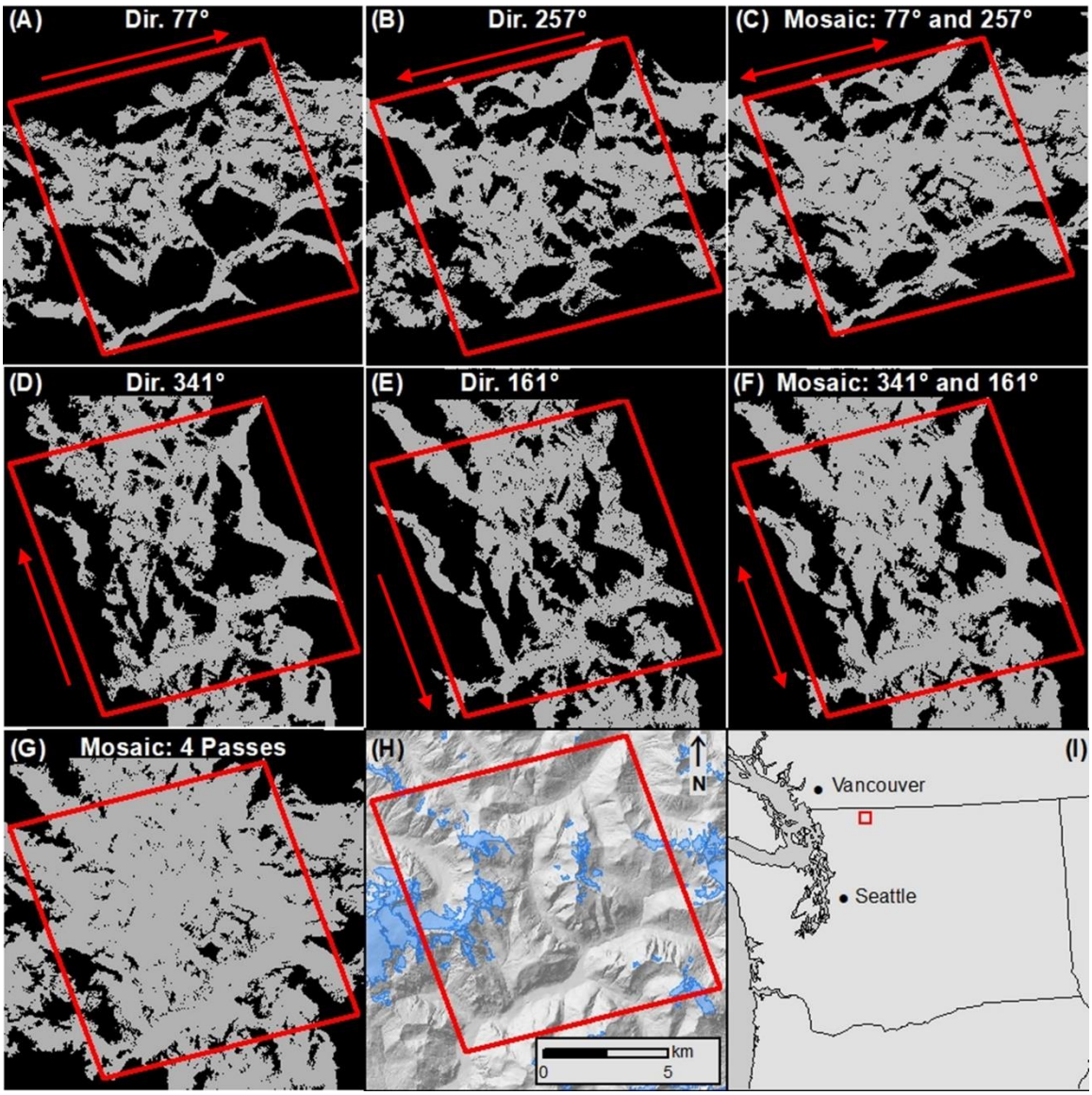

Figure 7. The change in GLISTIN data coverage due to different flight orientations and mosaiced processing over the same area in the northern Cascade Range, WA. The red rhombus outlines the overlapped area and the arrows indicate flight direction, with the actual direction identified by text. Grey fill represents collected data and black indicates no data. Panels A, B, D, E, show single pass results, C, F show mosaic results for the passes in that row, G shows the results of all 4 passes mosaiced. Panels H and I shows the location. Shaded relief topography with blue indicating glacier extent.

To understand the cause of the missing data. I created a simple model to estimate areas of radar shadow caused by terrain. These areas can be separated from the population of missing data to infer other causes, due to decorrelation induced by layover and foreshortening (Y. Zheng, Per. Comm., 2019). The model, based on the ArcGIS viewshed tool, used the planned flight path and the NED elevations to estimate the radar viewshed at a point every 500 m. The actual flight path was < 5m from the planned flight trajectory. The view extent for each point is the area perpendicular and to the left of the flight path/direction and is limited to 250 meters to the fore and aft of the observation point along the flight line. The model also constrains the range of vertical angles of observations to the planned range of look angles. The look angle is the angle between nadir and the line of sight of GLISTIN. Documentation from ESRI does not describe how the viewshed tool iterates through the range of angles. The model output is a binary raster, where pixels are classified as visible or shadowed. The model results were split into the near range, the half of the raster closest to the flight line, and the far range, the half farthest from the flight line.

The model was applied to a pair of flights over Mount Baker in the North Cascades, WA (Figure 8). The flight directions were 77° and 257°, with an altitude of 12,497 m, and look angles between 15 and 48.5 degrees. The results for both flights look similar, only the 77° flight direction is shown here (Figure 9), the other is in the appendix (Figure A4). Based on the 2016 NLCD (https://www.mrlc.gov/data/nlcd-2016-land-cover-conus), 2% (30.41 km^2) and 3% (25.55 km^2) of the model area for the 77° and 257° flights, respectively was water, which absorbs the radar energy, and was excluded from

further analysis. Results show that terrain shadow accounts for 52% and 53% of the missing data in the 77° and 257° flights, respectively. More data is missing due to terrain shadow in the near range than the far range for both flights, 65% (265.78km^2) for the 77° flight, and 61% (258.12 km^2) for the 257° flight. The actual missing data shows a similar pattern, 64% (506.31km^2) for the 77° flight, and 57% (449.64 km^2) for the 257° flight. Note that the model underpredicts the missing data in the near range along the outer edge of the swath (see green arrows in Figure 9).

The model also predicts missing data in places where GLISTIN data exists, a total of 43 km^2 (10% of modeled missing data) and 40 km^2 (9%) for flights at 77°, and 257°, respectively. Variations in the flight path from planned, < 5 m, changes the predicted missing data by < 1% and does not account for the observed data predicted to be missing.

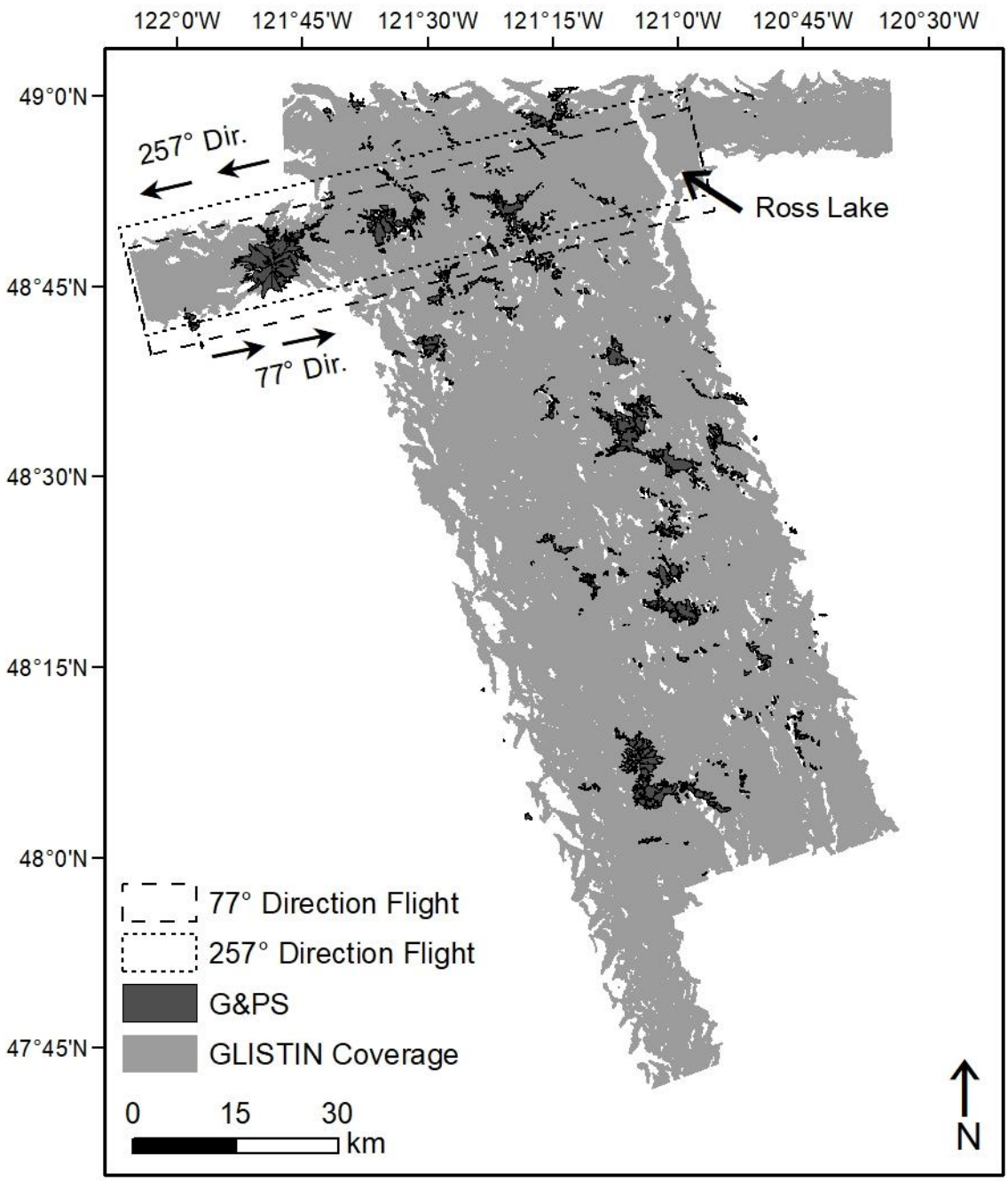

Figure 8. Map of GLISTIN coverage over the northern Cascades, WA. The light grey represents the GLISTIN coverage, the white is missing data, and the dark grey polygons are glaciers and perennial snowfields, and dash boxes represent the two flights used in the viewshed model. The arrows indicate the flight direction. See Figure 1 for the location of the GLISTIN mosaic.

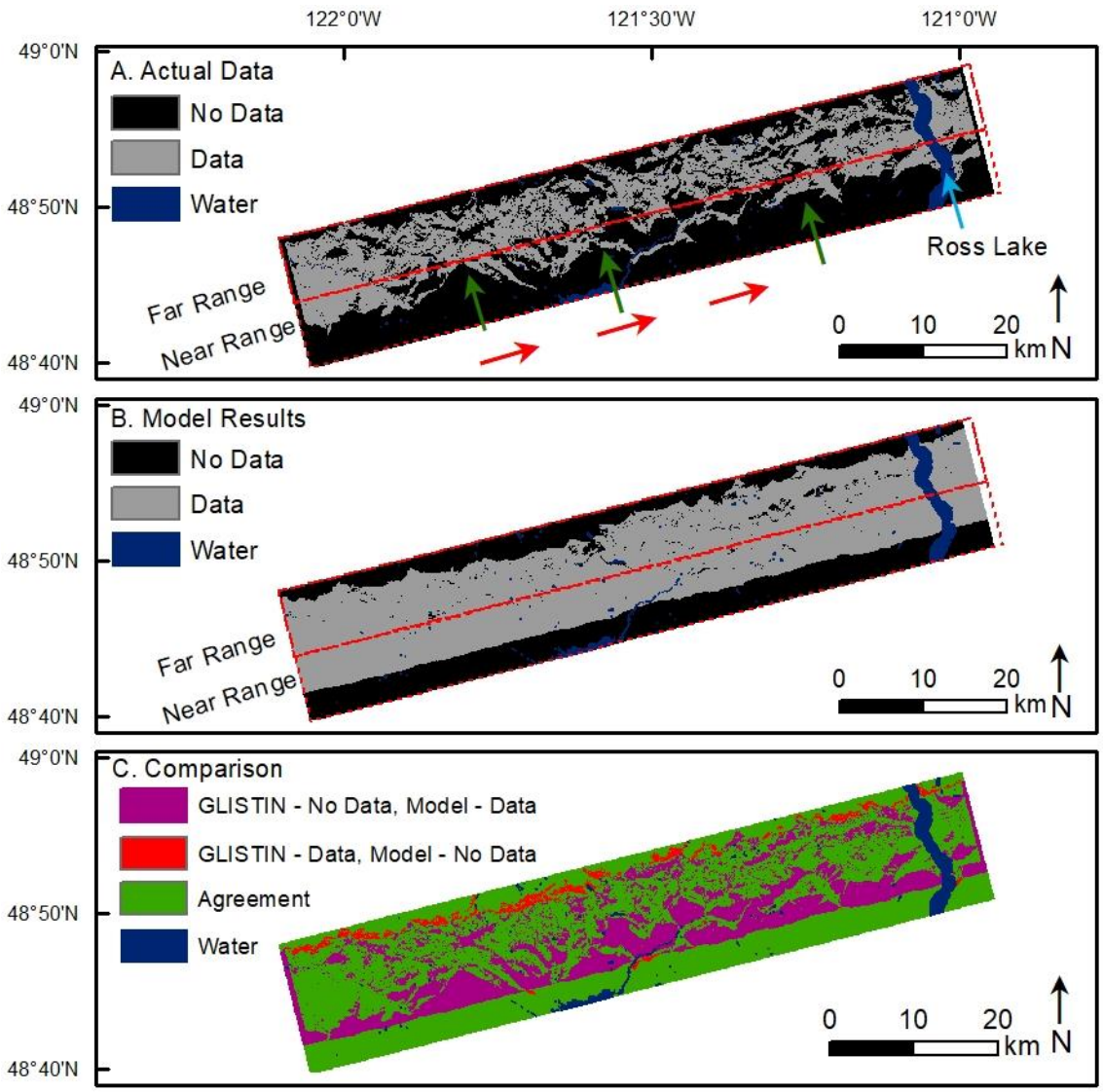

Figure 9. GLISTIN coverage for the 77° direction flight over the northern Cascades, WA. Panel A shows the data collected by GLISTIN, Panel B shows the modeled results from the viewshed analysis, and Panel C shows a comparison between the actual and modeled data. In panel A, the green arrows are examples of indents of missing data thought to be the result of radar foreshortening and layover. The red arrows in panel A indicate the flight direction. The dashed red boxes in panel A and B indicate the near and far ranges of GLISTIN.

The uncertainty of GLISTIN surface elevations was examined using height-precision and a comparison with lidar elevations. Height precision was compared between control zones and glacier surfaces (Table 5). For all control zones (421.30 km^2,

n = 4,6384,717), height precision ranged from 0.07 m to 12.59 m, with a mean and standard deviation of 0.84 ± 0.79 m, and a median of 0.58 m. For G&PS surfaces (440.74 km^2, n = 48,631,339) height-precision ranged from 0.08 m to 13.07 m, with a mean and standard deviation of 1.20 ± 1.02 m, and a median of 0.85 m. Less than 1% of pixels in control zones and ~ 1% of pixels on G&PS had a height-precision greater than 5 m (Figure 10). The median height-precision of G&PS is statistically different ($p < 0.01$) from the height-precision of control zones using the Wilcoxon Rank Sum Test.

Table 5. Height-precision of glaciers and perennial snowfields (G&PS), and control zones. Height-precision is in meters. 'Region' refers to the region of the mosaicked GLISTIN DEM, 'Min' is the minimum, 'Med' is median, 'Max' is the maximum, and 'Std' is the standard deviation. All values except for area are in meters. 'northern Cascades' and 'southern Cascades' refers to regions in the Washington Cascades. 'Bear/Abs' refers to Beartooth-Absaroka, MT. See Table 2 for the location of mountain ranges.

	G&PS						Control Zones					
Region	**Area (km^2)**	**Min**	**Mean**	**Med**	**Max**	**Std**	**Area (km^2)**	**Min**	**Mean**	**Med**	**Max**	**Std**
northern Cascades	194.38	0.08	1.32	1.04	12.81	1.01	61.33	0.12	1.21	0.79	12.51	1.07
southern Cascades	104.94	0.14	1.29	0.86	13.07	1.14	27.95	0.15	1.23	0.78	12.59	1.08
Mount Hood	25.63	0.11	1.03	0.67	13.00	0.99	10.39	0.13	1.10	0.65	10.99	1.10
Three Sisters	11.08	0.18	0.97	0.65	11.29	0.89	23.50	0.15	1.07	0.59	12.41	1.17
Sierra Nevada	18.70	0.11	0.91	0.57	10.98	0.87	191.92	0.07	0.63	0.50	10.63	0.45
Lewis	25.88	0.09	1.24	0.97	12.44	0.96	22.23	0.09	0.65	0.61	9.55	0.25
Bear/Abs	10.52	0.14	0.94	0.64	10.86	0.85	8.74	0.11	1.03	0.71	9.90	0.87
Teton	3.56	0.14	1.06	0.66	10.84	0.95	0.94	0.19	0.66	0.57	10.10	0.51
Wind River	43.73	0.19	0.73	0.52	10.17	0.67	8.09	0.12	0.90	0.70	9.99	0.65
Front	1.18	0.17	1.12	0.77	8.80	0.96	37.56	0.13	0.81	0.58	9.93	0.72
Gore	1.14	0.15	0.90	0.65	7.78	0.71	28.67	0.10	0.89	0.61	9.97	0.78
Total	440.74	0.08	1.20	0.85	13.07	1.02	421.30	0.07	0.84	0.58	12.59	0.79

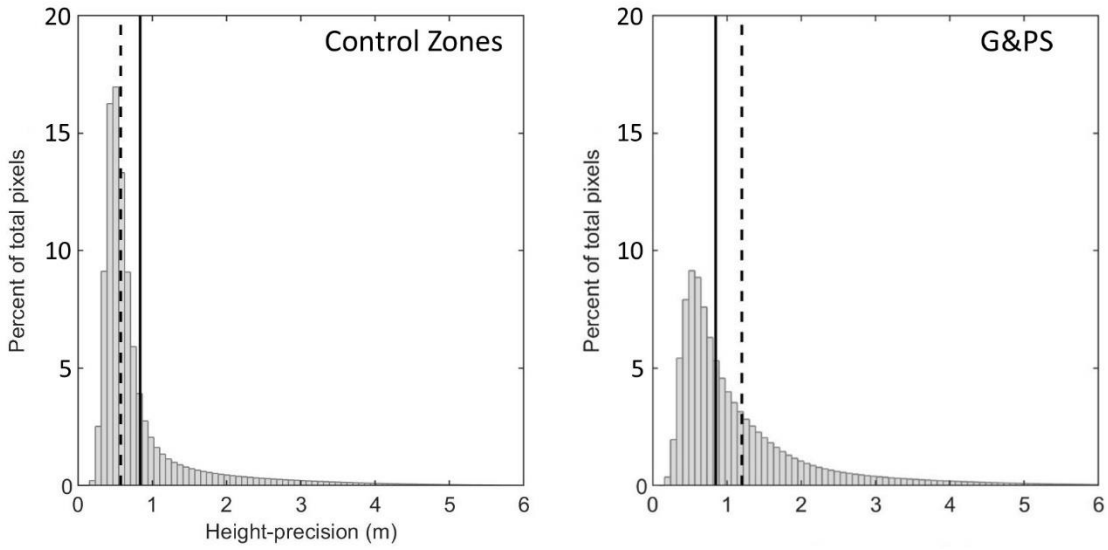

Figure 10. Histograms of height-precision for control zones and glaciers and perennial snowfields (G&PS). The solid black line indicates the mean, and the dashed line indicates the median.

The two groups have statistically different median slopes 21° and 15° for GP&S and control zones, respectively ($p < 0.01$, Wilcoxon Rank Sum Test). To examine how height precision may vary with surface slope the mean height-precision for G&PS within each glaciated region was calculated for 10° slope bins (Figure 11). Height-precision increases linearly with slope at a rate of +0.013 m per 10-degree slope bin ($R^2 = 0.61$, $p < 0.01$). The standard deviation of height-precision for each slope bin was fairly constant for slope bins less than 70°, varying between 0.16 m - 0.20 m: the deviation for the 70° bin was 1.07 m, and for 80°, 1.23 m.

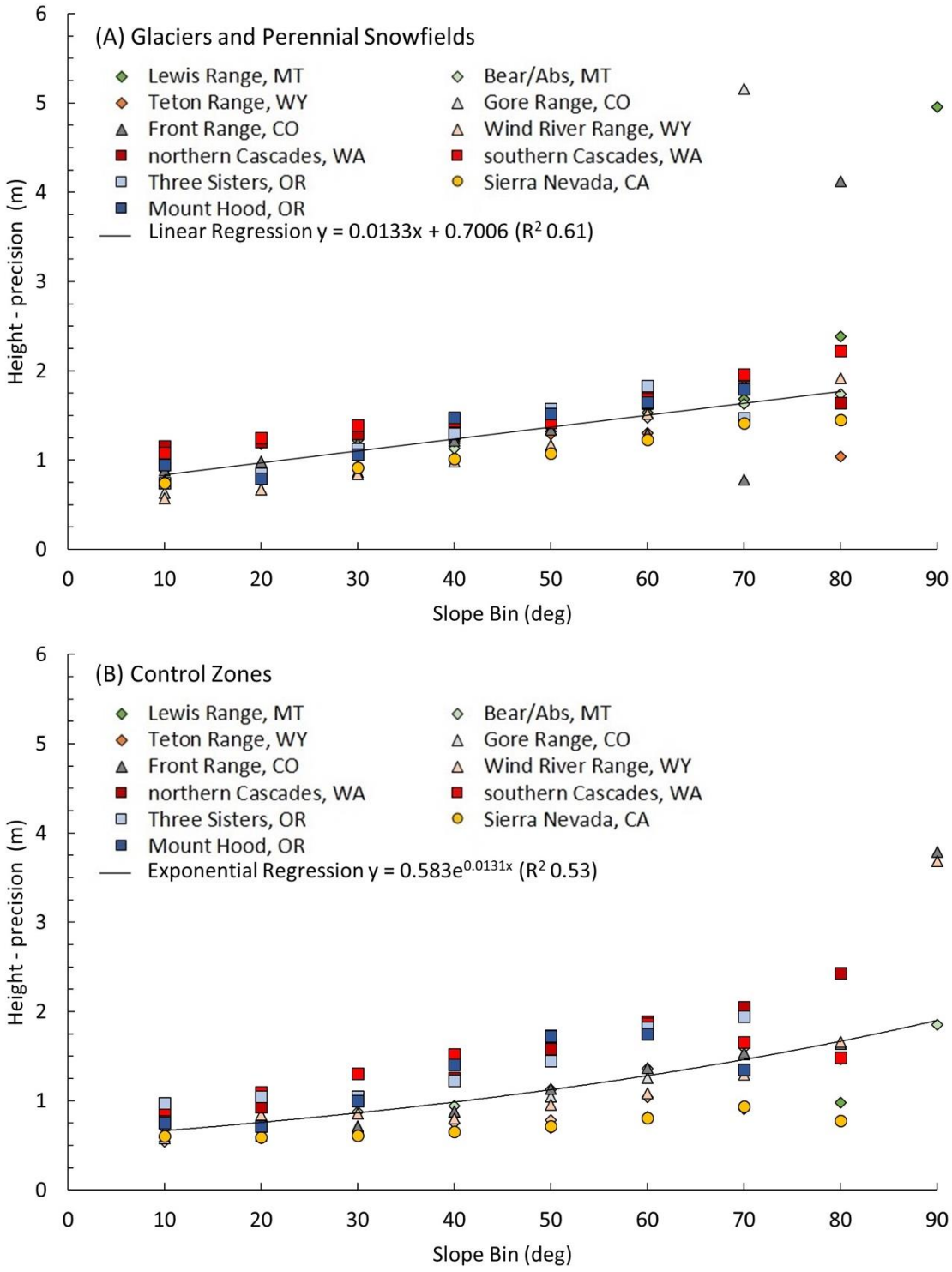

Figure 11. Average height-precision for glacier and perennial snowfields (A) and control zones (B) binned by 10° slopes. The slope label represents the maximum of that bin. The 10° slope bin includes slopes of 0°.

GLISTIN-derived elevations were compared to aerial lidar elevation on control zones, areas of barren earth near G&PS, for the Cascade Range (Oregon and Washington; Table 6). The RMSE for control zones in the northern Cascade Range in Washington (1.61 m^2) was 3.87 m, Mount Rainier, WA (3.10 m^2) 1.86 m, Mount Adams, WA (12.74 m^2) 3.19 m, and Three Sisters, OR (1.95 m^2) 2.99 m. The elevation differences visually appear to be normally distributed for all regions (Figure 12), but statistically are non-normally distributed (Anderson-Darling test, $p < 0.05$). Elevation differences were compared to slope and showed no relationship (Figure 13A). The height-precision was also compared to slope (Figure 13B). For all four regions there is a weak trend of the minimum height-precision increasing with slope. The mean height precision for all four regions was less than 1 m (Table 6). Also, no relationship exists between height precision and elevation differences (Figure 14). To examine how height precision may vary with surface slope, the mean height-precision for control zones was calculated for 10° slope bins (Figure 15A). There appear to be no trends between mean height-precision and slope. For slope bins > 30°, the mean height-precision for control zones on Mount Adams were greater than the mean of other regions. This may be the result from the GLISTIN data for Mount Adams being limited to data from a single flight pass rather than multiple passes, like the other regions examined. The RMSE for control zones was also calculated for 10° slope bins (Figure 15B). The RMSE increases with slope. The relationship fits both linear ($y = 0.08 + 0.01$, $R^2 = 0.62$) and exponential ($y = 1.01e^{0.02x}$, $R2 = 0.63$) regressions.

The Mount Adams lidar was collected 28 day prior to GLISTIN. Unfortunately, no simultaneous data were collected with GLISTIN, so the Mount Adams lidar provides the closest temporal collection of elevation data to GLISTIN. This provides the best opportunity to compare GLISTIN elevation on ice surfaces. The comparison of elevations is limited to a single pass rather than a GLISTIN mosaic because of collection problems on the second pass. We expect no difference in surface elevation of control zones, but the GLISTEN-derived elevations of snow and ice surfaces should be slightly lower due to melt during the month-long delay. The mean and median elevation differences (GLISTIN minus lidar) for control zones was + 0.38 ± 1.83 m and +0.001 m respectively. For ice surfaces the mean and median elevation difference were -0.86 ± 3.76 m and -0.97 m, respectively.

The RMSE of G&PS (19.67 km2) was 3.86 m. The histogram of elevation differences (Figure 16) looks normally distributed but statically the data is non-normally distributed (Anderson-Darling test, $p < 0.05$). Elevation differences were compared to slope and show a weak trend of elevation differences increasing with slope (Figure 17A). The height-precision was also compared to the slope (Figure 17B). There is a weak trend of the minimum height-precision increasing with slope on glacier surfaces. The mean and median height precision for glacier surfaces was 1.45 ± 1.12 m and 1.02 m, respectively. No relationship exists between height precision and elevation differences (Figure 18). There is a cluster, indicated by the red circle in Figure 18, of large elevation difference (> 75 m) found at low height precision (< 4 m). All of the pixels in the cluster are found on the White Salmon-Avalanche Glacier. The cluster contains 176 pixels, <0.01% of all the

glacier pixels on Mount Adams. The large elevation differences are likely due to the steep slope of the area the cluster is located. The cluster had a significantly steeper median slope (41°, $p < 0.05$, Mann-Whitney U) than the median slope of all glacier pixels (20°). The mean height precision for glacier surfaces was calculated for 10° slope bins (Figure 19A). Mean height precision increases linearly with slope for shallower slopes (≤ 30° bin). There is no trend between height- precision and slope for steeper slopes. The RMSE of elevation difference of glaciers surfaces was also calculated for 10° slope bins (Figure 19B). RMSE increases exponentially with slope ($y = 1.77e^{0.02x}$, $R^2 = 0.99$, $p < 0.01$). Aspect was also compared and showed surfaces facing away from GLISTIN had a higher error than surfaces facing GLISTIN (Appendix C).

To understand how a glacier's surface affects the error, height-precision and the RMSE, for control zones and glaciers were compared for Mount Adams. The mean height-precision for control zones, 1.34 m, was slightly smaller than that of glaciers, 1.45 m. Looking at mean height-precision grouped by 10° slope bins (Figure 19A) shows that glacier surfaces have a larger height-precision at shallower slopes (≤ 30° bin) than control zones. RMSE of control zones (12.74 km^2), 3.19 m, was slighter less than the RMSE of glaciers (19.67 km^2), 3.86 m. For control zones, the RMSE was 1.72 m and 9.52 m for the 10° and 80° bins, respectively; for glaciers, 2.28 m, and 13.33 m respectively.

Table 6. Elevation uncertainty for control zones expressed as the root mean square error (RMSE), the mean elevation difference (GLISTIN minus lidar), and mean height-precision (prc). 'std' refers to standard deviation. 'Region' refers to the region of the mosaicked GLISTIN DEMs. 'Year' is the acquisition year of the lidar data. The listed area is the area of the control zones.

Region	Year	RMSE (m)	Mean Elevation Difference ± std	Mean prc ± std	Area (km^2)
northern Cascades, WA	2009	3.87	-0.14 ± 1.78	0.91 ± 0.62	1.61
Mount Rainier, WA	2007/08	1.86	0.00 ± 3.20	0.60 ± 0.16	3.10
Mount Adams, WA	2016	3.19	0.38 ± 1.83	1.34 ± 1.23	12.74
Three Sisters, OR	2010	2.99	0.10 ± 1.63	0.69 ± 0.57	1.95

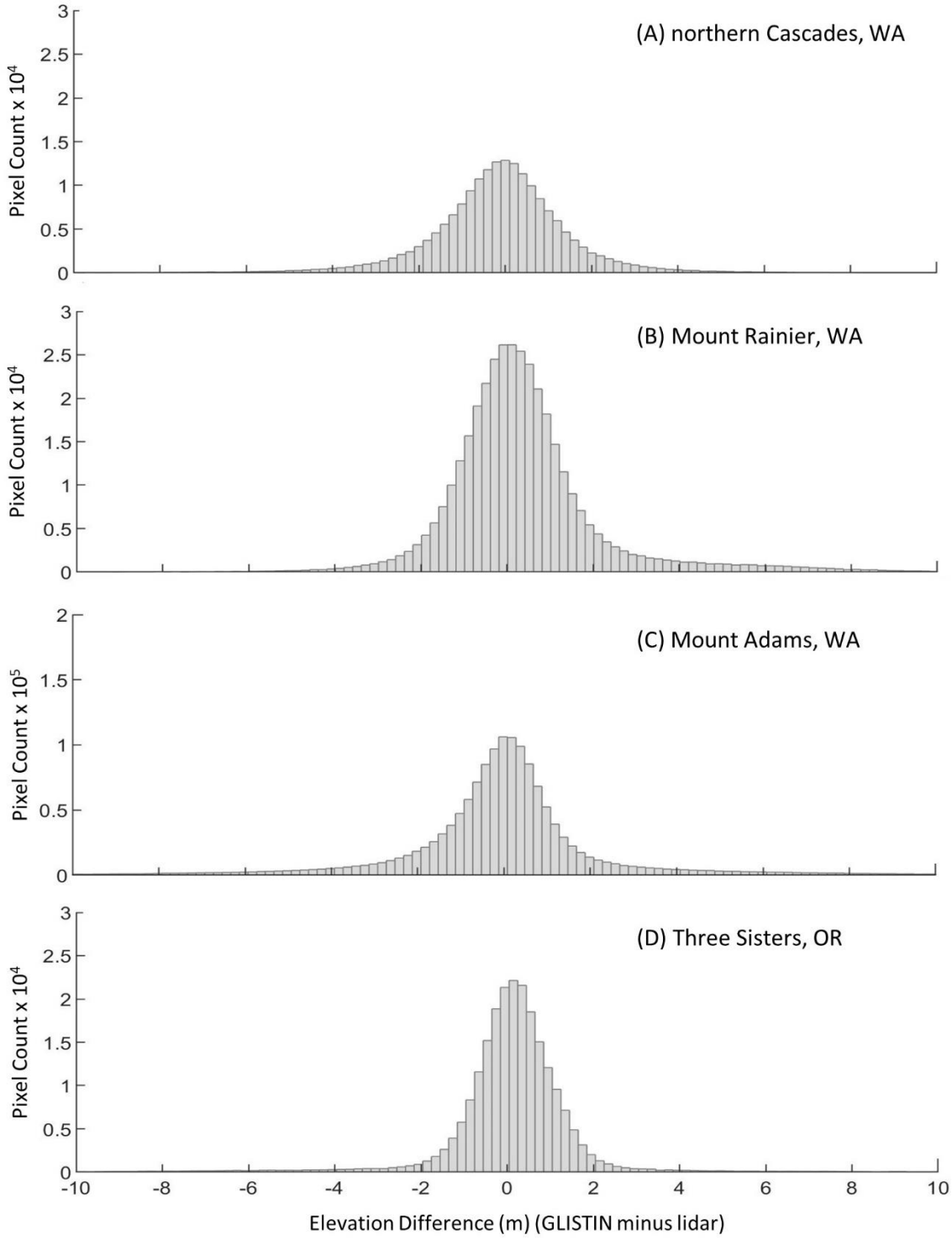

Figure 12. Histograms of elevation differences between GLISTIN and lidar for control zones in the northern Cascade Range (A), Mount Rainier, WA (B), Mount Adams, WA (C), and the Three Sisters, OR. Note the different scale on the y-axis in panel C. See Figures 1 and A1 for the location of the regions.

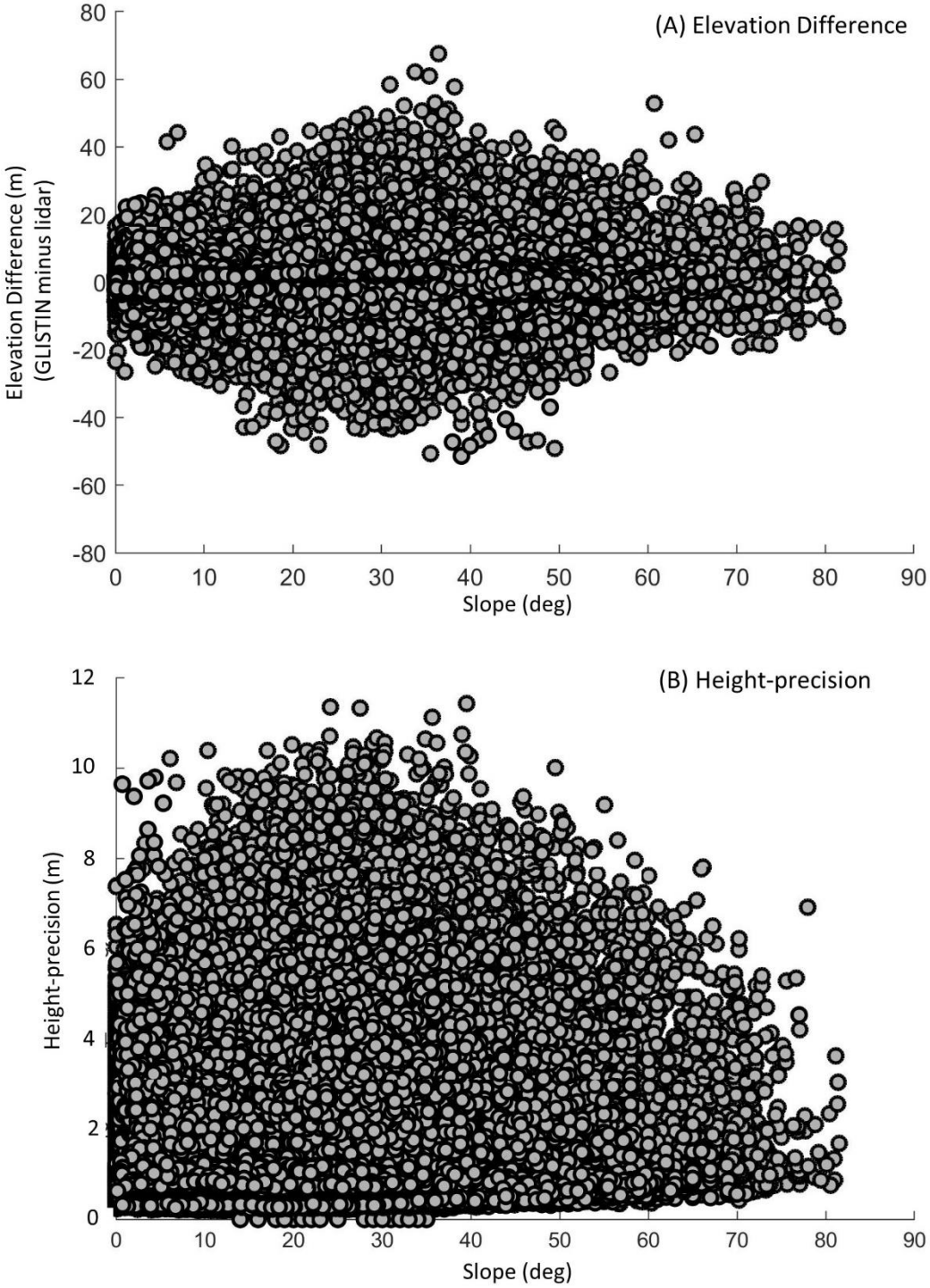

Figure 13. Elevation differences (GLISTIN minus lidar) (A) and Height-precision (B) versus slope for all four lidar datasets.

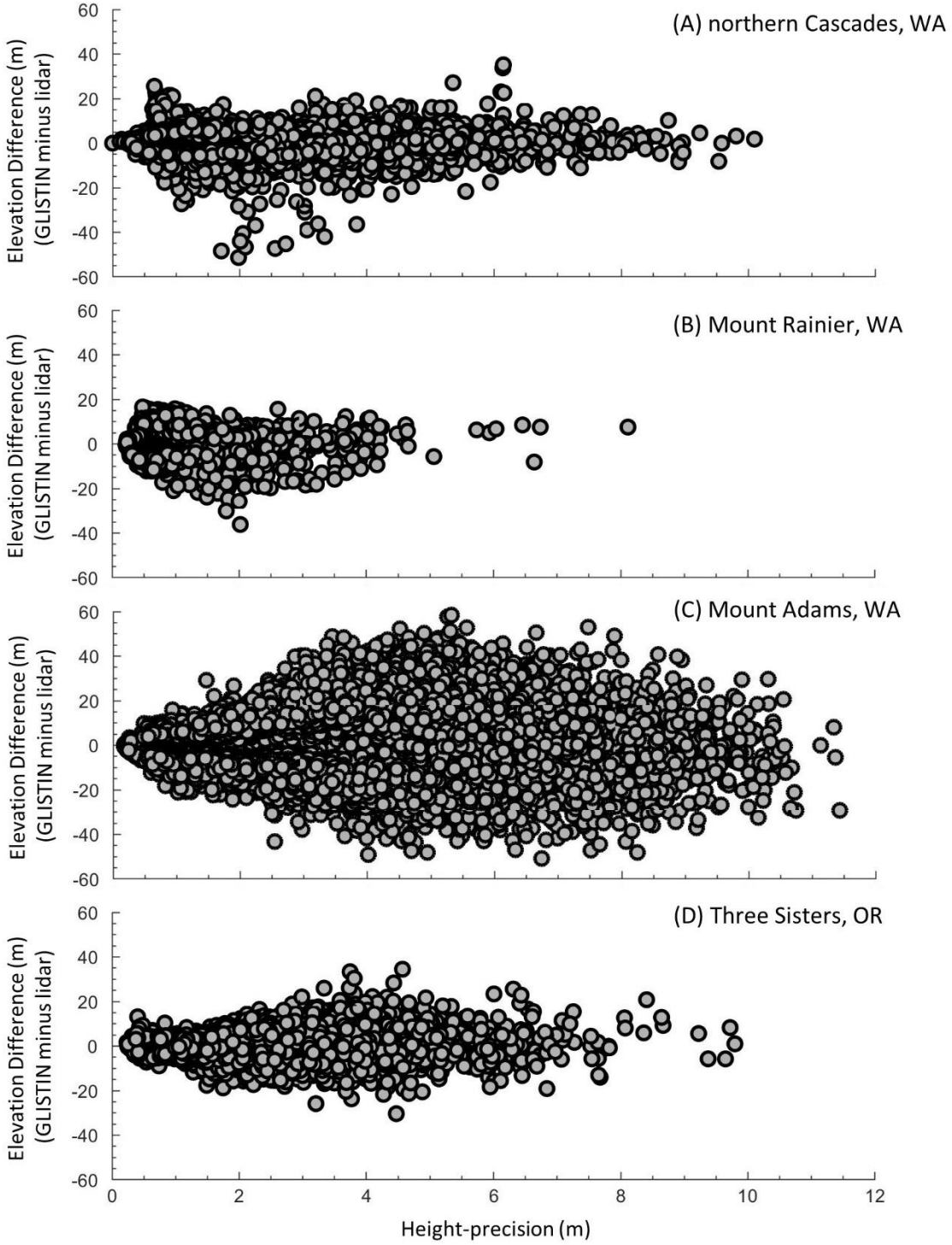

Figure 14. Elevation differences (GLISTIN minus lidar) versus height-precision for the northern Cascades in Washington(A), Mount Rainier, WA (B), Mount Adams, WA (C) and the Three Sisters, OR (D). See Figures 1 and A1 for the location of the regions.

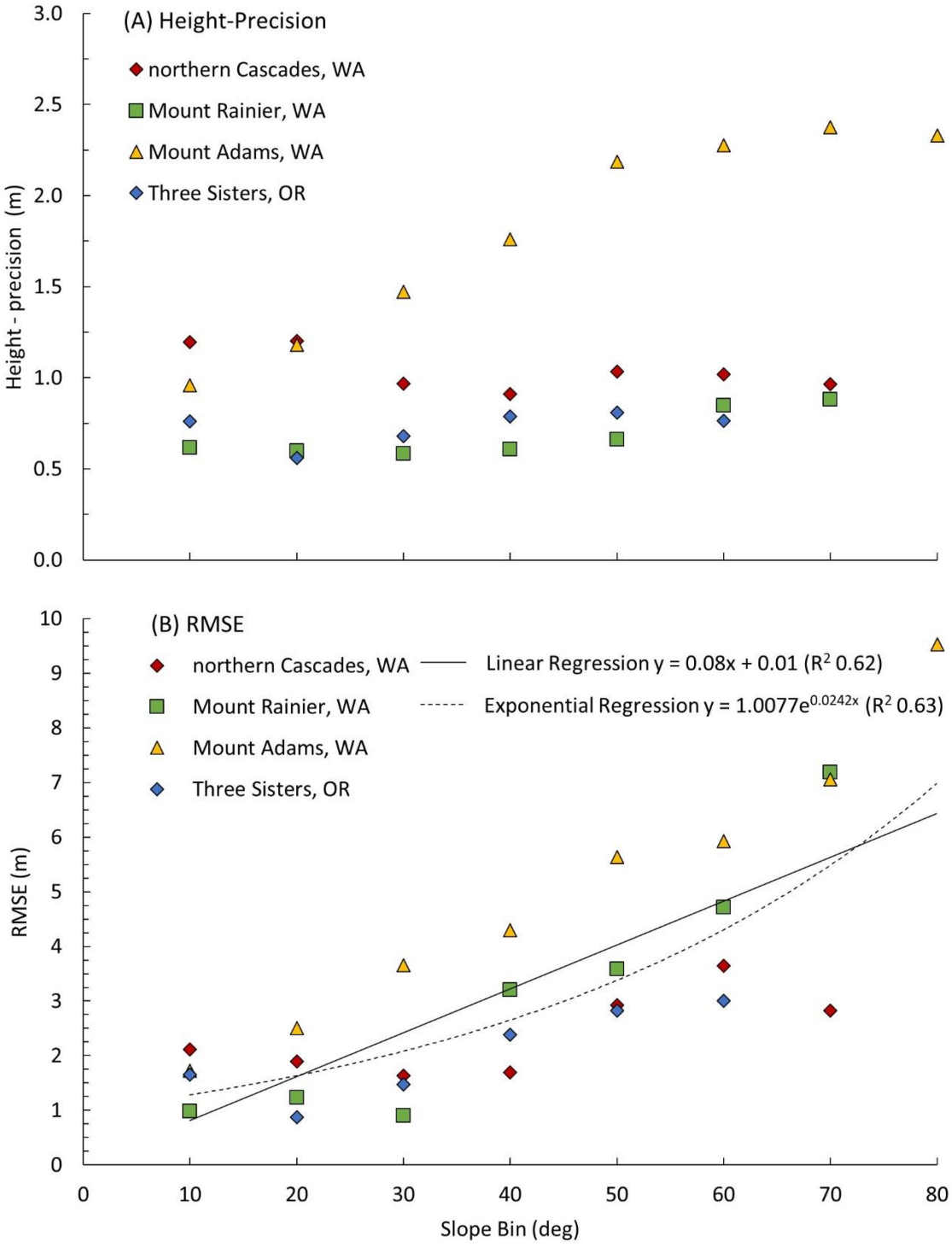

Figure 15. Mean height-precision (A) and root mean square error (RMSE, B) for control zones binned by 10° slopes. The slope label represents the maximum of that bin. The 10° slope bin includes slopes of 0°.

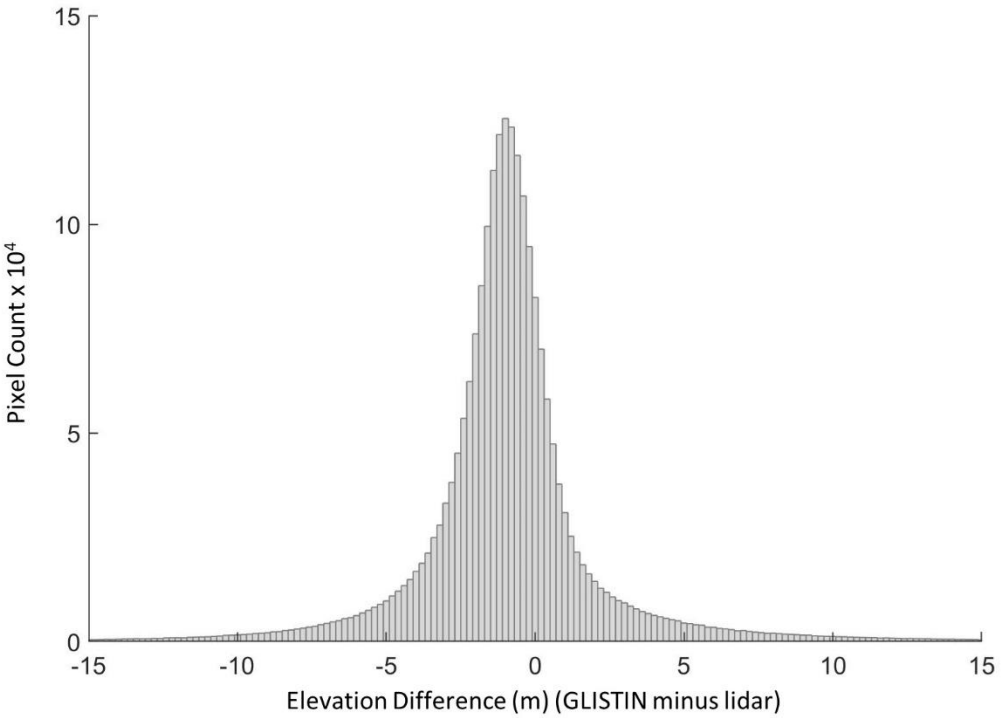

Figure 16. Histograms of elevation differences between GLISTIN and lidar for glaciers on Mount Adam, WA. See Figure A1 for the location.

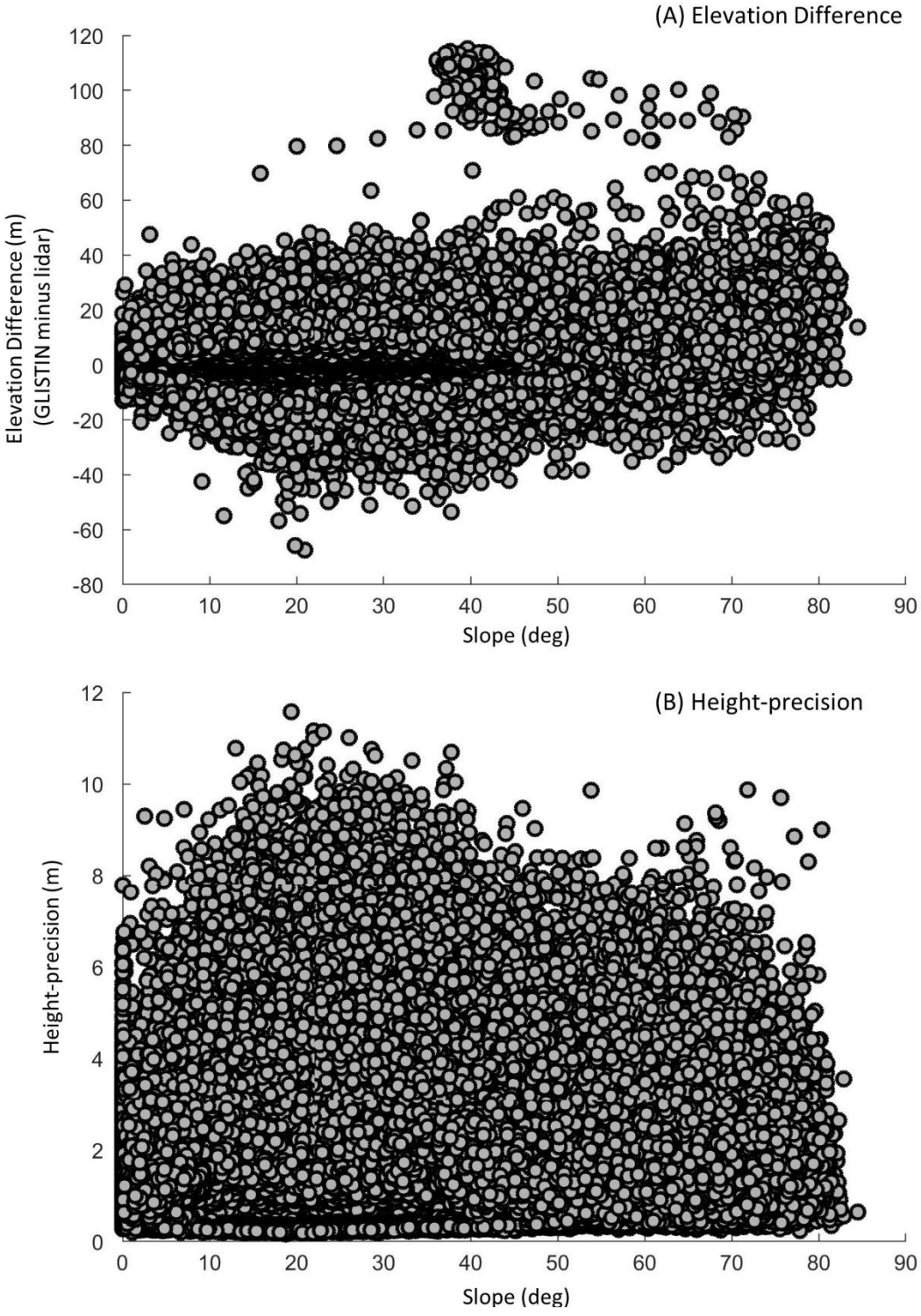

Figure 17. Elevation differences (GLISTIN minus lidar) (A) and Height-precision (B) versus slope for glaciers on Mount Adams, WA. See Figure A1 for the location.

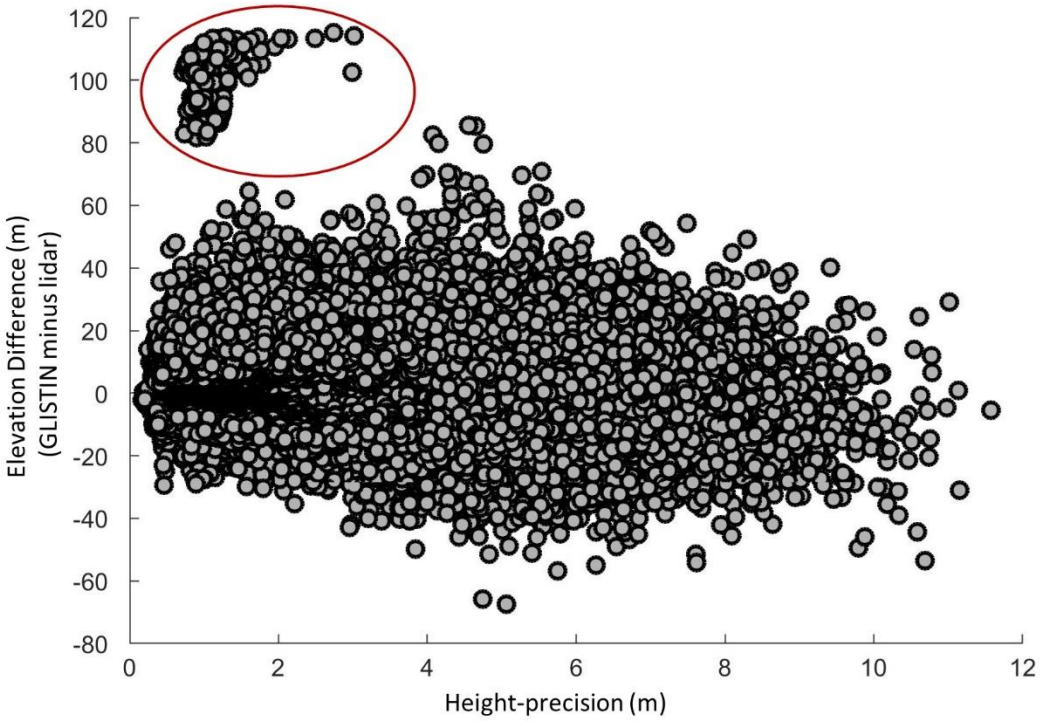

Figure 18. Elevation differences (GLISTIN minus lidar) versus height-precision for glacier surfaces on Mount Adams, WA. The red circle indicates a cluster of larger elevation differences. See A1 for the location of the regions.

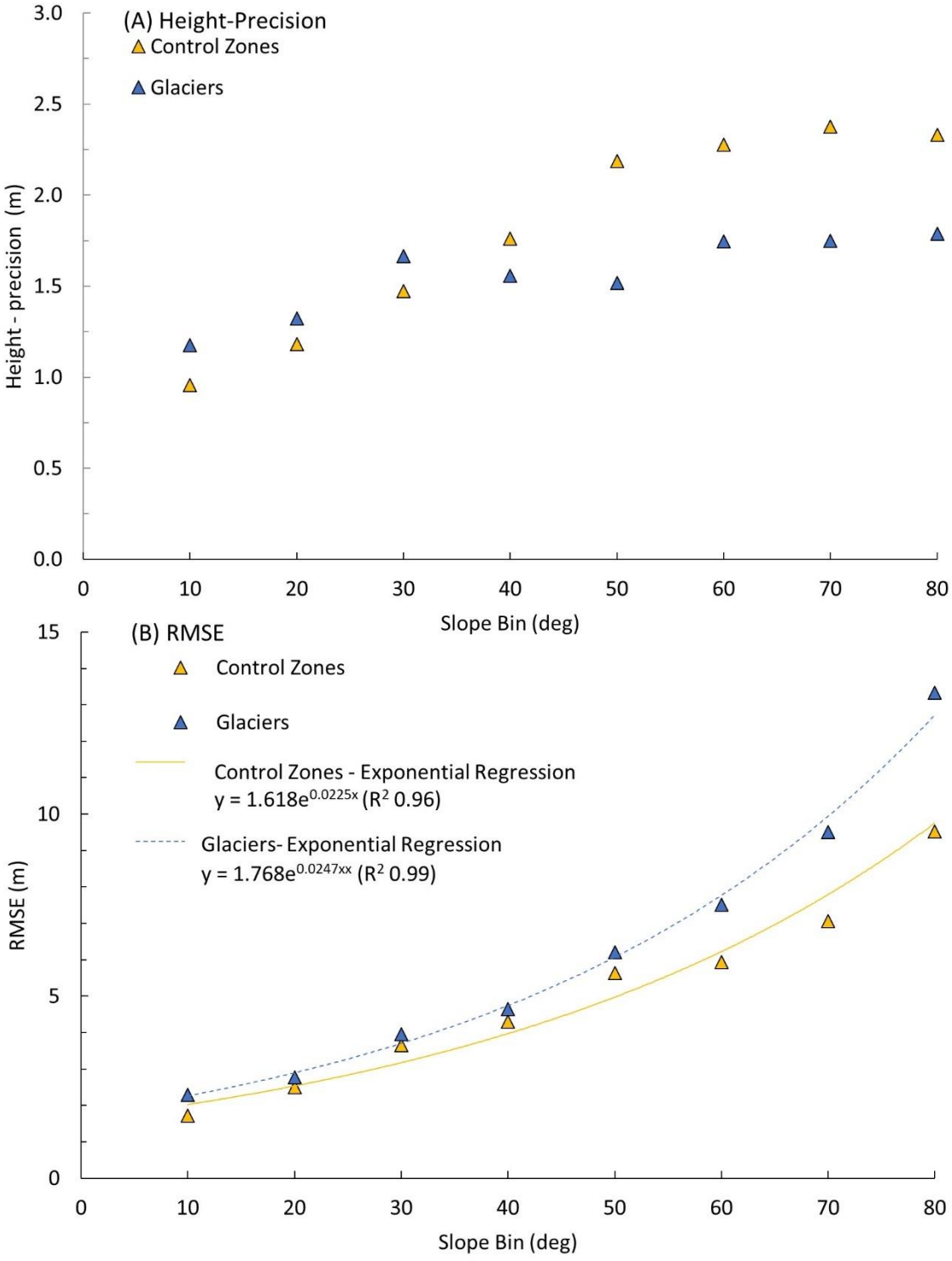

Figure 19. Mean height-precision (A) and root mean square error (RMSE, B) for glaciers and control zones binned by 10° slopes for Mount Adams, WA. The slope label represents the maximum of that bin. The 10° slope bin includes slopes of 0°.

To define the vertical uncertainty for elevations relative to the NED, control zones of barren earth were compared to GLISTIN-derived elevations. Knowing this uncertainty is important for assessing G&PS volume change. The RMSE of the NED itself is 3.74 m (Gesch, 2007). The RMSE for control zones in different regions ranged from 3.53 m (Teton Range, WY, 0.93 km^2, n=9301) to 10.57 m (Beartooth-Absaroka, MT, 7.83 km^2, n=78304; Table 7) with associated mean height-precision of 0.66 ± 0.51 m (standard deviation), 1.03 ± 0.87 m, respectively. For all regions, the mean height-precision was lower than the RMSE of control zones.

Table 7. Elevation uncertainty for control zones expressed as the root mean square error (RMSE) and mean height-precision (prc). 'std' refers to standard deviation. 'Region' refers to the region of the mosaicked GLISTIN DEMs. Area is the total area of the control zones.

Region	RMSE (m)	Mean prc ± std	Area (km^2)
northern Cascades, WA	7.97	1.21 ± 1.07	109.65
southern Cascades, WA	5.81	1.23 ± 1.08	27.06
Mount Hood, OR	8.26	1.11 ± 1.10	10.21
Three Sisters, OR	6.07	1.07 ± 1.17	23.19
Sierra Nevada, CA	6.48	0.63 ± 0.45	194.74
Lewis, MT	8.89	0.65 ± 0.25	22.16
Beartooth-Absaroka, MT	10.57	1.03 ± 0.87	7.83
Teton, WY	3.53	0.66 ± 0.51	0.93
Wind River, WY	6.55	0.90 ± 0.65	7.81
Front, CO	8.31	0.81 ± 0.72	36.54
Gore, CO	8.15	0.89 ± 0.78	27.43

The effects of slope on the uncertainty between the NED and GLISTIN was also examined at the control zones. The mean height-precision was calculated for 10º slope bins. There is a weak non-linear trend (Figure 20; $y = 3.11e^{0.02x}$, $R^2 = 0.76$). For the 10º bin, the mean height-precision was 0.73 ± 0.15 m (standard deviation) and 1.51 ± 0.46 m for the 80° bin. The RMSE was also calculated for 10º slope bins, RMSE and its standard deviation increased non-linearly with the slope (Figure 20). For the 10º bin, the mean

RMSE was 4.94 ± 1.86 m and 28.19 ± 6.83 m for the 80° bin. Similar relationships between slope and elevation RSME were identified in previous studies of the Three Sisters, OR (Ohlschlager, 2015), the Lewis Range, MT (Brett, 2017), and the Swiss Alps (Fischer et al., 2015). Both height precision and RMSE increase non-linearly with slope, suggesting a correlation between height-precision and RMSE. However, the difference in the strength of the trends suggests the relationship may be weak, and that other factors may influence the RMSE.

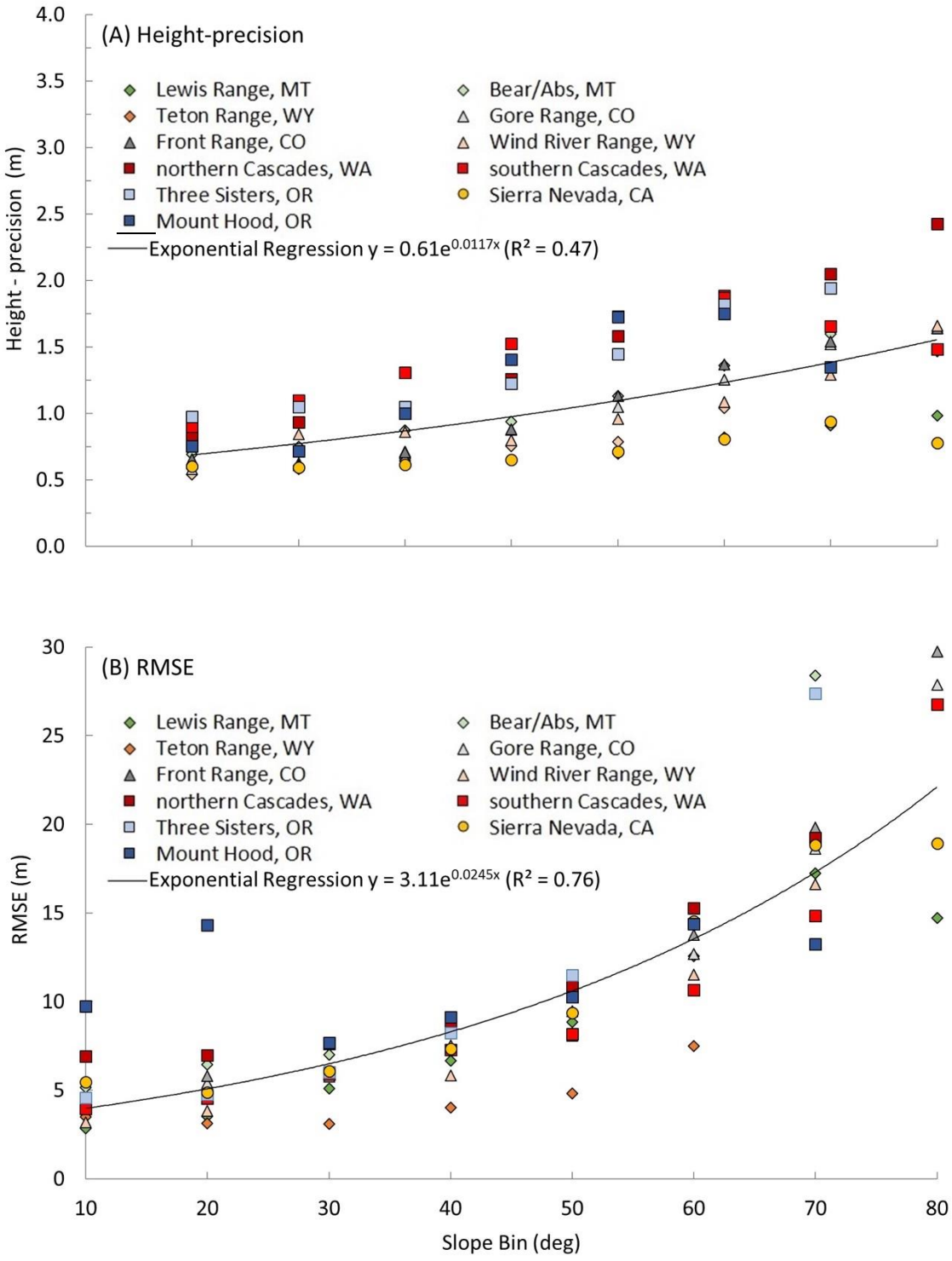

Figure 20. Height-precision (A) and root mean square error (RMSE; B) for control zones binned by 10° slopes. The slope label represents the maximum of that bin. The 10° slope bin includes slopes of 0°.

V Volume Change Results and Analysis

To quantify G&PS change over the last ~50 years volume change was estimated by differencing the GLISTIN-derived topography from the NED. However, only 19% (619) of the 3289 imaged G&PS were completely mapped by GLISTIN. To increase the number of available G&PS for analysis, with minimal reduction in accuracy, only G&PS with ≥ 80% GLISTIN coverage were examined. McNabb et al. (2018) showed that volume change estimates were still accurate when data covered only 40% of a glacier. The standard deviation between interpolated and actual glacier volume change drastically increases when less than 40% of the glacier is covered (McNabb et al., 2018). To err on the side of caution, a threshold of ≥ 80% coverage was adopted. The same threshold was used by Le Bris and Paul (2011). Methods of interpolating missing elevations were considered but each method affects the final estimate differently (McNabb et al., 2019), and a threshold value provided a more consistent approach. Using the ≥ 80% coverage threshold resulted in a sample of 1770 G&PS (54%) consisting of 351 glaciers and 1419 perennial snowfields. This sample reduced by 988 G&PS because the uncertainty was larger than the change, yielding 782 G&PS (231 glaciers and 551 perennial snowfields). The remaining G&PS showed a total volume change of -3.22 ± 1.41 km^3. The specific volume change, volume change divided by area, is -14.6 ± 6.4 m and its rate of change for individual G&PS ranged from -1.3 ± 0.2 m yr^{-1} to +0.8 ± 0.3 m yr^{-1} with a median of -0.2 ± 0.2 m yr^{-1}. Glaciers account for most of the total volume loss, 93% (-3.00 ± 1.28 km^3). The specific volume change for the glaciers was 15.1 ± 6.4 m with rates from -1.3 ± 0.3 m yr^{-1} to +0.3 ± 0.2 m yr^{-1} with a median of -0.3 m yr^{-1}. For perennial snowfields,

the total specific volume change was -10.4 ± 6.1 m with rates between -1.1 ± 0.2 m yr^{-1} and +0.8 ± 0.3 m yr^{-1}, and a median of -0.2 m yr^{-1}.

Although the average change of G&PS was negative, 60 G&PS increased in volume (4 glaciers and 56 perennial snowfields; Table A4). These G&PS were typically small (median area = 0.02 km^2; Figure 21) with a significantly steeper median slope (28°, $p < 0.05$, Mann-Whitney U) than the median slope of G&PS with volume loss (25°) and significantly higher median elevation, 3100 m ($p < 0.05$, Mann-Whitney U) than the median elevation (2335 m) of G&PS with volume loss. For aspect, eastness was not significantly different ($p < 0.05$, Mann-Whitney U) between G&PS with volume increase and those with volume loss. However, northness was significant. G&PS with volume loss had more northly aspects (0.81) than G&PS with volume increases (0.47). These enlarging G&PS were not associated with any particular geographic location. The Cascade Range in Washington had the most glaciers (2) and the regions with the greatest number of increasing perennial snowfields were the Sierra Nevada, CA, the Teton Range, WY, and the Wind River Range, WY, each region containing 11. The Lewis Range, MT (1 glacier and 7 perennial snowfields), had the greatest total volume increase, a total specific volume change of +12.7 ± 8.3 m, and the largest change of an individual glacier (Ahern Glacier) +12.9 ± 8.3 m.

Evaluating volume change over time is not straightforward because the start date, defined by the NED, are spread over five decades (Figure 22). Volume changes were grouped into five-year intervals based on the NED starting date (Table 8; Figure 23). When referring to the five-year group, the last year in the group is used as the identifier

(e.g., 1955 is 1951 to 1955). Four of the periods (1955, 1965, 1990, and 1995) had 10 or fewer G&PS and are excluded from further analysis. The total rate of specific volume change of G&PS for each period ranged from -0.25 ± 0.11 m yr^{-1} (1970 to 2016) to -0.61 ± 0.25 m yr^{-1} (1985 to 2016). Glaciers lost more specific volume (ranging from-0.65 ± 0.26 m yr^{-1}, 1985 to 2016 to -0.25 ± 0.11 m yr^{-1}, 1970 to 2016) than perennial snowfields (-0.41 ± 0.21 m yr^{-1} ,1980 to 2016 to -0.14 ± 0.10 m yr^{-1}, 1970 to 2016).

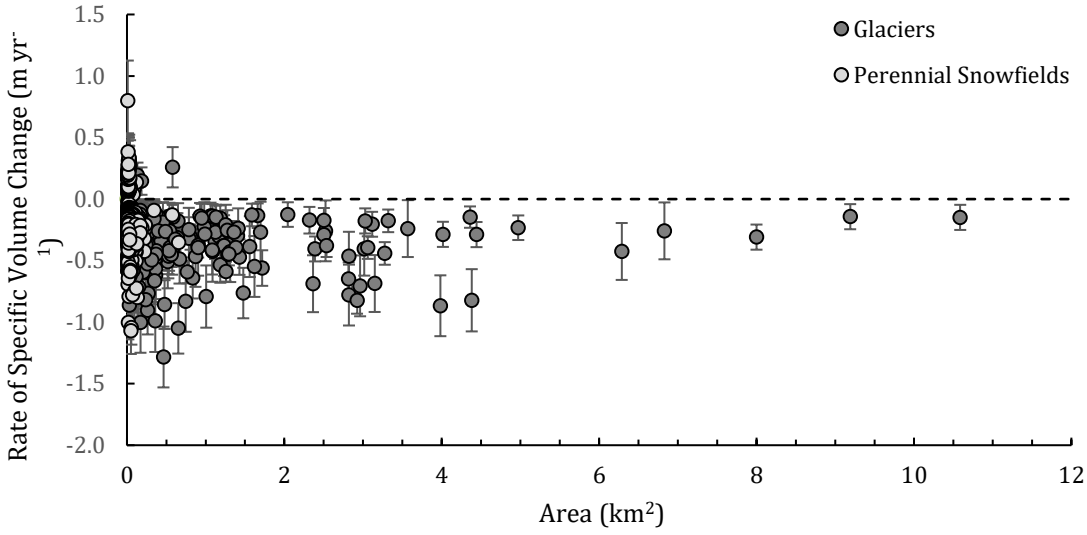

Figure 21. Specific volume change of glaciers and perennial snowfields (G&PS). Light grey circles represent perennial snowfields, and dark grey circles represent glaciers. The 'whiskers' represent uncertainty. Initial area refers to the area from the U.S. Geological Survey's 1:24000 map series.

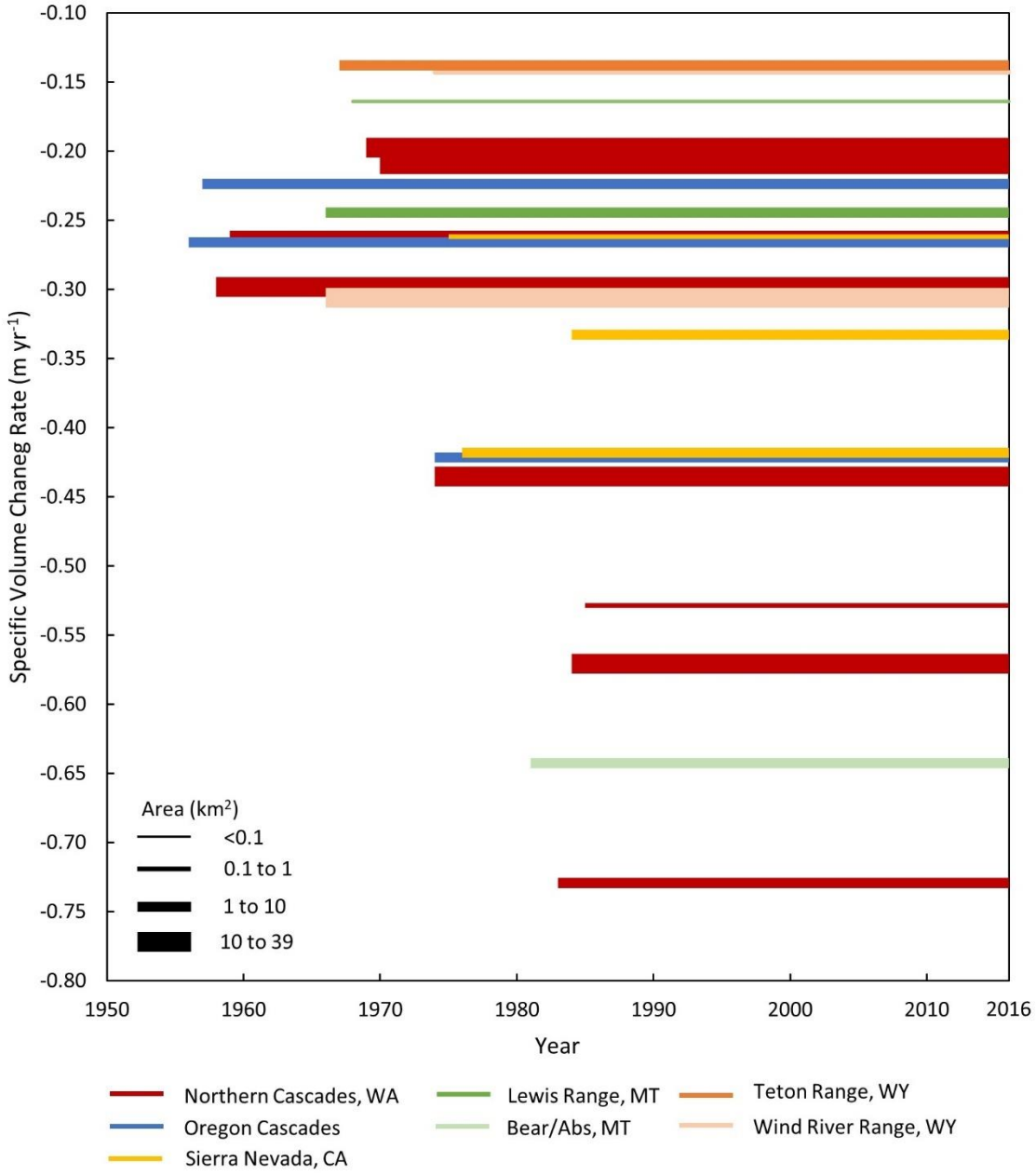

Figure 22. Specific volume change rate for glaciers and perennial snowfields grouped by start year. The width of each bar is scaled to the area of glaciers and perennial snowfields in the year group. 'Bear/Abs' refers to Beartooth-Absaroka, MT. See Figure 1 for mountain range locations. The figure only includes groups with more than 10 G&PS.

Table 8. Volume change estimates between the initial NED year and the GLISTIN year of 2016 for glaciers and perennial snowfields with ≥ 80% GLISTIN coverage grouped by 5-year intervals. The year listed is the last in the 5-year interval (e.g., 1955 = 1951 to 1955). 'Num' is the number of G&PS for that category. '---' indicates no data.

Year/ Type	Num	Volume Change (m^3 x10^6)		Specific Vol Change (m)		Rate of Specific Vol Change (m yr^{-1})	
1955	5	-0.75 ±	0.45	-6.7 ±	4.0	-0.11 ±	0.07
Glacier	0	--- ±	---	--- ±	---	---	---
Snowfield	5	-0.75 ±	0.45	-6.7 ±	4.0	-0.11 ±	0.07
1960	119	-551.88 ±	207.79	-16.1 ±	6.1	-0.29 ±	0.11
Glacier	42	-500.85 ±	182.72	-16.7 ±	6.1	-0.30 ±	0.11
Snowfield	77	-51.03 ±	25.07	-12.0 ±	5.9	-0.22 ±	0.11
1965	10	-27.38 ±	13.65	-11.0 ±	5.5	-0.22 ±	0.11
Glacier	3	-23.78 ±	11.81	-11.1 ±	5.5	-0.22 ±	0.11
Snowfield	7	-3.59 ±	1.84	-10.3 ±	5.3	-0.20 ±	0.10
1970	202	-996.71 ±	452.73	-11.3 ±	5.1	-0.25 ±	0.11
Glacier	71	-962.96 ±	428.65	-11.6 ±	5.2	-0.25 ±	0.11
Snowfield	131	-33.75 ±	24.08	-6.6 ±	4.7	-0.14 ±	0.10
1975	147	-441.47 ±	180.72	-17.7 ±	7.2	-0.43 ±	0.18
Glacier	36	-389.65 ±	150.28	-18.8 ±	7.2	-0.46 ±	0.18
Snowfield	111	-51.82 ±	30.45	-12.4 ±	7.3	-0.30 ±	0.18
1980	55	-363.07 ±	199.19	-15.1 ±	8.3	-0.42 ±	0.23
Glacier	20	-344.50 ±	189.56	-15.1 ±	8.3	-0.42 ±	0.23
Snowfield	35	-18.57 ±	9.63	-14.8 ±	7.7	-0.41 ±	0.21
1985	233	-786.71 ±	322.73	-18.8 ±	7.7	-0.61 ±	0.25
Glacier	55	-726.64 ±	289.03	-20.2 ±	8.0	-0.65 ±	0.26
Snowfield	178	-60.07 ±	33.70	-10.5 ±	5.9	-0.34 ±	0.19
1990	10	-53.32 ±	28.52	-11.5 ±	6.2	-0.44 ±	0.24
Glacier	4	-51.47 ±	26.73	-11.9 ±	6.2	-0.46 ±	0.24
Snowfield	6	-1.85 ±	1.79	-6.3 ±	6.1	-0.24 ±	0.24
1995	1	0.16 ±	0.07	18.4 ±	7.7	0.88 ±	0.37
Glacier	0	---	---	---	---	---	---
Snowfield	1	0.16 ±	0.07	18.4 ±	7.7	0.88 ±	0.37
Total	782	-3221.12 ±	1405.84	-14.6 ±	6.4	---	---
Glacier	231	-2999.86 ±	1278.77	-15.1 ±	6.4	---	---
Snowfield	551	-221.26 ±	127.08	-10.4 ±	6.0	---	---

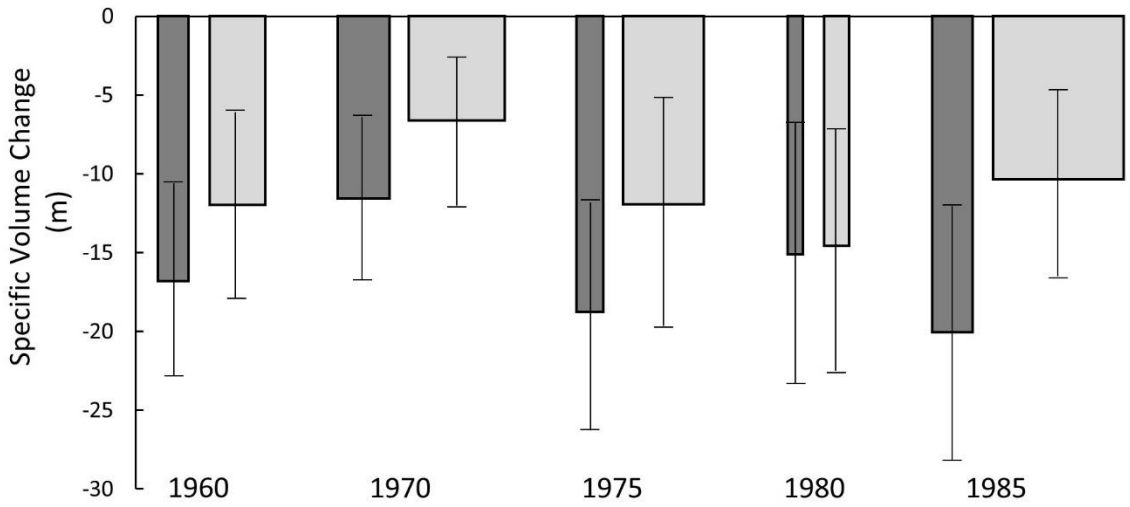

Figure 23. Specific volume change for all glaciers (dark grey boxes) and all perennial snowfields (light grey boxes) in the American West, with ≥ 80% GLISTIN coverage and with change greater than uncertainty, grouped by 5-year intervals. The width of the bar is scaled to represent the number of G&PS for that group. The year listed is the last in the 5-year interval (e.g., 1960 = 1956 to 1960). The 'whiskers' represent uncertainty. The figure only includes groups with more than ten glaciers or perennial snowfields.

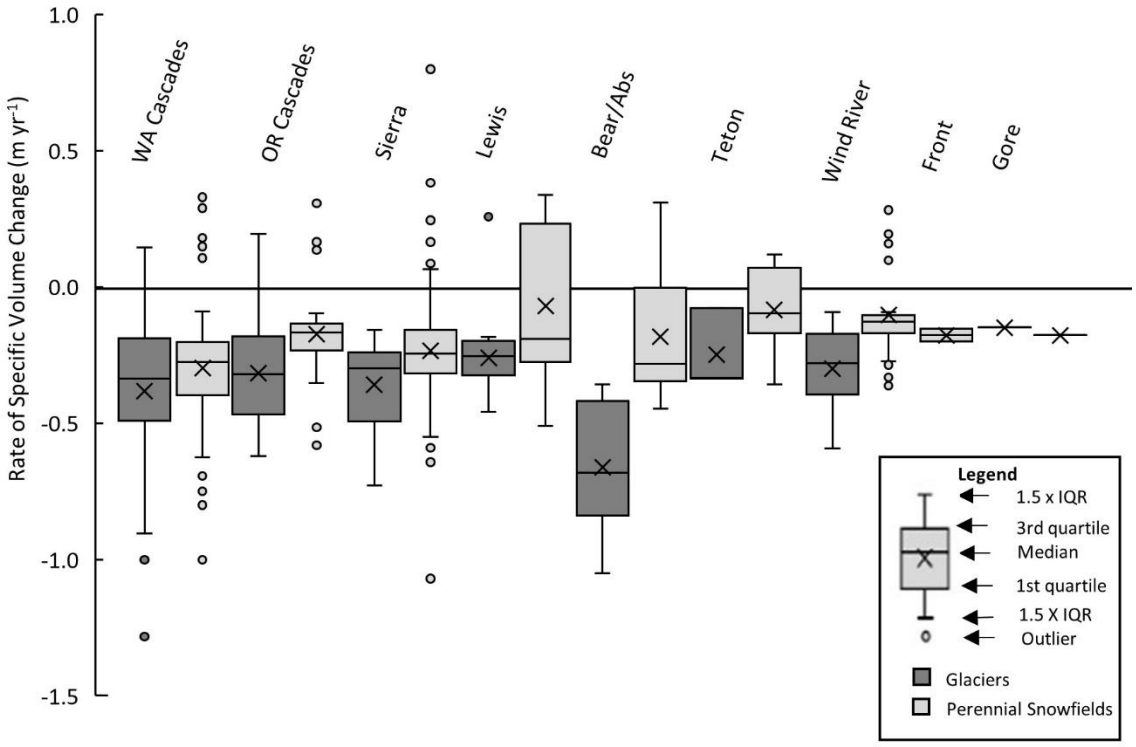

Figure 24. Volume change rates for glaciers and perennial snowfields for each region for all periods. The line within the boxes indicates the median, and the 'x' indicates the mean. The bottom and top of the boxes represent the 1st and 3rd quartile, respectively. Values that exceed 1.5 times the interquartile (IQR) below the first quartile or above the third quartile are considered outliers and are displayed as points. The 'whiskers' represent the smallest and largest values not considered outliers. 'Bear/Abs' refers to Beartooth-Absaroka, MT. See Table 2 for the location of mountain ranges.

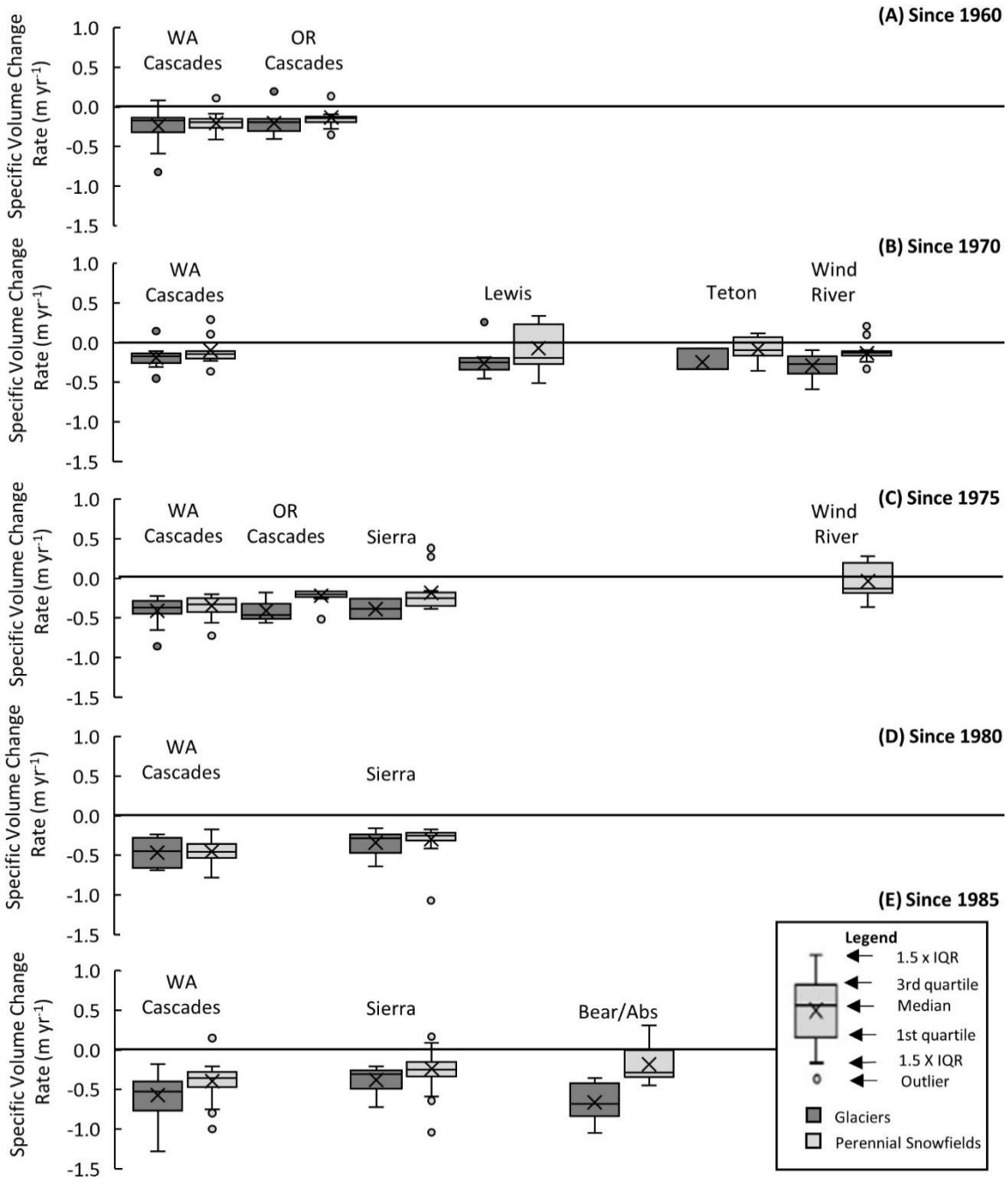

Figure 25. Volume change rates for all glaciers (dark grey boxes) and all perennial snowfields (light grey boxes), with ≥ 80% GLISTIN coverage and with change greater than uncertainty for each region for the periods of 1960 (1956 to 1960) to 2016 (A), 1970 (1966 to 1970) to 2016 (B), 1975 (1971 to 1975) to 2016 (C), 1980 (1976 to 1980) to 2016 (D), and 1985 (1981 to 1985) to 2016 (E). The line in the boxes indicates the median, and the 'x' indicates the mean. The values that exceed 1.5 times the interquartile range (IQR) below the first quartile or above the third quartile are considered outliers. The 'whiskers' represent the smallest and largest values not considered outliers. Points indicate outliers. This figure only includes regions with more than ten glaciers or perennial snowfields 'Bear/Abs' refers to Beartooth-Absaroka, MT. See table 2 for mountain range locations.

The imagery used to create the NED was flown on multiple years for different areas of the same mountain range. If we can assume that glacier change is more or less the same within a mountain range, then we can infer how volume change varies over time. These regions included, the Cascade Range in Washington, the Sierra Nevada, CA, and to a lesser degree, the Cascade Range, OR, and the Wind River Range, WY (Table 9, Figure 26). As shown previously, glaciers had a greater loss rate than perennial snowfields for every region and time period. For the Cascade Range in Washington volume change loss is greater over time. There appear to be no strong trends for the other regions.

Table 9. Volume change estimates for glaciers and perennial snowfields in select regions and periods. Volume change was estimated between the initial NED year and the GLISTIN year of 2016 for glaciers and perennial snowfields with ≥ 80% GLISTIN. The change was grouped by region and year. The year listed is the last in the 5-year interval (e.g., 1955 = 1951 to 1955). 'Num' is the number of G&PS for that category.

Region/Year/Type	Num	Area (km^2)	Volume Change (m^3 x 10^6)	Specific Vol Change (m)	Specific Vol Change Rate (m yr^{-1})
WA Cascades					
1960	75	19.70	-336.81 ± 117.49	-17.10 ± 5.96	-0.31 ± 0.11
Glacier	29	17.75	-312.42 ± 106.56	-17.60 ± 6.00	-0.31 ± 0.11
Snowfield	46	1.95	-24.40 ± 10.93	-12.48 ± 5.59	-0.22 ± 0.10
1970	53	53.36	-507.94 ± 255.44	-9.52 ± 4.79	-0.21 ± 0.10
Glacier	23	52.40	-501.59 ± 250.65	-9.57 ± 4.78	-0.21 ± 0.10
Snowfield	30	0.96	-6.35 ± 4.79	-6.62 ± 5.00	-0.14 ± 0.11
1975	82	15.88	-290.34 ± 124.61	-18.29 ± 7.85	-0.45 ± 0.19
Glacier	24	13.14	-249.19 ± 102.35	-18.96 ± 7.79	-0.46 ± 0.19
Snowfield	58	2.73	-41.16 ± 22.26	-15.05 ± 8.14	-0.37 ± 0.20
1980	20	21.40	-320.08 ± 180.75	-14.95 ± 8.44	-0.42 ± 0.23
Glacier	8	20.81	-309.81 ± 175.82	-14.89 ± 8.45	-0.41 ± 0.23
Snowfield	12	0.59	-10.27 ± 4.94	-17.32 ± 8.33	-0.48 ± 0.23
1985	101	34.14	-662.12 ± 275.94	-19.39 ± 8.08	-0.63 ± 0.26
Glacier	40	31.54	-628.40 ± 257.10	-19.92 ± 8.15	-0.64 ± 0.26
Snowfield	61	2.60	-33.71 ± 18.83	-12.97 ± 7.25	-0.42 ± 0.23
OR Cascades					
1960	44	14.47	-215.07 ± 90.29	-14.86 ± 6.24	-0.27 ± 0.11
Glacier	13	12.19	-188.44 ± 76.15	-15.46 ± 6.25	-0.28 ± 0.11
Snowfield	31	2.28	-26.63 ± 14.14	-11.67 ± 6.19	-0.21 ± 0.11
1975	25	8.09	-143.32 ± 50.91	-17.71 ± 6.29	-0.43 ± 0.15
Glacier	9	7.44	-137.50 ± 46.93	-18.48 ± 6.31	-0.45 ± 0.15
Snowfield	16	0.65	-5.83 ± 3.98	-8.97 ± 6.13	-0.22 ± 0.15
Sierra Nevada					
1975	16	0.39	-4.19 ± 2.38	-10.74 ± 6.09	-0.26 ± 0.15
Glacier	2	0.13	-1.85 ± 0.73	-14.57 ± 5.73	-0.36 ± 0.14
Snowfield	14	0.26	-2.35 ± 1.65	-8.90 ± 6.26	-0.22 ± 0.15
1980	35	2.61	-42.98 ± 18.44	-16.44 ± 7.05	-0.46 ± 0.20
Glacier	12	1.95	-34.69 ± 13.74	-17.76 ± 7.04	-0.49 ± 0.20
Snowfield	23	0.66	-8.30 ± 4.70	-12.55 ± 7.10	-0.35 ± 0.20
1985	109	3.87	-40.62 ± 18.78	-10.50 ± 4.86	-0.34 ± 0.16
Glacier	9	1.40	-19.27 ± 8.63	-13.79 ± 6.18	-0.44 ± 0.20
Snowfield	100	2.47	-21.35 ± 10.15	-8.64 ± 4.11	-0.28 ± 0.13
Wind River					
1970	64	23.95	-365.80 ± 115.43	-15.28 ± 4.82	-0.33 ± 0.10
Glacier	19	21.17	-345.41 ± 102.55	-16.31 ± 4.84	-0.35 ± 0.11
Snowfield	45	2.77	-20.40 ± 12.89	-7.35 ± 4.64	-0.16 ± 0.10
1975	24	0.60	-3.61 ± 2.82	-6.01 ± 4.70	-0.15 ± 0.11
Glacier	1	0.05	-1.12 ± 0.27	-20.90 ± 4.96	-0.51 ± 0.12
Snowfield	23	0.55	-2.49 ± 2.56	-4.55 ± 4.68	-0.11 ± 0.11

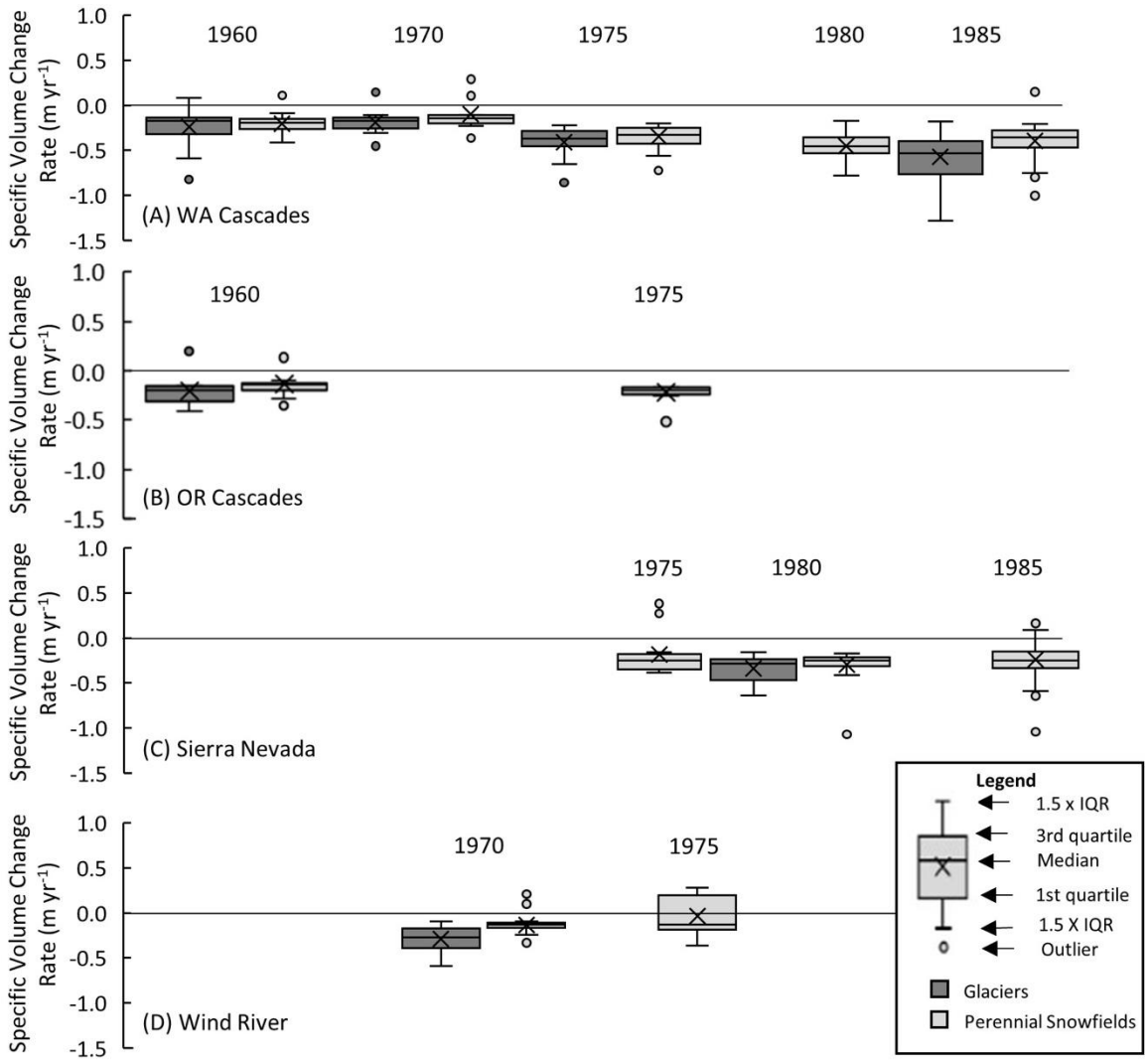

Figure 26. Volume change rates for glaciers (dark grey boxes) and perennial snowfields (light grey boxes) for the Cascade Range in Washington (A) and in Oregon (B), Sierra Nevada, CA (C) and the River Wind River Range, WY (D) by year. The line in the boxes indicates the median, and the 'x' indicates the mean. Values that exceed 1.5 times the interquartile, below the first quartile, or above the third quartile are considered outliers. The bottom and top of the boxes represent the 1st and 3rd quartile, respectively. The 'whiskers' represent the smallest and largest values not considered outliers. Points indicate outliers.

Volume change results of this study were compared to previous work on Mount Rainier, WA (Cascade Range), Three Sisters, OR (Cascade Range), and the Lewis Range (Sisson et al., 2011; Ohlschlager, 2015; and Brett, 2017). To account for the difference in length of time and differences in the number of G&PS in my study versus previous

studies, specific volume change rates were calculated for the subset of overlapping glaciers between studies (Table 10). In all cases, the rate of loss estimated in this paper was less than the previous studies.

Table 10. Specific volume change for subset of glaciers on Mount Rainier WA, Three Sisters, OR, and the Lewis Range, MT. Specific volume change was calculated by dividing the total volume change by total area. All values were calculated by me using the published data in the source. --- indicated missing data.

Region/Source	Date	Count	Specific Volume Change (m)	Specific Volume Change Rate (m yr^{-1})
Mount Rainier, WA				
This Paper	1970-2016	7	-9.7 ± 4.8	-0.21 ± 0.10
Sisson et al. (2011)	1970-2007/08	7	-8.6 ± ---	-0.23 ± ---
Three Sisters, OR				
This Paper	1957-2016	9	-15.1 ± 6.2	-0.26 ± 0.11
Ohlschlager (2015)	1957-2010	9	-10.8 ± 1.2	-0.28 ± 0.02
Lewis Range, MT				
This Paper	1966-2016	12	-12.3 ± 8.6	-0.25 ± 0.17
Brett (2017)	1966-2015	12	-16.4 ± 2.7	-0.38 ± 0.06

To compare the volume change from this study to global studies, the specific volume change rates were converted to area-averaged specific mass rates (average mass balance rate; Table A3) by multiplying the specific volume change rate by a conversion factor (unitless) of 0.850 (Fischer et al., 2015). The conversion factor represents the assumed density of ice 850 ± 60 kg m^{-3} (Sapiano et al., 1998; Huss, 2013). Huss (2013) shows that 850 kg m^{-3} is a reasonable value for density for studies longer than five years on glaciers with a stable mass balance gradient, that have a firn zone, and where volume change is not close to zero.

To evaluate the effect of topography on glacier volume change, mean elevation, mean slope, mean aspect, latitude, and longitude were compared to rates of specific volume change (Figures A5 – A9). Topographic variables were derived from the NED. For aspect, which is based on compass directions, has a discontinuity at 360°, it was transformed into northness (cosine of aspect) and eastness (sine of aspect). Longitude is in decimal degrees with increasing negative values heading west. A correlation analysis was performed to determine the relationship between topographic variables and the specific volume change rate. Before calculating correlations, the normality of each variable was calculated using the Shapiro-Wilk Test. The normality of the data determines which correlation test should be used. The Pearson correlation test is used for normally distributed data; the non-parametric Spearman test is used for non-normal data. The correlation between the rate of specific volume change for the 5-year groupings and the topographic variables was calculated using the non-parametric Spearman because the rate of specific volume change was not normally distributed (Table 11). Considering only the statistically significant ($p < 0.05$) correlations, there were no strong patterns. The correlations for slope were mostly positive, indicating G&PS with shallower slopes experience more loss than glaciers with steeper slopes. The correlations of elevation were also mostly positive, indicating G&PS at lower elevations experience a greater loss than G&PS at higher elevations. Northness and eastness were equivocal, latitude was always negative, indicating a greater loss for G&PS to the south than glaciers to the north. Longitude was always positively correlated. Because longitude becomes more negative to

the west, a positive correlation indicates G&PS to the west have greater loss than G&PS in the east.

To assess whether the use of the whole data set may include spurious results leading to poor correlations the correlations were reexamined for three specific regions where the sample sizes were relatively large (G&PS count >50), Cascade Range in Washington, the Cascade Range in Oregon, and the Sierra Nevada, CA (Table 12). Summarizing only the significant ($p < 0.05$) correlations no strong patterns were evident except for latitude, which was negative for the Cascade Range (both Washington and Oregon) and equivocal for the Sierra Nevada. The negative correlation for the Cascade Range indicate a greater loss for G&PS in the south than G&PS to the north. Slope and eastness had no significant correlations, and elevation and longitude correlations were equivocal.

Table 11. Spearman correlation between the rate of specific volume change of glaciers and perennial snowfield (G&PS) and topographic variables, grouped by 5-year intervals for periods-with 30 or more features. The year refers to the last year in the 5-year interval (e.g., 1960 = 1956 to 1960). 'All' under type includes all G&PS for that year. 'G' refers to glaciers, and 'PS' is perennial snowfield. 'Num' is the number of G&PS for that category. 'Lat' is the latitude, and 'Long' is longitude. Bold numbers indicated significant correlations (95% confidence).

Year	Type	Num	Slope	Elevation	Northness	Eastness	Lat	Long
1960	All	119	0.023	0.95	**-0.329**	-0.027	-0.115	-0.023
	G	42	**0.527**	0.067	-0.203	-0.062	0.199	0.240
	PS	77	-0.207	0.121	**-0.382**	-0.016	**-0.248**	-0.139
1970	All	202	-0.061	0.083	-0.090	0.058	**-0.155**	0.027
	G	71	0.123	-0.059	-0.144	0.060	0.076	**-0.257**
	PS	131	-0.064	0.031	-0.121	0.059	-0.057	-0.034
1975	All	147	-0.032	**0.405**	-0.133	0.109	**-0.482**	**0.277**
	G	36	0.138	-0.072	-0.252	**0.500**	0.006	0.133
	PS	111	0.010	**0.482**	-0.038	0.022	**-0.575**	**0.325**
1980	All	55	**0.366**	0.215	**0.312**	0.084	-0.457	0.436
	G	20	0.211	0.189	**0.235**	**-0.454**	-0.214	0.083
	PS	35	**0.400**	0.259	0.333	**0.464**	**-0.578**	**0.568**
1985	All	233	-0.074	**0.301**	0.003	0.024	**-0.345**	**0.276**
	G	55	**0.294**	**0.345**	-0.167	0.120	-0.245	0.063
	PS	178	**-0.171**	**0.212**	0.092	-0.009	**-0.221**	**0.208**

Table 12. Correlation statistics for specific volume change rate for glaciers and perennial snowfield (G&PS) grouped by region. 'All' under type includes all G&PS for that year. 'G' refers to glaciers, and 'PS' is perennial snowfield. 'Num' is the number of G&PS for that category. 'Lat.' is the latitude, and 'Long.' is the longitude. Bold numbers indicated significant correlations (95% confidence). In most cases the Spearman correlation is reported, Pearson coefficients are denoted by '*'. See Table 2 for region location.

Region	Type	Num	Slope	Elevation	Northness	Eastness	Lat	Long
WA Cascades	All	338	-0.033	**0.246**	**-0.175**	-0.035	**-0.350**	0.022
	G	126	0.147	**0.325**	**-0.269**	-0.001	-0.149	-0.018
	PS	212	-0.131	**0.275**	-0.098	-0.049	-0.**513**	0.071
OR Cascades	All	80	-0.176	-0.130	**-0.226**	0.108	-0.**417**	0.140
	G	26	-0.131 *	-0.152 *	-0.147	-0.002	**-0.424**	0.149
	PS	54	-0.097	0.059	-0.178	0.119	**-0.389**	0.171
Sierra Nevada	All	164	-0.122	**-0.455**	-0.073	0.015	0.**347**	**-0.328**
	G	23	0.137	-0.213	0.131	-0.098	-0.202	0.054
	PS	141	-0.124	**-0.446**	-0.001	-0.005	**0.373**	**-0.342**

To examine the pattern of specific volume change at all ice-covered elevations within the Sierra Nevada and the Cascade Range in Washington, the specific volume change for 50 m elevation bins was calculated for the periods 1960-2016, 1970-2016, 1975-2016, 1980-2016, and 1985-2016 with initial glacier area at each elevation bin. For the Sierra Nevada (Figure 27), volume loss was greatest at higher elevations for all periods. For 1975-2016 and 1980 to 2016, there were several elevation bins with volume increases. In all cases, these volume increases were found in perennial snowfields and not glaciers. Examining G&PS together for the Cascade Range in Washington shows volume loss at most elevations (Figure 28-30). Generally, the greatest loss for G&PS was at lower elevations. Appendix D shows a similar analysis, except volume change for all regions were grouped for each 5-year group.

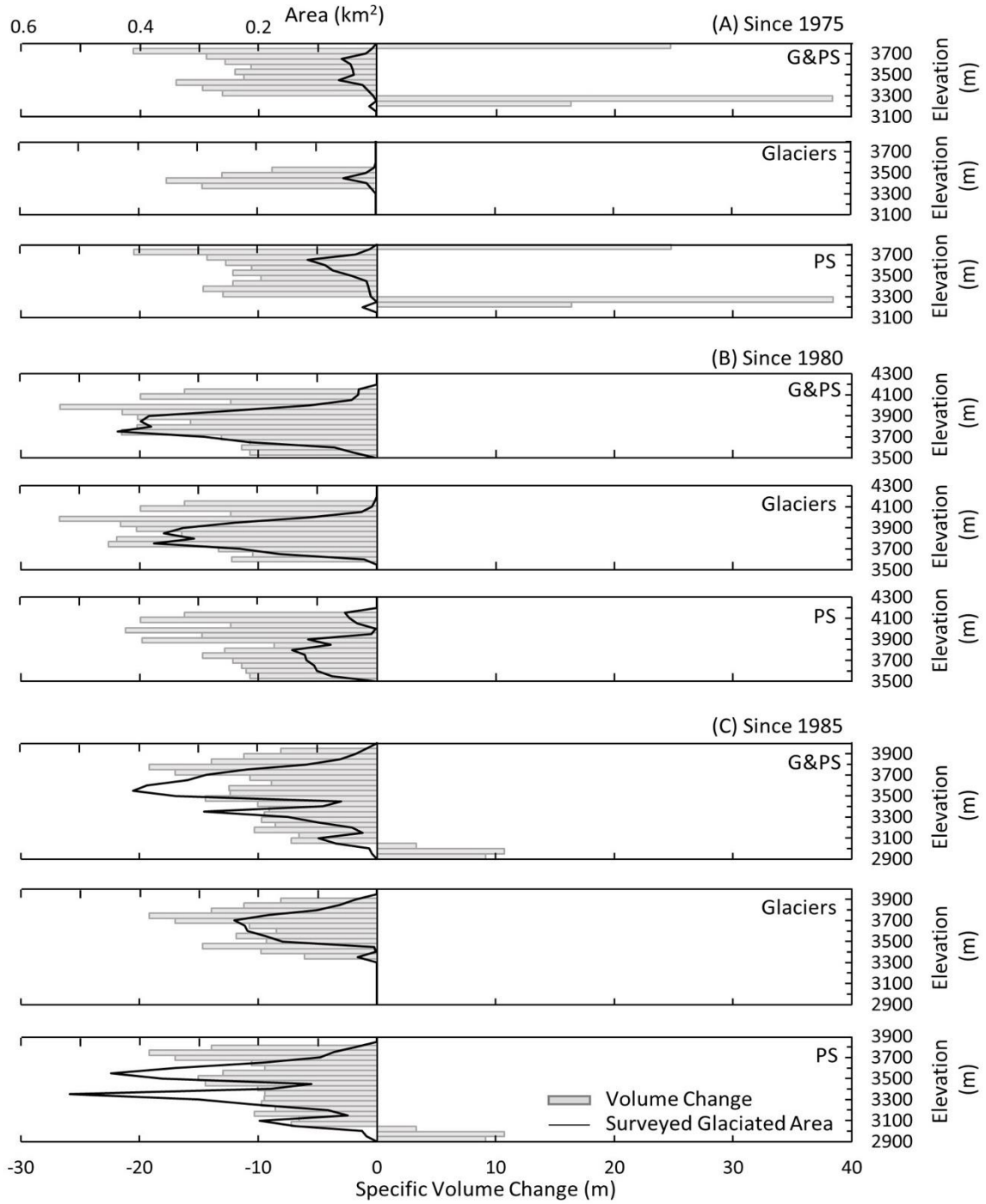

Figure 27. Specific volume change for glaciers and perennial snowfields (G&PS) as a function of elevation for the Sierra Nevada for the periods of 1975 (A), 1980 (B), and 1985 (C) to 2016. The initial year refers to the 5-year interval (e.g., 1975 = 1971 to 1975). The specific volume change was calculated for each 50 m elevation bin. The value on the y-axis is the maximum elevation of that bin. The grey bars represent average specific volume change for each 50 m bin, and the black lines represent the glaciated area for each bin. Numbers indicate the region where the positive change is located. Specific volume change is the total volume change divided by total area for each elevation bin.

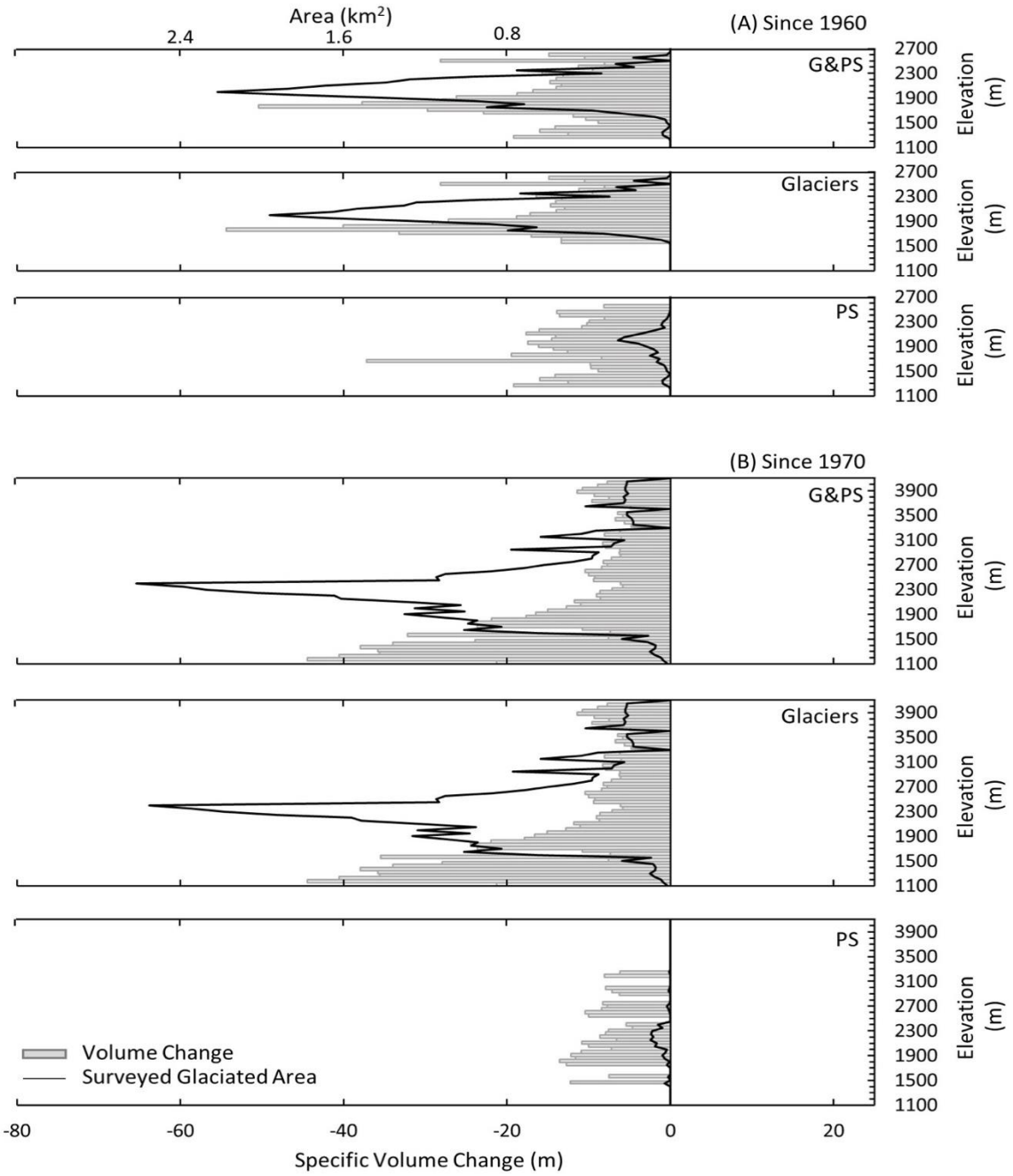

Figure 28 Specific volume change for glaciers and perennial snowfields (G&PS) as a function of elevation for the Cascade Range in Washington for the periods of 1960 (A), and 1970 (B) to 2016. The initial year refers to the 5-year interval (e.g., 1960 = 1956 to 1960). The specific volume change was calculated for each 50 m elevation bin. The value on the y-axis is the maximum elevation of that bin. The grey bars represent average specific volume change for each 50 m bin, and the black lines represent the glaciated area for each bin. Numbers indicate the region where the positive change is located. Specific volume change is the total volume change divided by total area for each elevation bin.

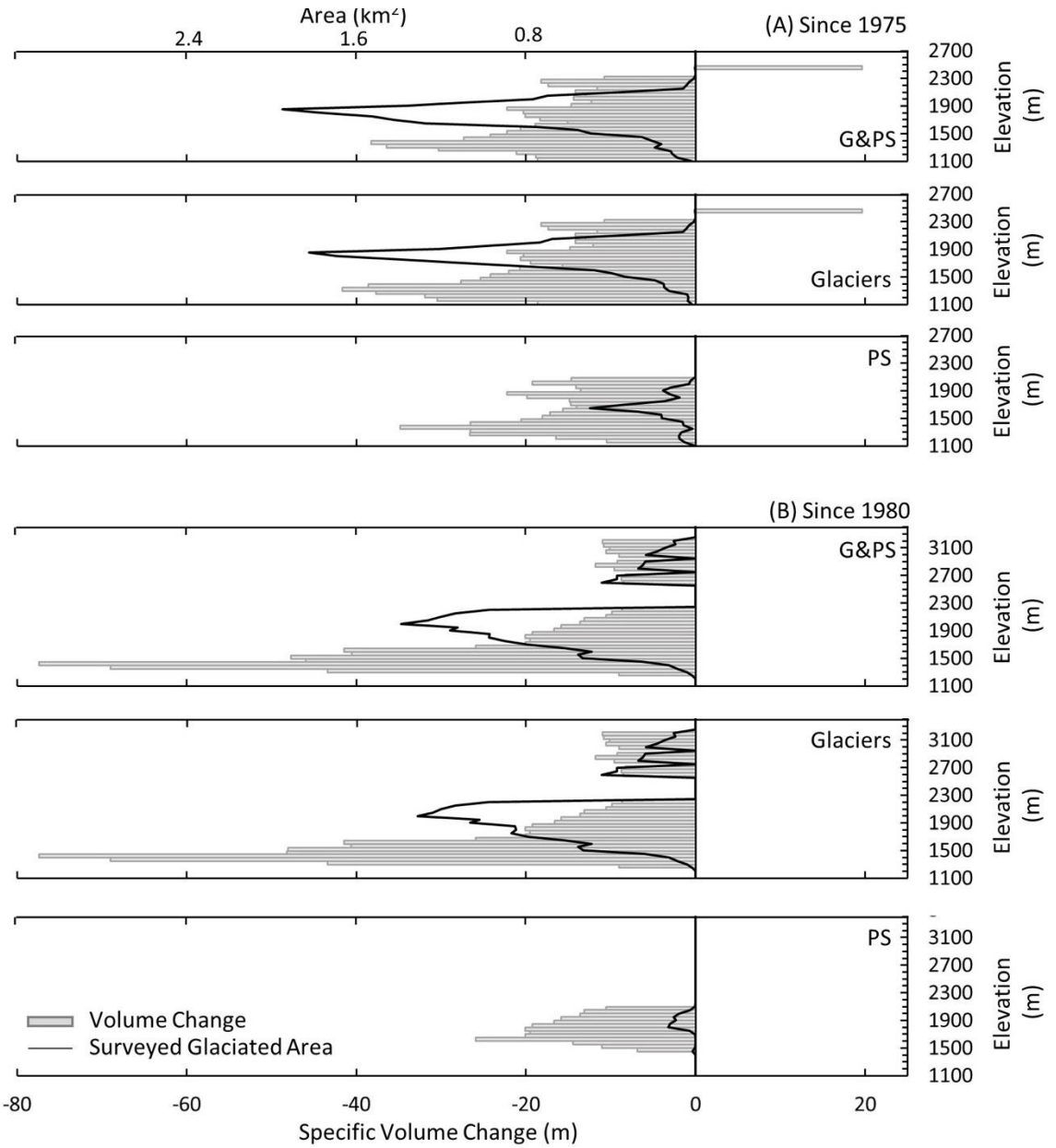

Figure 29. Specific volume change for glaciers and perennial snowfields (G&PS) as a function of elevation for the Cascade Range in Washington for the periods of 1975 (A), and 1980 (B) to 2016. The initial year refers to the 5-year interval (e.g., 1975 = 1971 to 1975). The specific volume change was calculated for each 50 m elevation bin. The value on the y-axis is the maximum elevation of that bin. The grey bars represent average specific volume change for each 50 m bin, and the black lines represent the glaciated area for each bin. Numbers indicate the region where the positive change is located. Specific volume change is the total volume change divided by total area for each elevation bin.

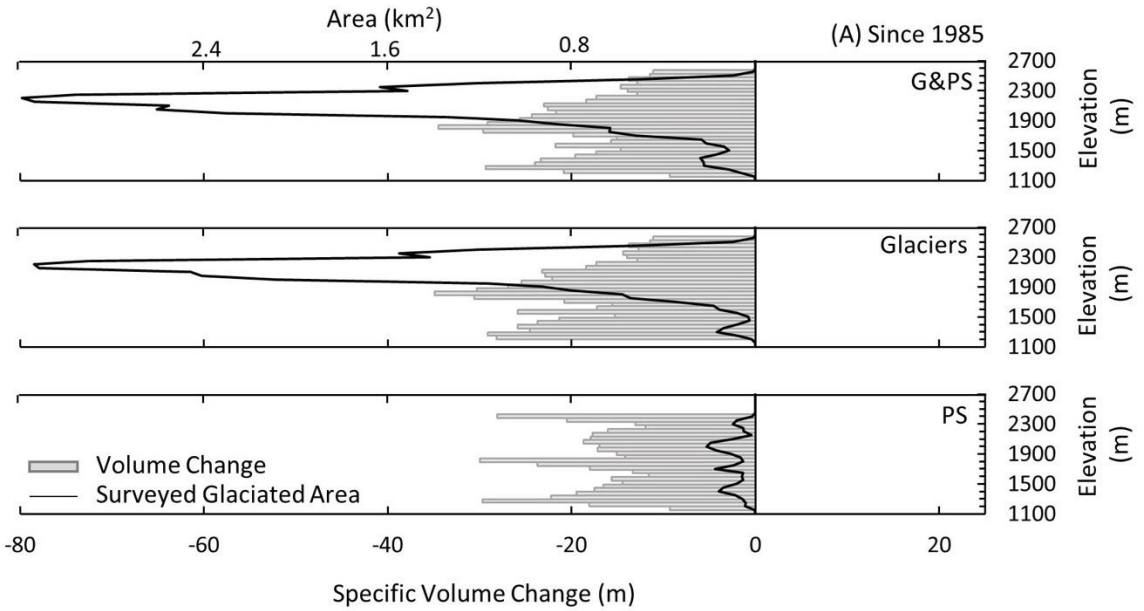

Figure 30. Specific volume change for glaciers and perennial snowfields (G&PS) as a function of elevation for the Cascade Range in Washington for the periods of 1985 to 2016. The initial year refers to the 5-year interval (e.g., 1985 = 1981 to 1985). The specific volume change was calculated for each 50 m elevation bin. The value on the y-axis is the maximum elevation of that bin. The grey bars represent average specific volume change for each 50 m bin, and the black lines represent the glaciated area for each bin. Numbers indicate the region where the positive change is located. Specific volume change is the total volume change divided by total area for each elevation bin.

VI Discussion and Conclusions

An important metric of GLISTIN's utility is its elevation precision and accuracy. As an error assessment, GLISTIN and lidar elevations were compared for control zones in several regions in the Cascade Range. The mean GLISTIN height-precision was between 0.69 ± 0.57 m (Three Sisters, OR) and 1.34 ± 1.23 m (Mount Adams, WA). The mean elevation difference (GLISTIN minus lidar) for control zones ranged from -0.14 ± 1.78 m (northern Cascade Range, WA) to 0.38 ± 1.83 m (Mount Adams, WA). Previous work in Greenland using GLISTIN showed a similar bias, 0.32 ± 0.95 m, on rocky regions near glaciers (Moller et al., 2019). Although the mean difference for this study was similar, the standard deviation was about double that of the Greenland study. The RMSE increased with surface slope. The relationship between slope and elevation uncertainty is also common to other studies, such as lidar and DEMs derived from topographic maps (Fischer et al., 2015; Ohlschlager 2015). Terrain facing away from GLISTIN has a higher RMSE than surfaces facing the instrument (see Appendix C). In a previous study the standard deviation of elevation differences for surfaces with slopes 0-10° was 0.372 m and 0.390 m for surfaces facing towards and away from GLISTIN, respectively, and for surfaces with 40°+ slopes, they were 0.643 m and 0.903 m, respectively (Moller et al., 2016).

The accuracy of GLISTIN on ice surfaces was also examined. For this project, no simultaneous lidar was collected; however, the USGS collected lidar 28 days prior to the GLISTIN flight over Mount Adams, WA. Unfortunately, the Mount Adams GLISTIN data relied on data from a single flight rather than a mosaic of data from multiple flights. The mean elevation difference (GLISTIN minus lidar) over snow and ice surfaces was

-0.87 ± 3.8 m (standard deviation) on Mount Adams. However, GLISTIN was flown 28 days after the lidar and the lower elevations of GLISTIN are expected. Previous studies comparing GLISTIN elevations to lidar elevations of two glaciers in south-central Alaska show differences of 0.8 ± 1.7 m (mean ± standard deviation) and 1.2 ± 3.7 m. Here, GLISTIN was flown in spring four to six weeks earlier than the lidar (Moller et al., 2019). Together these results suggest that GLISTIN elevations are very similar to lidar elevations over snow and ice surfaces as they are over bedrock surfaces.

Elevations were acquired for 75% of the G&PS-covered area, but only 16% of the G&PS were completely mapped by GLISTIN and 45% had ≥ 80% coverage. Missing data was caused by radar shadow (~50%) and layover, and foreshortening effects, resulting from steep terrain. Somewhat more elevation data were missing from the accumulation zones (58%, 69.01 km^2) of the glaciers than the ablation zones (42%, 50.39 km^2). Increased number of flight passes increased data coverage. From an analysis of flight lines in the northern Cascade Range, WA, coverage for single flight lines ranged from 45%- 47%, for two flights in opposite but parallel directions, and mosaicked together, coverage increases to 57% - 70%, and when a perpendicular flight line is included coverage increases to 89%.

Volume change results for the last 60 years showed that the G&PS of the American West lost at least -3.22 ± 1.41 km^3. To account for differences in time interval and in the number of G&PS in various intervals, specific volume change rates were used. My estimates of specific volume change on Mount Rainier, WA; Three Sisters, OR: and the Lewis Range are similar to prior studies and within the uncertainty. My results are

also consistent with glacier mass change rates globally. For example, in the Swiss Alps, the average mass balance rate for 120 glaciers was -0.62 ± 0.07 m w.e. yr^{-1} for the period of 1980-2010 (Fischer et al., 2015) and for the eastern Italian Alps, -0.69 ± 0.09 m w.e. yr^{-1} (1980s - 2000s; Carturan et al., 2013). These rates are comparable to the average mass balance rate of -0.62 ± 0.22m w.e. yr^{-1} over (1983- 2016) for the Cascade Range in Washington. For a different place and period, Austrian Alps 1969 - 1998, the rate of glacier mass change was -0.25 m w.e. yr^{-1} (Lambrecht and Kuhn, 2007) and the Coast Range, Canada, 1965- 2002, -0.15 ± 0.03 m w.e. yr^{-1} (DeBeer and Sharp, 2007). These rates are similar to the average mass balance rates of -0.26 ± 0.08 m w.e. yr^{-1} over (1966 - 2016) for the Wind River Range, WY, and -0.14 ± 0.09 m w.e. yr^{-1} over (1968 - 2016) for the Cascade Range in Washington.

An analysis of topographic controls (slope, elevation, aspect [northness and eastness], latitude, longitude) on volume change rate showed somewhat different statistically significant results for different regions. For the Cascade Range, WA, elevation is positively correlated, indicating G&PS at lower elevations experience a greater loss than G&PS at higher elevations. Northness was negatively correlated, indicating G&PS with more northerly aspects experienced greater loss than G&PS with southerly aspects. Latitude was also negatively correlated, indicating a greater loss for G&PS in the south compared to G&PS in the north. Northness and latitude were also negatively correlated with volume change in the Oregon Cascades. However, in the Sierra Nevada, elevation was negatively correlated, indicating G&PS at higher elevations experience a greater loss than G&PS at lower elevations. Latitude was positively

correlated, indicating a greater loss for G&PS in the north compared to glaciers in the south. Longitude was also negatively correlated. Because longitude becomes more negative going west, a negative correlation indicates G&PS to the east have greater loss than G&PS in the west. No statistically significant correlations were found with slope. Ohlschlager (2015) found no significant correlation between volume change and slope, elevation, or aspect for the Three Sisters (Oregon Cascades). For the Sierra Nevada; Basagic and Fountain (2011) found no correlation between area change, a proxy for volume change, and topography (slope, elevation, and aspect). Studies in other regions globally also found little or conflicting correlations with topographic variables. Fischer et al. (2015) found no correlation between the glacier mass change in the Swiss Alps and aspect. They did find correlations with elevation and slope only for the lower ablation zone of the glaciers. For the Eastern Italian Alps, Carturan et al. (2013) found volume changes of large glaciers to be correlated with slope, elevation, and elevation range, but smaller glaciers (< 0.3 km$^{2)}$ were not because they were more influenced by local effects of debris cover and snow accumulation by avalanching. The influence of such local effects on volume change was also observed in western Canada (DeBeer and Sharp, 2007). The correlations between glacier size and topographic variables was beyond the scope of this project but future work should address this issue.

Considering future aerial surveys, several improvements could be made to improve GLISTN's coverage and accuracy. First, modeling the potential coverage based on planned flights would optimize coverage in complex terrain. Apparently, current models need significant improvement for operational application (Y. Zheng, Per. Comm.,

2019), however, a first step would be to anticipate terrain shadow as this thesis attempted to quantify. Perhaps modeling could be used to anticipate the number of flights required to adequately cover a region and whether they should be flown in parallel or with perpendicular orientations. One important oversight in this project was the lack of ground-truthing. Although some of the GLISTIN coverage overlapped exciting lidar data, the overlapping regions were limited, and most of the GLISTIN mosaics did not overlap lidar datasets. Additionally, for some GLISTIN mosaics, limited areas of bedrock were available for control zones. Targets should have been identified, such as large expanses of bedrock that have been mapped using lidar. These predefined control zones should have been incorporated into the planned flight path. If possible, it would have been very helpful to have simultaneous lidar over snow and ice surfaces.

GLISTIN allows for the rapid collection of glacier surface measurements regardless of cloud cover and light conditions. As demonstrated, glacier surfaces across a large region, such as the western U.S., can be surveyed in a short time (two weeks). GLISTIN can capture a comprehensive snapshot of all glaciers in the region when surface conditions are likely the same. Although the accuracy was ± 3.19 m (RMSE) over snow and ice surfaces, the error is small enough to estimate volume change over decadal time periods. Depending on the project's objective, other tools and methods may be more appropriate for measuring glacier change. Field measurements are ideal for monitoring seasonal or annual changes of a single glacier. Lidar is more suitable for monitoring the change of a small number of glaciers annually. GLISTIN is best suited to measure glacier change for a broad region on a decadal scale.

References

Bakker W, Feringa WF, Gieske A, Grabmaier KA, Hecker C, Horn J, Meer FD, Parodi G, Pohl C, Reeves CV, Ruitenbeek FJA, Schetselaar E, Weir M, Westinga E and Woldai T (2009) *Principles of remote sensing : an introductory textbook.* The International Institute for Geo-Information Science and Earth Observation, Enschede, The Netherlands

Basagic HJ and Fountain AG (2011) Quantifying 20th Century Glacier Change in the Sierra Nevada, California. *Arctic, Antarctic, and Alpine Research* **43**(3), 317–330 (doi:10.1657/1938-4246-43.3.317)

Berthier E, Arnaud Y, Kumar R, Ahmad S, Wagnon P and Chevallier P (2007) Remote sensing estimates of glacier mass balances in the Himachal Pradesh (Western Himalaya, India). *Remote Sensing of Environment* **108**(3), 327–338 (doi:10.1016/j.rse.2006.11.017)

Brett, MC (2017) Glacier Inventories and Change in Glacier National Park. Portland State University, Portland Oregon.

Brunt KM, Neumann TA and Smith BE (2019) Assessment of ICESat-2 Ice Sheet Surface Heights, Based on Comparisons Over the Interior of the Antarctic Ice Sheet. *Geophys. Res. Lett.* **46**(22), 13072–13078 (doi:10.1029/2019GL084886)

Carturan L, Filippi R, Seppi R, Gabrielli P, Notarnicola C, Bertoldi L, Paul F, Rastner P, Cazorzi F, Dinale R and Dalla Fontana G (2013) Area and volume loss of the glaciers in the Ortles-Cevedale group (Eastern Italian Alps): controls and imbalance of the remaining glaciers. *The Cryosphere* **7**(5), 1339–1359 (doi:10.5194/tc-7-1339-2013)

Cogley GJ (2009) Geodetic and direct mass-balance measurements: comparison and joint analysis. *Ann. Glaciol.* **50**(50), 96–100 (doi:10.3189/172756409787769744)

Cuffey K and Paterson WSB (2010) *The Physics of Glaciers.*, 4th edn. Elsevier, New York

DeBeer CM and Sharp MJ (2007) Recent changes in glacier area and volume within the southern Canadian Cordillera. *Annals of Glaciology* **46**(1), 215–221

DeVisser MH and Fountain AG (2015) A century of glacier change in the Wind River Range, WY. *Geomorphology* **232**, 103–116 (doi:10.1016/j.geomorph.2014.10.017)

Dick KA (2013) Glacier Change in the North Cascades, Washington: 1900-2009. Portland State University.

Eineder M and Holzner J (2000) Interferometric DEMs in alpine terrain-limits and options for ERS and SRTM. *IGARSS 2000. IEEE 2000 International Geoscience and Remote Sensing Symposium. Taking the Pulse of the Planet: The Role of Remote Sensing in Managing the Environment. Proceedings (Cat. No.00CH37120)*. IEEE, Honolulu, HI, USA, 3210–3212 (doi:10.1109/IGARSS.2000.860385)

Farr TG, Rosen PA, Caro E, Crippen R, Duren R, Hensley S, Kobrick M, Paller M, Rodriguez E, Roth L, Seal D, Shaffer S, Shimada J, Umland J, Werner M, Oskin M, Burbank D and Alsdorf D (2007) The Shuttle Radar Topography Mission. *Rev. Geophys.* **45**(2), RG2004 (doi:10.1029/2005RG000183)

Fischer M, Huss M and Hoelzle M (2015) Surface elevation and mass changes of all Swiss glaciers 1980–2010. *The Cryosphere* **9**(2), 525–540 (doi:10.5194/tc-9-525-2015)

Fountain AG, Glenn B and Basagic HJ (2017) The Geography of Glaciers and Perennial Snowfields in the American West. *Arctic, Antarctic, and Alpine Research* **49**(3), 391–410 (doi:10.1657/AAAR0017-003)

Fountain AG, Hoffman M, Jackson K, Basagic H, Nylen T and Percy D (2007) Digital outlines and topography of the glaciers of the American West. US Geological Survey

Fountain AG and Tangborn WV (1985) The Effect of Glaciers on Streamflow Variations. *Water Resources Research* **21**(4), 579–586 (doi:10.1029/WR021i004p00579)

Frey H, Paul F and Strozzi T (2012) Compilation of a glacier inventory for the western Himalayas from satellite data: methods, challenges, and results. *Remote Sensing of Environment* **124**, 832–843 (doi:10.1016/j.rse.2012.06.020)

Fricker HA (2005) Assessment of ICESat performance at the salar de Uyuni, Bolivia. *Geophys. Res. Lett.* **32**(21), L21S06 (doi:10.1029/2005GL023423)

Gardner AS, Moholdt G, Cogley JG, Wouters B, Arendt AA, Wahr J, Berthier E, Hock R, Pfeffer WT, Kaser G, Ligtenberg SRM, Bolch T, Sharp MJ, Hagen JO, van den Broeke MR and Paul F (2013) A Reconciled Estimate of Glacier Contributions to Sea Level Rise: 2003 to 2009. *Science* **340**(6134), 852–857 (doi:10.1126/science.1234532)

Gesch D, Oimoen M, Greenlee S, Nelson C, Steuck M and Tyler D (2002) The national elevation dataset. *Photogrammetric engineering and remote sensing* **68**(1), 5–32

Hall MH and Fagre DB (2003) Modeled climate-induced glacier change in Glacier National Park, 1850–2100. *AIBS Bulletin* **53**(2), 131–140

Hensley S, Moller D, Oveisgharan S, Michel T and Wu X (2016) Ka-Band Mapping and Measurements of Interferometric Penetration of the Greenland Ice Sheets by the GLISTIN Radar. *IEEE Journal of Selected Topics in Applied Earth Observations and Remote Sensing* **9**(6), 2436–2450 (doi:10.1109/JSTARS.2016.2560626)

Hoffman MJ, Fountain AG and Achuff JM (2007) 20th-century variations in area of cirque glaciers and glacierets, Rocky Mountain National Park, Rocky Mountains, Colorado, USA. *Annals of Glaciology* **46**(1), 349–354

Huss M (2013) Density assumptions for converting geodetic glacier volume change to mass change. *The Cryosphere* **7**(3), 877–887 (doi:10.5194/tc-7-877-2013)

Huss M and Farinotti D (2012) Distributed ice thickness and volume of all glaciers around the globe: GLOBAL GLACIER ICE THICKNESS AND VOLUME. *J. Geophys. Res.* **117**(F4), (doi:10.1029/2012JF002523)

Kaser G, Fountain AG and Jansson P (2003) A manual for monitoring the mass balance of mountain glaciers.

Kohler J, James TD, Murray T, Nuth C, Brandt O, Barrand NE, Aas HF and Luckman A (2007) Acceleration in thinning rate on western Svalbard glaciers. *Geophys. Res. Lett.* **34**(18), L18502 (doi:10.1029/2007GL030681)

Lambrecht A and Kuhn M (2007) Glacier changes in the Austrian Alps during the last three decades, derived from the new Austrian glacier inventory. *Ann. Glaciol.* **46**, 177–184 (doi:10.3189/172756407782871341)

Le Bris R and Paul F (2015) Glacier-specific elevation changes in parts of western Alaska. *Ann. Glaciol.* **56**(70), 184–192 (doi:10.3189/2015AoG70A227)

McNabb R, Nuth C, Kääb A and Girod L (2019) Sensitivity of glacier volume change estimation to DEM void interpolation. *The Cryosphere* **13**(3), 895–910 (doi:10.5194/tc-13-895-2019)

Meier MF (1984) Contribution of small glaciers to global sea level. *Science* **226**, 1418–1421

Meier MF, Tangborn WV, Mayo LR and Post A Combined Ice and Water Balances of Gulkana and Wolverine Glaciers, Alaska, and South Cascade Glacier, Washington, 1965 and 1966 Hydrologic Years. 715-A. U.S. Department of the Interior, Geological Survey

Menounos B, Hugonnet R, Shean D, Gardner A, Howat I, Berthier E, Pelto B, Tennant C, Shea J, Noh M, Brun F and Dehecq A (2018) Heterogeneous changes in western North American glaciers linked to decadal variability in zonal wind strength. *Geophysical Research Letters* (doi:10.1029/2018GL080942)

Moller D, Andreadis KM, Bormann KJ, Hensley S and Painter TH (2017) Mapping Snow Depth From Ka-Band Interferometry: Proof of Concept and Comparison With Scanning Lidar Retrievals. *IEEE Geoscience and Remote Sensing Letters* **14**(6), 886–890

Moller D, Hensley S, Mouginot J, Willis J, Wu X, Larsen C, Rignot E, Muellerschoen R and Khazendar A (2019) Validation of Glacier Topographic Acquisitions from an Airborne Single-Pass Interferometer. *Sensors* **19**(17), 3700 (doi:10.3390/s19173700)

Moller D, Hensley S, Sadowy GA, Fisher CD, Michel T, Zawadzki M and Rignot E (2011) The Glacier and Land Ice Surface Topography Interferometer: An Airborne Proof-of-Concept Demonstration of High-Precision Ka-Band Single-Pass Elevation Mapping. *IEEE Transactions on Geoscience and Remote Sensing* **49**(2), 827–842 (doi:10.1109/TGRS.2010.2057254)

Moore RD, Fleming SW, Menounos B, Wheate R, Fountain A, Stahl K, Holm K and Jakob M (2009) Glacier change in western North America: influences on hydrology, geomorphic hazards and water quality. *Hydrol. Process.* **23**(1), 42–61 (doi:10.1002/hyp.7162)

NGS, 2006. "Whitney". *NGS data sheet*. U.S. National Geodetic Survey. www.ngs.noaa.gov/cgi-bin/ds_mark.prl?PidBox=GT1811 Retrieved 2008-10-31.

Nuth C, Moholdt G, Kohler J, Hagen JO and Kääb A (2010) Svalbard glacier elevation changes and contribution to sea level rise. *J. Geophys. Res.* **115**(F1), F01008 (doi:10.1029/2008JF001223)

Oerlemans J (2005) Extracting a Climate Signal from 169 Glacier Records. *Science* **308**(5722), 675–677 (doi:10.1126/science.1107046)

Oerlemans J and Reichert BK (2000) Relating glacier mass balance to meteorological data by using a seasonal sensitivity characteristic. *Journal of Glaciology* **46**(152), 1–6 (doi:10.3189/172756500781833269)

Ohlschlager JG (2015) Glacier Change on the Three Sisters Volcanoes, Oregon: 1900-2010. M.S., Portland State University, Portland.

Osborn K, List J, Gesch D, Crowe J, Merrill G, Constance E, Mauck J, Lund C, Caruso V and Kosovich J National Digital Elevation Program (NDEP). , 38

Østrem G and Haakensen N (1999) Map Comparison or Traditional Mass-Balance Measurements: Which Method Is Better? *Geografiska Annaler. Series A, Physical Geography* **81**(4), 703–711

Paul F, Kääb A, Maisch M, Kellenberger T and Haeberli W (2002) The new remote-sensing-derived Swiss glacier inventory: I. Methods. *Ann. Glaciol.* **34**, 355–361 (doi:10.3189/172756402781817941)

Pfeffer WT, Arendt AA, Bliss A, Bolch T, Cogley JG, Gardner AS, Hagen J-O, Hock R, Kaser G, Kienholz C, Miles ES, Moholdt G, Mölg N, Paul F, Radić V, Rastner P, Raup BH, Rich J, Sharp MJ and The Randolph Consortium (2014) The Randolph Glacier Inventory: a globally complete inventory of glaciers. *Journal of Glaciology* **60**(221), 537–552 (doi:10.3189/2014JoG13J176)

Racoviteanu AE, Paul F, Raup B, Khalsa SJS and Armstrong R (2009) Challenges and recommendations in mapping of glacier parameters from space: results of the 2008 Global Land Ice Measurements from Space (GLIMS) workshop, Boulder, Colorado, USA. *Ann. Glaciol.* **50**(53), 53–69 (doi:10.3189/172756410790595804)

Radić V and Hock R (2010) Regional and global volumes of glaciers derived from statistical upscaling of glacier inventory data. *Journal of Geophysical Research* **115**(F1) (doi:10.1029/2009JF001373)

Rees WG (2000) Technical note: Simple masks for shadowing and highlighting in SAR images. *International Journal of Remote Sensing* **21**(11), 2145–2152 (doi:10.1080/01431160050029477)

Rignot E, Echelmeyer K and Krabill W (2001) Penetration depth of interferometric synthetic-aperture radar signals in snow and ice. *Geophys. Res. Lett.* **28**(18), 3501–3504 (doi:10.1029/2000GL012484)

Rosen PA, Hensley S, Joughin IR, Li FK, Madsen SN, Rodriguez E and Goldstein RM (2000) Synthetic aperture radar interferometry. *Proc. IEEE* **88**(3), 333–382 (doi:10.1109/5.838084)

Ruiz L, Berthier E, Viale M, Pitte P and Masiokas MH (2017) Recent geodetic mass balance of Monte Tronador glaciers, northern Patagonian Andes. *The Cryosphere* **11**(1), 619–634 (doi:10.5194/tc-11-619-2017)

Sapiano J, Harrison WD and Echelmeyer KA (1998) Elevation, voluIlle and terIllinus changes of nine glaciers in North AIllerica. *J ournal oJGlaciology* **44**(146), 119–135

Schumann GJ-P, Moller DK and Mentgen F (2016) High-Accuracy Elevation Data at Large Scales from Airborne Single-Pass SAR Interferometry. *Frontiers in Earth Science* **3** (doi:10.3389/feart.2015.00088)

Selkowitz DJ and Forster RR (2016) Automated mapping of persistent ice and snow cover across the western U.S. with Landsat. *ISPRS Journal of Photogrammetry and Remote Sensing* **117**, 126–140 (doi:10.1016/j.isprsjprs.2016.04.001)

Shean DE, Alexandrov O, Moratto ZM, Smith BE, Joughin IR, Porter C and Morin P (2016) An automated, open-source pipeline for mass production of digital elevation models (DEMs) from very-high-resolution commercial stereo satellite imagery. *ISPRS Journal of Photogrammetry and Remote Sensing* **116**, 101–117 (doi:https://doi.org/10.1016/j.isprsjprs.2016.03.012)

Sisson TW, Robinson JE and Swinney DD (2011) Whole-edifice ice volume change A.D. 1970 to 2007/2008 at Mount Rainier, Washington, based on LiDAR surveying. *Geology* **39**(7), 639–642 (doi:10.1130/G31902.1)

Thompson D, Tootle G, Asce M, Kerr G, Sivanpillai R and Pochop L Glacier Variability in the Wind River Range, Wyoming. , 8

Ulaby FT, Moore RK and Fung AK (1986) *Microwave Remote sensing Active and Passive.* Artech House, Norwood MA

Zemp M, Hoelzle M and Haeberli W (2009) Six decades of glacier mass-balance observations: a review of the worldwide monitoring network. *Ann. Glaciol.* **50**(50), 101–111 (doi:10.3189/172756409787769591)

Appendix A: Additional Tables and Figures

Table A1. List of sources compiled for the historical elevation data. The three sources used were the National Map, maintained by the U.S. Geological Survey (USGS), the Oregon office of the Bureau of Land Management (BLM), and the Geomorphological Research Group at the University of Washington (UW).

State/Range	Source	Website
California		
Sierra Nevada	USGS	https://viewer.nationalmap.gov/basic
Colorado		
Front	USGS	https://viewer.nationalmap.gov/basic
Gore	USGS	https://viewer.nationalmap.gov/basic
Montana		
Beartooth-Absaroka	USGS	https://viewer.nationalmap.gov/basic
Lewis	USGS	https://viewer.nationalmap.gov/basic
Oregon		
Cascade	BLM	http://earthexplorer.usgs.gov
Washington		
northern Cascades	UW	http://gis.ess.washington.edu/data/
northern Cascades	USGS	https://viewer.nationalmap.gov/basic
southern Cascades	BLM	http://earthexplorer.usgs.gov
Wyoming		
Teton	USGS	https://viewer.nationalmap.gov/basic
Wind River	USGS	https://viewer.nationalmap.gov/basic

Table A2. List of glaciated areas not covered by GLISTIN flights in September 2016, including the number of glaciers and perennial snowfields (G&PS) in each mountain range (Fountain et a., 2017).

State/Range	Number	Area ($km^{2)}$
California		
Cascade Range	15	5.04
Trinity Alps	29	1.87
Colorado		
Medicine Bow	5	0.13
Park	16	0.48
San Miguel	4	0.18
Sawatch	16	0.28
Tenmile-Mosquito	1	0.03
Idaho		
Sawtooth	69	1.99
Montana		
Cabinet	4	0.70
Crazy	44	1.85
Madison	2	0.04
Mission-Swan-Flathead	65	3.45
Nevada		
Snake	1	0.09
Oregon		
Wallowa	42	1.07
Washington		
Olympic	253	36.52
Wyoming		
Absaroka	221	8.14
Bighorn	16	0.97

Table A3. Average mass balance rates of glaciers and perennial snowfields in select regions and periods. Mass balance was estimated between the initial NED year and the GLISTIN year of 2016 for glaciers and perennial snowfields with ≥ 80% GLISTIN. The year listed is the NED year. 'Num' is the number of G&PS for that category. The region 'Beartooth' refers to the Beartooth-Absaroka range, MT. See Figure 1 for the location of regions.

Region	Year	Num	Average Mass Balance Rate (mw.e. yr)
OR Cascades	1956	13	-0.23 ± 0.09
OR Cascades	1957	31	-0.19 ± 0.09
WA Cascades	1958	62	-0.25 ± 0.09
WA Cascades	1959	12	-0.22 ± 0.07
Lewis	1966	42	-0.21 ± 0.14
Wind River	1966	62	-0.26 ± 0.08
Tetons	1967	41	-0.12 ± 0.06
WA Cascades	1968	11	-0.14 ± 0.09
WA Cascades	1969	22	-0.17 ± 0.09
WA Cascades	1970	20	-0.18 ± 0.09
OR Cascades	1974	25	-0.36 ± 0.13
WA Cascades	1974	82	-0.37 ± 0.16
Wind River	1974	24	-0.12 ± 0.10
Sierra Nevada	1975	16	-0.22 ± 0.13
Sierra Nevada	1976	32	-0.36 ± 0.15
WA Cascades	1980	10	-0.35 ± 0.20
Beartooth	1981	23	-0.55 ± 0.19
WA Cascades	1983	40	-0.62 ± 0.22
Sierra Nevada	1984	107	-0.28 ± 0.13
WA Cascades	1984	46	-0.49 ± 0.22
WA Cascades	1985	15	-0.45 ± 0.17
OR Cascades	1988	10	-0.35 ± 0.19

A4. Volume change estimates for G&PS with significant positive change. Volume change was estimated between the initial NED year and the GLISTIN year of 2016 for glaciers and perennial snowfields with ≥ 80% GLISTIN. The change was grouped by region and year. The year listed is the last in the 5-year interval (e.g., 1955 = 1951 to 1955). 'Num' is the number of G&PS for that category.

Region/Year/Type	Num	Area (km^2)	Volume Change (m^3 x 10^6)	Specific Vol Change (m)	Specific Vol Change Rate (m yr^{-1})
Washington Cascades	10	0.39	2.76 ± 1.96	7.1 ± 5.1	1.62 ±1.05
1960	2	0.10	0.48 ± 0.47	5.0 ± 4.9	0.20 ±0.19
Glacier	1	0.08	0.41 ± 0.40	4.8 ± 4.7	0.08 ±0.08
Snowfield	1	0.01	0.07 ± 0.07	6.5 ± 6.3	0.11 ±0.11
1970	7	0.27	2.18 ± 1.40	8.0 ± 5.1	1.28 ±0.72
Glacier	1	0.16	1.13 ± 0.87	7.0 ± 5.4	0.15 ±0.11
Snowfield	6	0.11	1.05 ± 0.54	9.4 ± 4.8	1.13 ±0.61
1985	1	0.02	0.09 ± 0.09	4.9 ± 4.6	0.15 ±0.14
Snowfield	1	0.02	0.09 ± 0.09	4.9 ± 4.6	0.15 ±0.14
Oregon Cascades	5	0.31	3.03 ± 1.91	9.7 ± 6.1	0.99 ±0.63
1960	4	0.28	2.78 ± 1.73	9.8 ± 6.1	0.68 ±0.41
Glacier	1	0.13	1.52 ± 0.82	11.4 ± 6.2	0.19 ±0.10
Snowfield	3	0.15	1.26 ± 0.91	8.4 ± 6.1	0.49 ±0.31
1990	1	0.03	0.25 ± 0.18	8.6 ± 6.1	0.31 ±0.22
Snowfield	1	0.03	0.25 ± 0.18	8.6 ± 6.1	0.31 ±0.22
Sierra Nevada, CA	11	0.22	0.93 ± 0.28	4.3 ± 1.3	2.15 ±1.63
1955	1	0.01	0.05 ± 0.00	4.1 ± 0.4	0.07 ±0.07
Snowfield	1	0.01	0.05 ± 0.00	4.1 ± 0.4	0.07 ±0.07
1975	2	0.02	0.31 ± 0.13	13.5 ± 5.5	0.65 ±0.26
Snowfield	2	0.02	0.31 ± 0.13	13.5 ± 5.5	0.65 ±0.26
1985	7	0.17	0.41 ± 0.08	2.4 ± 0.4	0.63 ±0.97
Snowfield	7	0.17	0.41 ± 0.08	2.4 ± 0.4	0.63 ±0.97
1995	1	0.01	0.16 ± 0.07	18.4 ± 7.7	0.80 ±0.33
Snowfield	1	0.01	0.16 ± 0.07	18.4 ± 7.7	0.80 ±0.33
Lewis, MT	8	0.70	8.91 ± 5.78	12.8 ± 8.3	1.93 ±1.31
1970	8	0.70	8.91 ± 5.78	12.8 ± 8.3	1.93 ±1.31
Glacier	1	0.56	7.26 ± 4.64	12.9 ± 8.3	0.26 ±0.16
Snowfield	7	0.14	1.65 ± 1.14	12.0 ± 8.3	1.68 ±1.15
Beartooth-Absaroka, MT	4	0.09	0.80 ± 0.63	9.2 ± 7.2	1.02 ±0.82
1985	4	0.09	0.80 ± 0.63	9.2 ± 7.2	1.02 ±0.82
Snowfield	4	0.09	0.80 ± 0.63	9.2 ± 7.2	1.02 ±0.82
Tetons, WY	11	0.23	0.95 ± 0.71	4.2 ± 3.1	0.95 ±0.70
1970	11	0.23	0.95 ± 0.71	4.2 ± 3.1	0.95 ±0.70
Snowfield	11	0.23	0.95 ± 0.71	4.2 ± 3.1	0.95 ±0.70
Wind River, WY	11	0.19	1.58 ± 0.89	8.3 ± 4.7	2.15 ±1.17
1970	2	0.03	0.27 ± 0.16	8.1 ± 4.7	0.31 ±0.18
Snowfield	2	0.03	0.27 ± 0.16	8.1 ± 4.7	0.31 ±0.18
1975	9	0.16	1.31 ± 0.73	8.3 ± 4.7	1.84 ±0.98
Snowfield	9	0.16	1.31 ± 0.73	8.3 ± 4.7	1.84 ±0.98
Total	60	2.12	18.96 ± 12.15	8.9 ± 5.7	10.81 ±7.29

Table A5. Volume change estimates between the initial NED year and the GLISTIN 2016 survey for glaciers and perennial snowfields with ≥ 80% GLISTIN coverage grouped by 5-year intervals. In the first column, 'Yr' is the 5-year interval, 'Reg' is the region, and 'Type refers' to either glaciers or perennial snowfields. 'Num' is the number of G&PS for that category. 'Vol' is volume. The year listed is the last in the 5-year interval (e.g., 1955 = 1951 to 1955). The region 'Beartooth' refers to the Beartooth-Absaroka range, MT. See Figure 1 for the location of regions. Specific volume change is calculated by dividing the total volume change by the total area.

Yr/Reg/Type	Num	Vol Change (m^3 x10^6)	Specific Vol Change (m)	Specific Vol Change Rate (m yr^{-1})
1955	**5**	**-0.75 ± 0.45**	**-6.7 ± 4.0**	**-0.1 ± 0.1**
Sierra Nevada	3	-0.13 ± 0.02	-2.5 ± 0.4	0.0 ± 0.0
Snowfield	3	-0.13 ± 0.02	-2.5 ± 0.4	0.0 ± 0.0
Front	2	-0.62 ± 0.43	-10.8 ± 7.5	-0.2 ± 0.1
Snowfield	2	-0.62 ± 0.43	-10.8 ± 7.5	-0.2 ± 0.1
1960	**119**	**-551.88 ± 207.79**	**-16.1 ± 6.1**	**-0.3 ± 0.1**
WA Cascades	75	-336.81 ± 117.49	-17.1 ± 6.0	-0.3 ± 0.1
Glacier	29	-312.42 ± 106.56	-17.6 ± 6.0	-0.3 ± 0.1
Snowfield	46	-24.40 ± 10.93	-12.5 ± 5.6	-0.2 ± 0.1
OR Cascades	44	-215.07 ± 90.29	-14.9 ± 6.2	-0.3 ± 0.1
Glacier	13	-188.44 ± 76.15	-15.5 ± 6.2	-0.3 ± 0.1
Snowfield	31	-26.63 ± 14.14	-11.7 ± 6.2	-0.2 ± 0.1
1965	**10**	**-27.38 ± 13.65**	**-11.0 ± 5.5**	**-0.2 ± 0.1**
WA Cascades	7	-25.15 ± 12.14	-11.0 ± 5.3	-0.2 ± 0.1
Glacier	2	-22.01 ± 10.68	-10.9 ± 5.3	-0.2 ± 0.1
Snowfield	5	-3.14 ± 1.46	-11.2 ± 5.2	-0.2 ± 0.1
OR Cascades	1	-0.34 ± 0.31	-6.6 ± 6.1	-0.1 ± 0.1
Snowfield	1	-0.34 ± 0.31	-6.6 ± 6.1	-0.1 ± 0.1
Lewis	1	-1.77 ± 1.13	-13.0 ± 8.3	-0.3 ± 0.2
Glacier	1	-1.77 ± 1.13	-13.0 ± 8.3	-0.3 ± 0.2
Wind River	1	-0.11 ± 0.08	-6.9 ± 4.6	-0.1 ± 0.1
Snowfield	1	-0.11 ± 0.08	-6.9 ± 4.6	-0.1 ± 0.1
1970	**202**	**-996.71 ± 452.73**	**-11.3 ± 5.1**	**-0.2 ± 0.1**
WA Cascades	53	-507.94 ± 255.44	-9.5 ± 4.8	-0.2 ± 0.1
Glacier	23	-501.59 ± 250.65	-9.6 ± 4.8	-0.2 ± 0.1
Snowfield	30	-6.35 ± 4.79	-6.6 ± 5.0	-0.1 ± 0.1
Lewis	42	-113.05 ± 76.70	-12.2 ± 8.3	-0.3 ± 0.1
Glacier	25	-111.52 ± 73.62	-12.6 ± 8.3	-0.3 ± 0.1
Snowfield	17	-1.53 ± 3.08	-4.1 ± 8.3	-0.1 ± 0.1
Tetons	41	-8.68 ± 4.13	-6.8 ± 3.2	-0.1 ± 0.1
Glacier	3	-3.29 ± 0.86	-12.7 ± 3.3	-0.3 ± 0.1
Snowfield	38	-5.39 ± 3.26	-5.3 ± 3.2	-0.1 ± 0.1
Wind River	64	-365.80 ± 115.43	-15.3 ± 4.8	-0.3 ± 0.1
Glacier	19	-345.41 ± 102.55	-16.3 ± 4.8	-0.4 ± 0.1
Snowfield	45	-20.40 ± 12.89	-7.4 ± 4.6	-0.2 ± 0.1
Gore	2	-1.24 ± 1.03	-7.1 ± 5.9	-0.2 ± 0.1
Glacier	1	-1.15 ± 0.97	-7.0 ± 5.9	-0.2 ± 0.1
Snowfield	1	-0.09 ± 0.06	-8.3 ± 5.9	-0.2 ± 0.1

Yr/Reg/Type	Num	Vol Change (m^3 x10^6)	Specific Vol Change (m)	Specific Vol Change Rate (m yr^{-1})
1975	**147**	**-441.47 ± 180.72**	**-17.7 ± 7.2**	**-0.4 ± 0.2**
WA Cascades	82	-290.34 ± 124.61	-18.3 ± 7.8	-0.4 ± 0.2
Glacier	24	-249.19 ± 102.35	-19.0 ± 7.8	-0.5 ± 0.2
Snowfield	58	-41.16 ± 22.26	-15.0 ± 8.1	-0.4 ± 0.2
OR Cascades	25	-143.32 ± 50.91	-17.7 ± 6.3	-0.4 ± 0.2
Glacier	9	-137.50 ± 46.93	-18.5 ± 6.3	-0.5 ± 0.2
Snowfield	16	-5.83 ± 3.98	-9.0 ± 6.1	-0.2 ± 0.1
Sierra Nevada	16	-4.19 ± 2.38	-10.7 ± 6.1	-0.3 ± 0.1
Glacier	2	-1.85 ± 0.73	-14.6 ± 5.7	-0.4 ± 0.1
Snowfield	14	-2.35 ± 1.65	-8.9 ± 6.3	-0.2 ± 0.2
Wind River	24	-3.61 ± 2.82	-6.0 ± 4.7	-0.1 ± 0.1
Glacier	1	-1.12 ± 0.27	-20.9 ± 5.0	-0.5 ± 0.1
Snowfield	23	-2.49 ± 2.56	-4.6 ± 4.7	-0.1 ± 0.1
1980	**55**	**-363.07 ± 199.19**	**-15.1 ± 8.3**	**-0.4 ± 0.2**
WA Cascades	20	-320.08 ± 180.75	-15.0 ± 8.4	-0.4 ± 0.2
Glacier	8	-309.81 ± 175.82	-14.9 ± 8.4	-0.4 ± 0.2
Snowfield	12	-10.27 ± 4.94	-17.3 ± 8.3	-0.5 ± 0.2
Sierra Nevada	35	-42.98 ± 18.44	-16.4 ± 7.1	-0.5 ± 0.2
Glacier	12	-34.69 ± 13.74	-17.8 ± 7.0	-0.5 ± 0.2
Snowfield	23	-8.30 ± 4.70	-12.6 ± 7.1	-0.3 ± 0.2
1985	**233**	**-786.71 ± 322.73**	**-18.8 ± 7.7**	**-0.6 ± 0.2**
WA Cascades	101	-662.12 ± 275.94	-19.4 ± 8.1	-0.6 ± 0.3
Glacier	40	-628.40 ± 257.10	-19.9 ± 8.2	-0.6 ± 0.3
Snowfield	61	-33.71 ± 18.83	-13.0 ± 7.2	-0.4 ± 0.2
Sierra Nevada	109	-40.62 ± 18.78	-10.5 ± 4.9	-0.3 ± 0.2
Glacier	9	-19.27 ± 8.63	-13.8 ± 6.2	-0.4 ± 0.2
Snowfield	100	-21.35 ± 10.15	-8.6 ± 4.1	-0.3 ± 0.1
Beartooth-Absaroka	23	-83.97 ± 28.01	-22.5 ± 7.5	-0.7 ± 0.2
Glacier	6	-78.97 ± 23.29	-25.6 ± 7.6	-0.8 ± 0.2
Snowfield	17	-5.00 ± 4.72	-7.7 ± 7.2	-0.2 ± 0.2
1990	**10**	**-53.32 ± 28.52**	**-11.5 ± 6.2**	**-0.4 ± 0.2**
OR Cascades	10	-53.32 ± 28.52	-11.5 ± 6.2	-0.4 ± 0.2
Glacier	4	-51.47 ± 26.73	-11.9 ± 6.2	-0.5 ± 0.2
Snowfield	6	-1.85 ± 1.79	-6.3 ± 6.1	-0.2 ± 0.2
1995	**1**	**0.16 ± 0.07**	**18.4 ± 7.7**	**0.7 ± 0.3**
Sierra Nevada	1	0.16 ± 0.07	18.4 ± 7.7	0.7 ± 0.3
Snowfield	1	0.16 ± 0.07	18.4 ± 7.7	0.7 ± 0.3

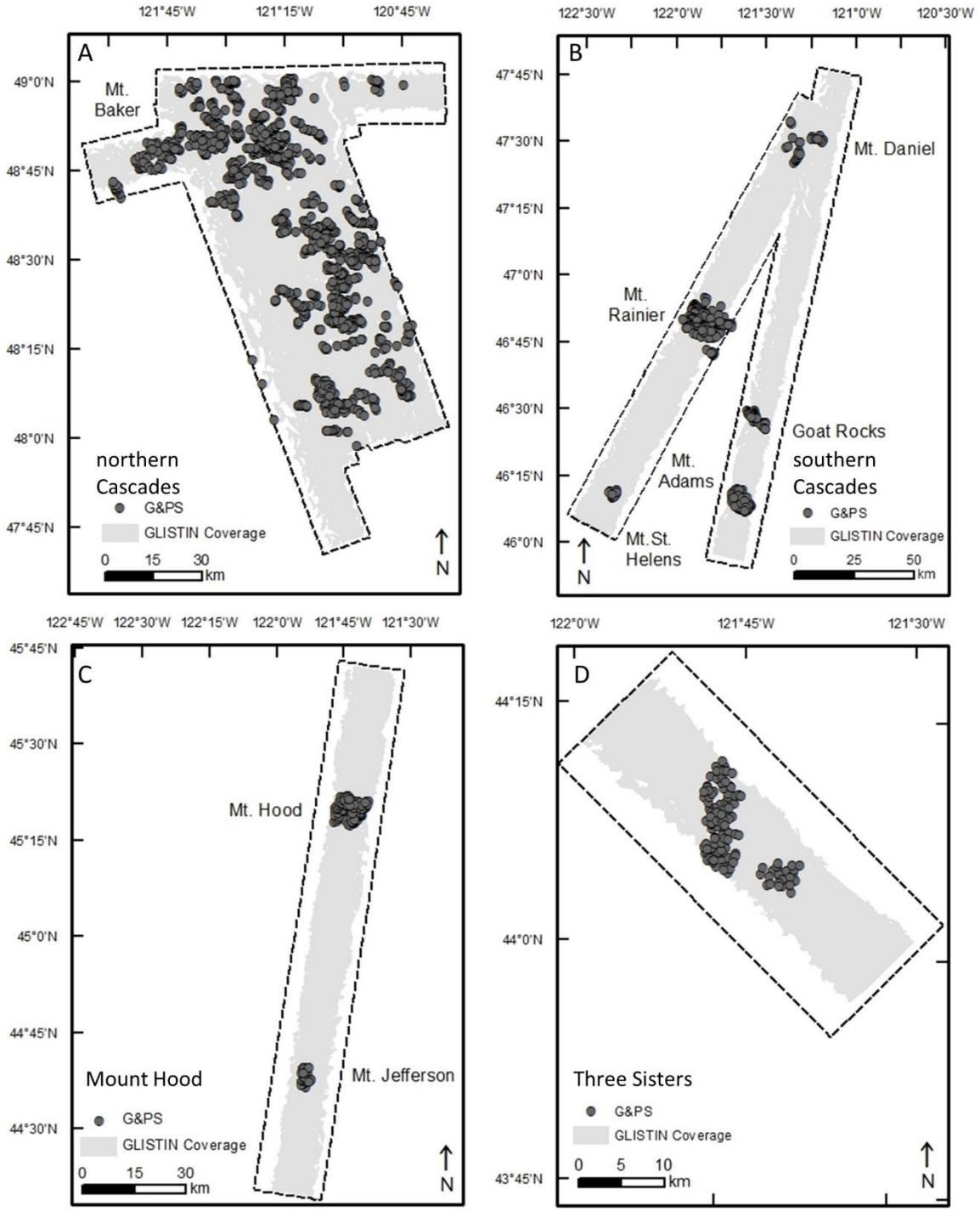

Figure A1. GLISTIN coverage for mountain ranges in Washington (A and B) and Oregon (C and D). Dark grey points represent glaciers and perennial snowfields (G&PS). G&PS location is based on U.S. Geological Survey 1:240000 topographic map series. Light grey outlines represent the 2016 GLISTIN coverage. The black dashed box is the maximum extent of the GLISTIN flights. The white space inside the maximum extent represents missing data. See Figure **1** for the location of coverage.

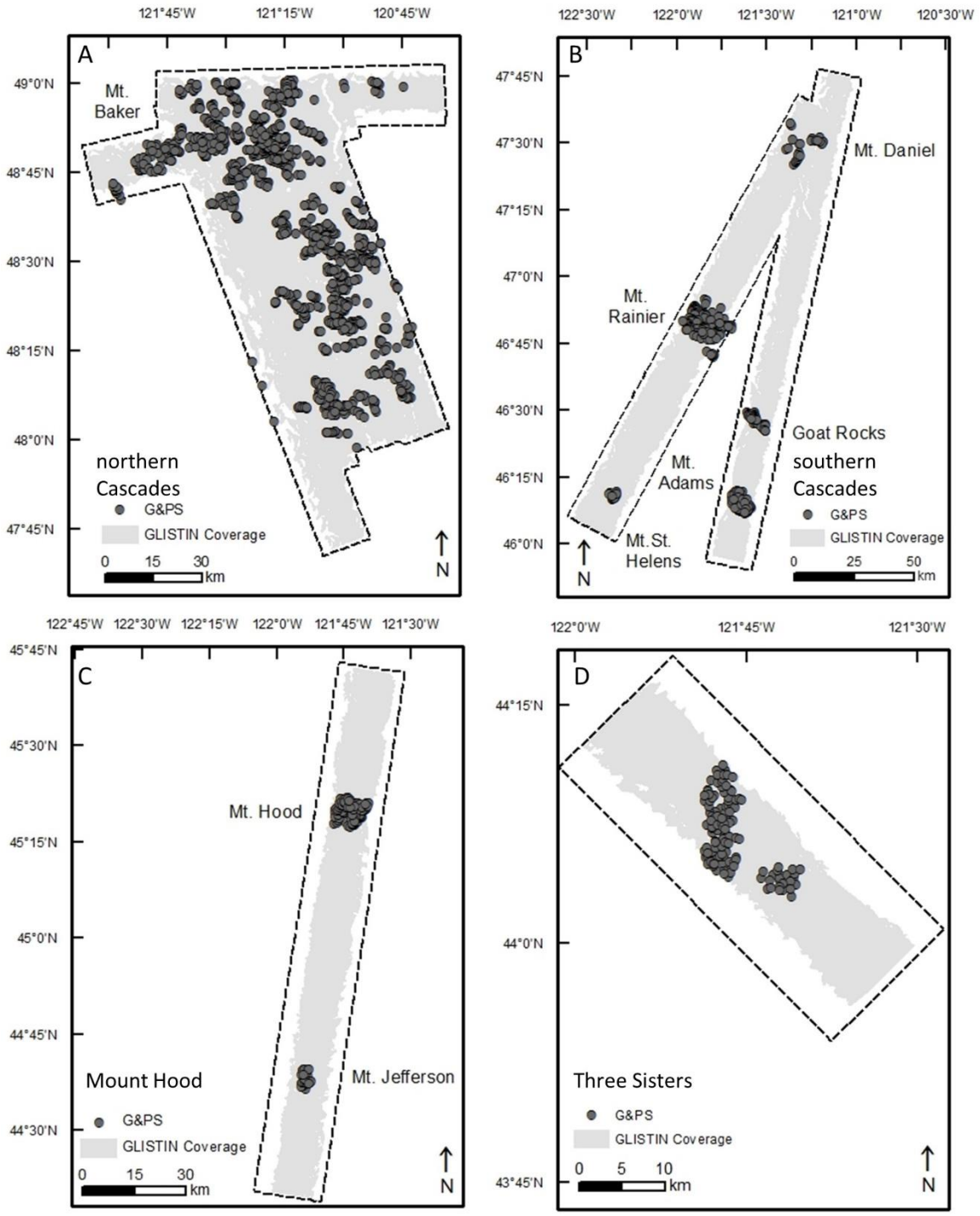

Figure A2. GLISTIN coverage for mountain ranges in Montana (A and B) and Wyoming (C and D). Dark grey points represent glaciers and perennial snowfields (G&PS). G&PS location is based on U.S. Geological Survey 1:240000 topographic map series. Light grey outlines represent the 2016 GLISTIN coverage. The black dashed box is the maximum extent of the GLISTIN flights. The white space inside the maximum extent represents missing data. See Figure **1** for the location of coverage.

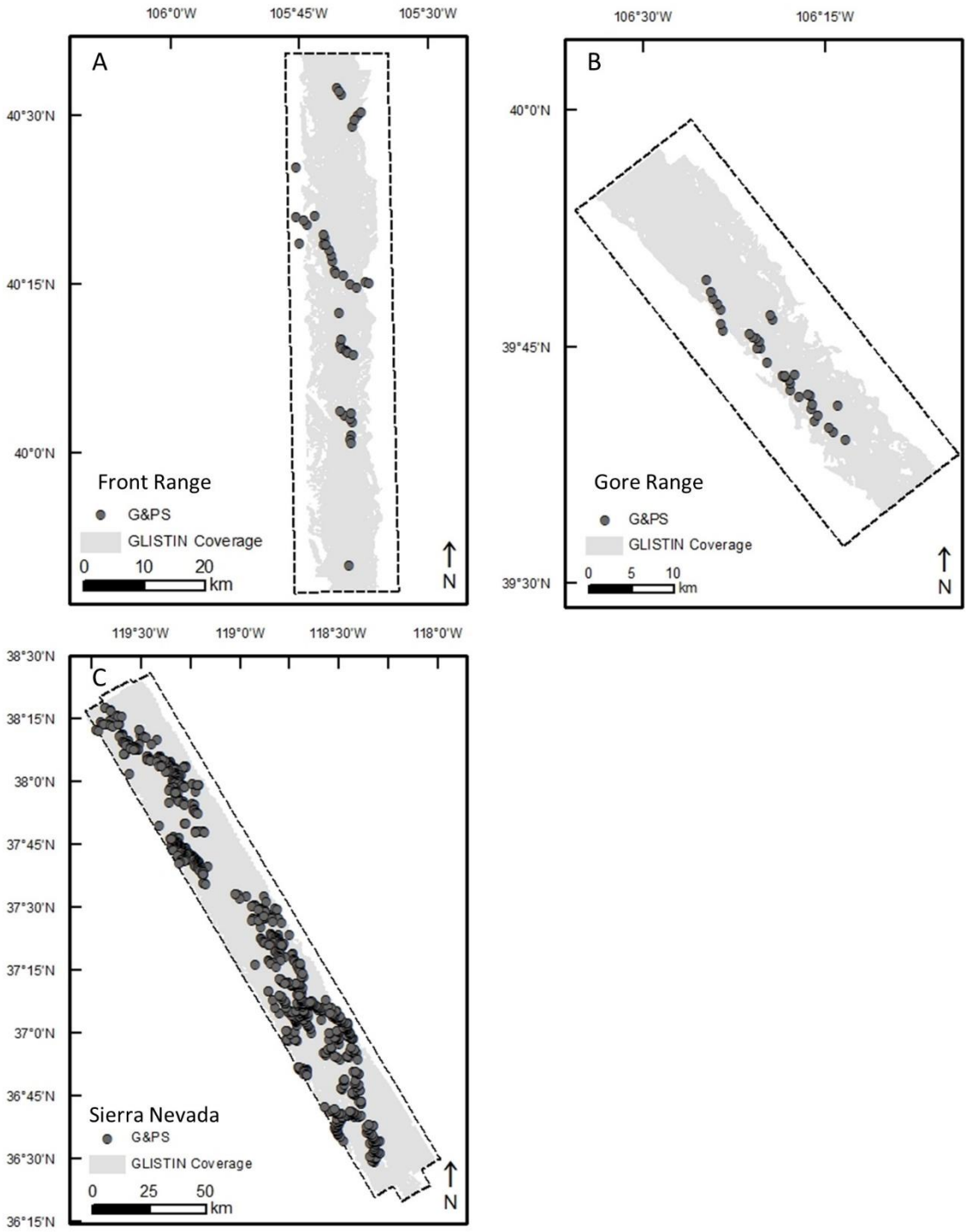

Figure A3. GLISTIN coverage for mountain ranges in Colorado (A and B) and California (C). Dark grey points represent glaciers and perennial snowfields (G&PS). G&PS location is based on U.S. Geological Survey 1:240000 topographic map series. Light grey outlines represent the 2016 GLISTIN coverage. The black dashed box is the maximum extent of the GLISTIN flights. The white space inside the maximum extent represents missing data. See Figure 1 for the location of coverage.

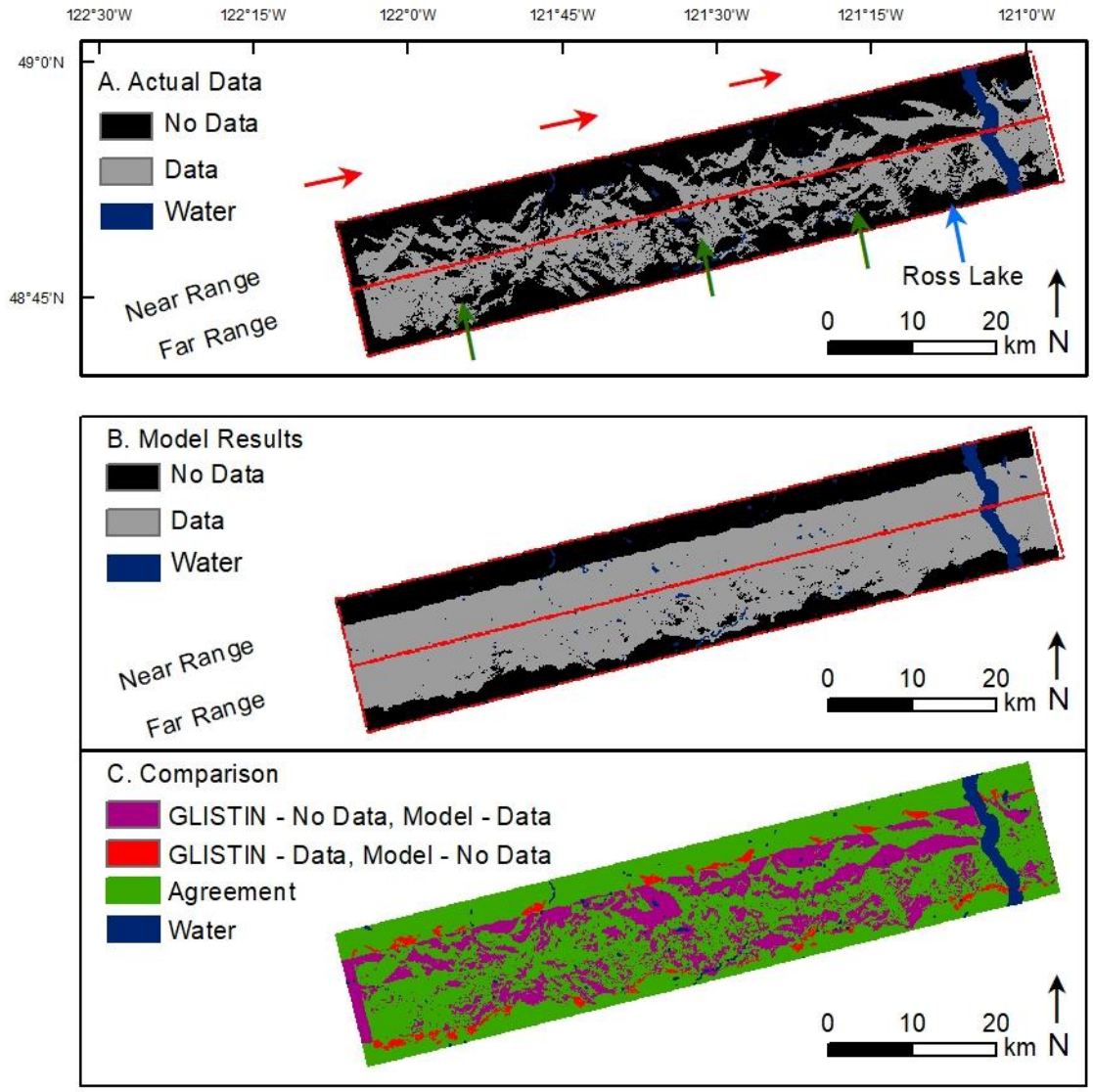

Figure A4. GLISTIN coverage for the 257° direction flight over the North Cascades, WA. Panel A shows the data collected by GLISTIN, Panel B shows the modeled results from the viewshed analysis, and Panel C shows a comparison between the observed and modeled data. The red arrows in panel A are examples of indents of missing data thought to be the result of radar foreshortening and layover.

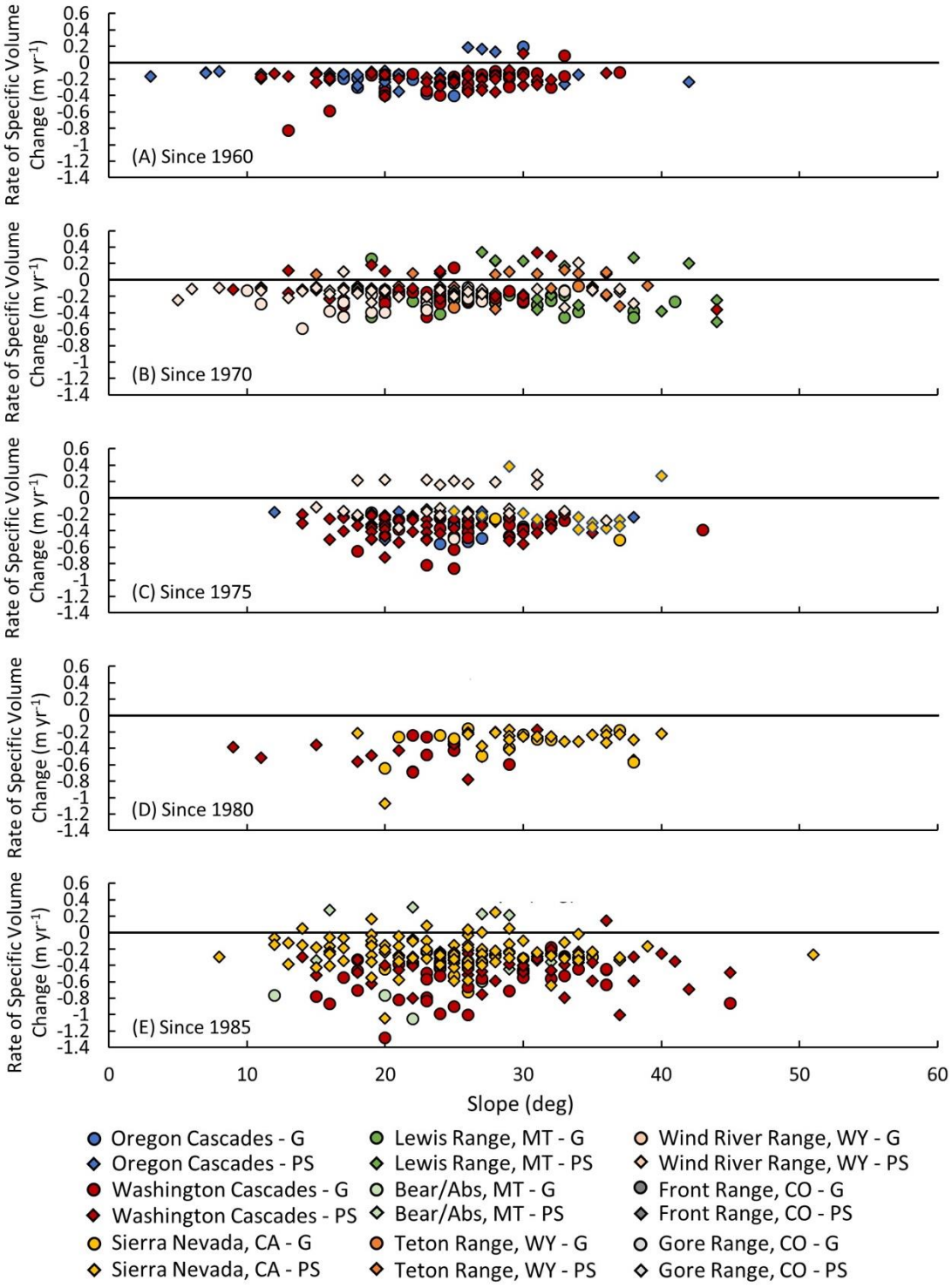

Figure A5. Rate of Specific volume change versus slope for all glaciers and perennial snowfields.

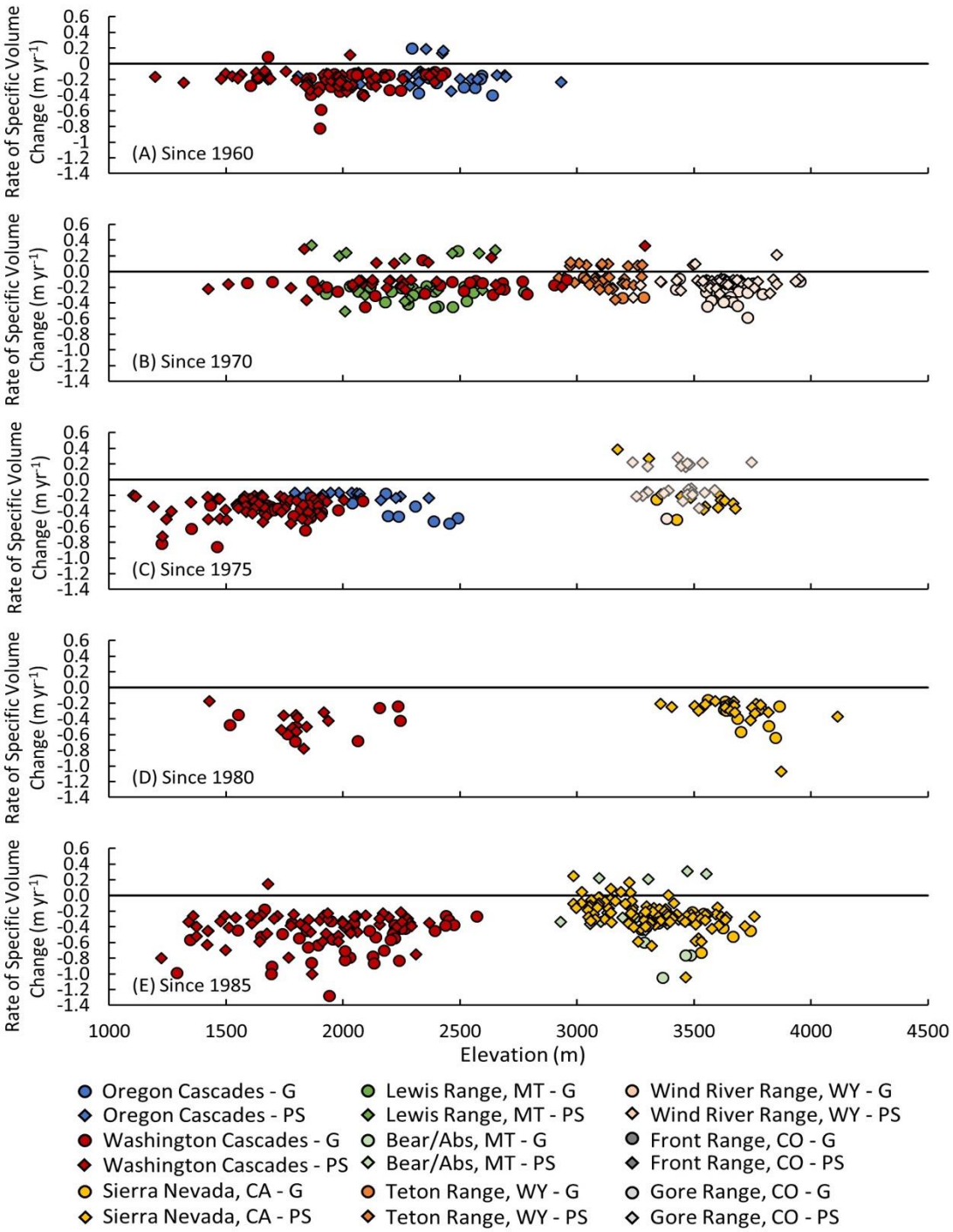

Figure A5. Rate of specific volume change versus slope for all glaciers and perennial snowfields.

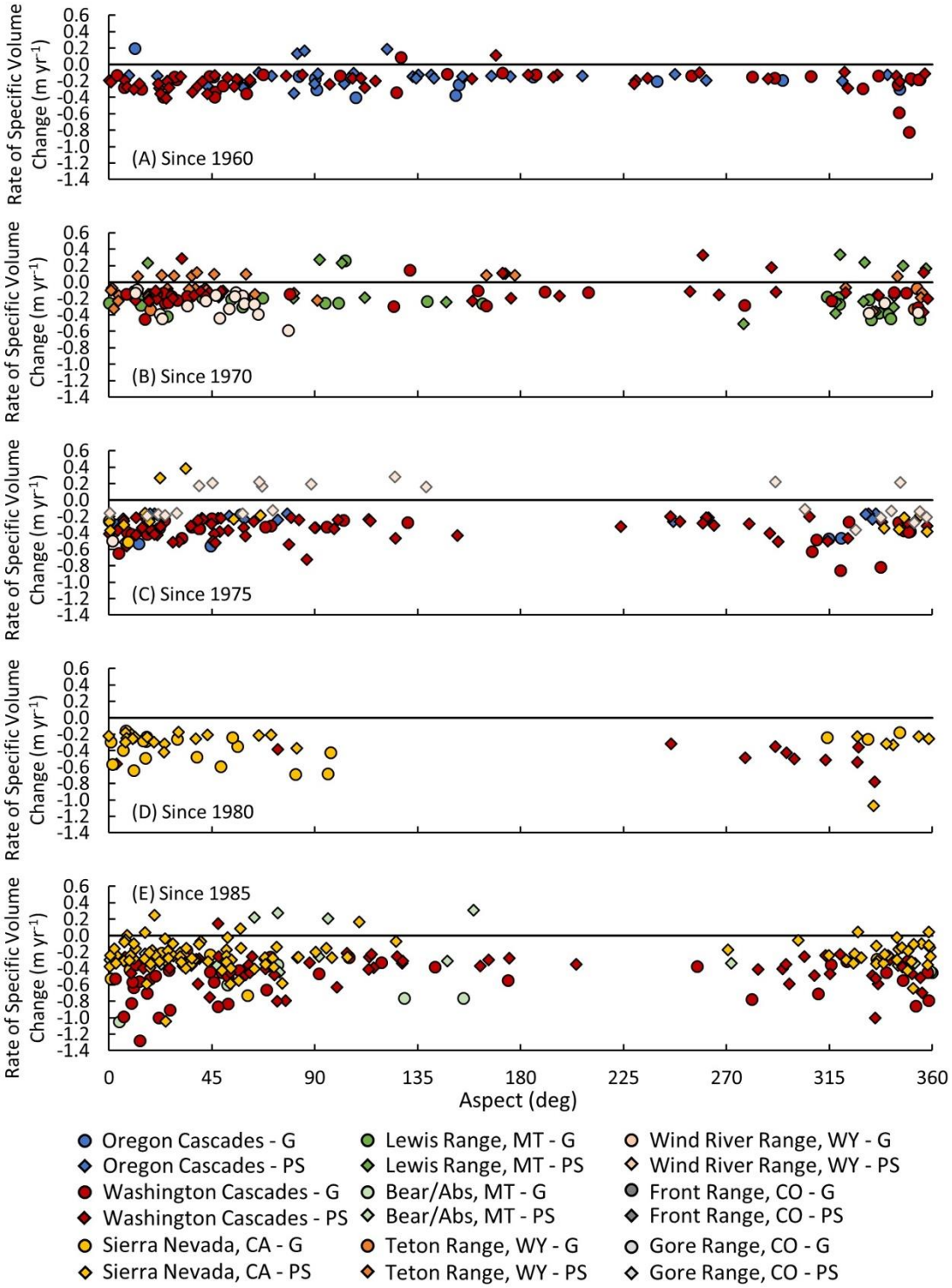

Figure A7. Rate of specific volume change versus aspect for all glaciers and perennial snowfields.

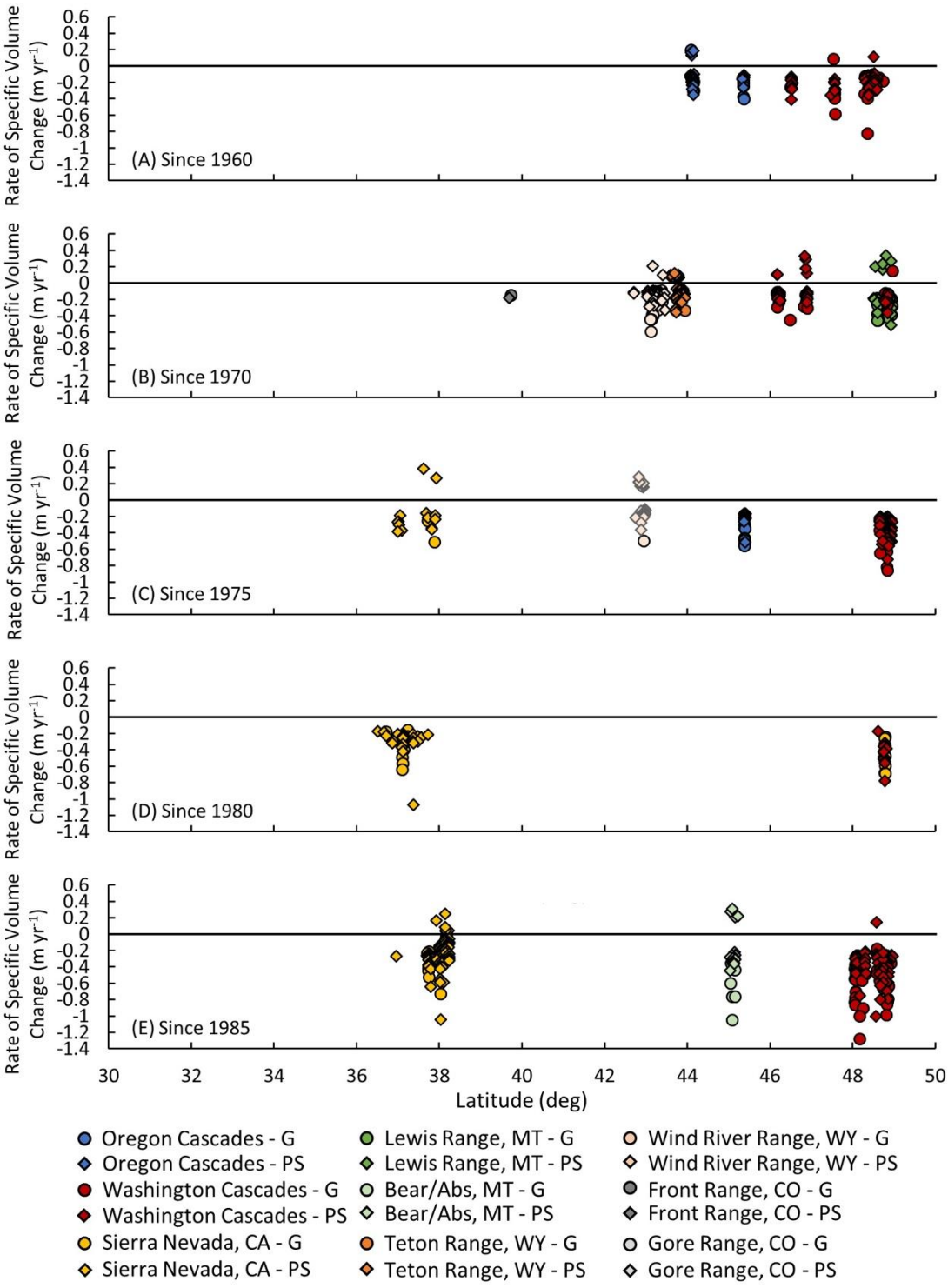

Figure A8. Rate of specific volume change versus latitude for all glaciers and perennial snowfields.

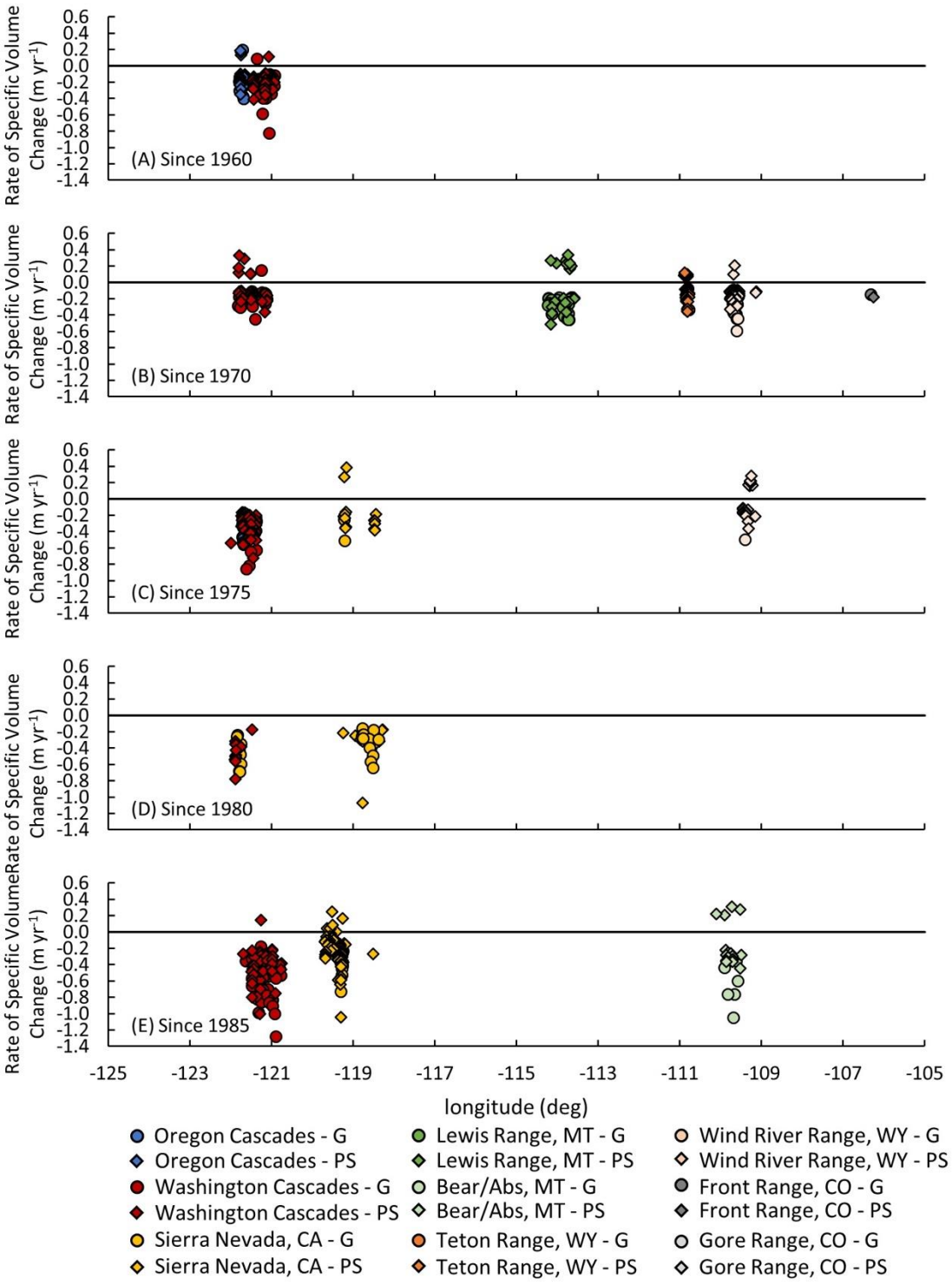

Figure A9. Rate of specific volume change versus longitude for all glaciers and perennial snowfields.

Appendix B: Probability Density Functions

Probability density functions (pdf) were plotted for missing data and all pixels within a G&PS outline, as well as the ratio, for each topographic variable of slope, aspect, and elevation to examine if topography had an influence on missing data (Figures B1-B17). If missing data were uniformly distributed over the terrain, then the pdf for the missing data would match that of the terrain data and the ratio would be constant at one. Any variability in the distribution of missing data would result in a pdf different from the terrain pdf. The pdf ratio for slope follows similar patterns for all regions; however, the magnitude and peak vary between regions. For slope, the ratio is < 1 for small slopes (< 20°) and > 1 for slopes between about 20° and 35°. For elevation, the pdf ratio tends to be > 1 at higher elevations for all regions. For some regions, also a pdf ratio > 1 also occurs at lower elevations, most notable at Mount Hood, OR (Fig. A18). No clear pattern exists for aspects for any region. This is probably the result of the flight direction of GLISTIN, the number of flights used for the mosaicked DEM, and the overall aspect of the terrain.

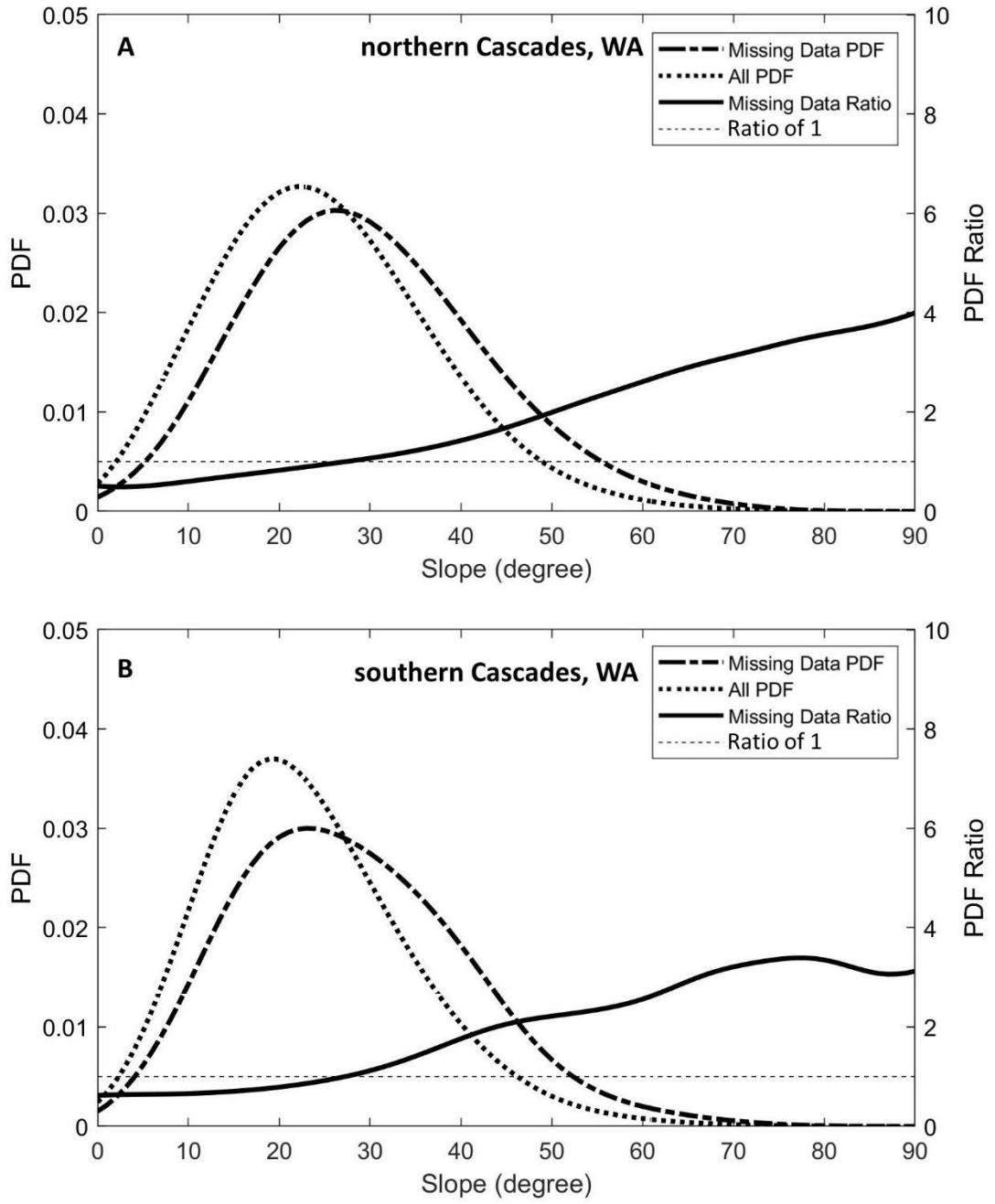

Figure B1. Plots of probability density functions (pdf) and pdf ratios of slope for all glacier and perennial snowfield (G&PS) surfaces and the missing data on G&PS surfaces for the northern Cascades, WA (A), and the southern Cascades, WA (B).

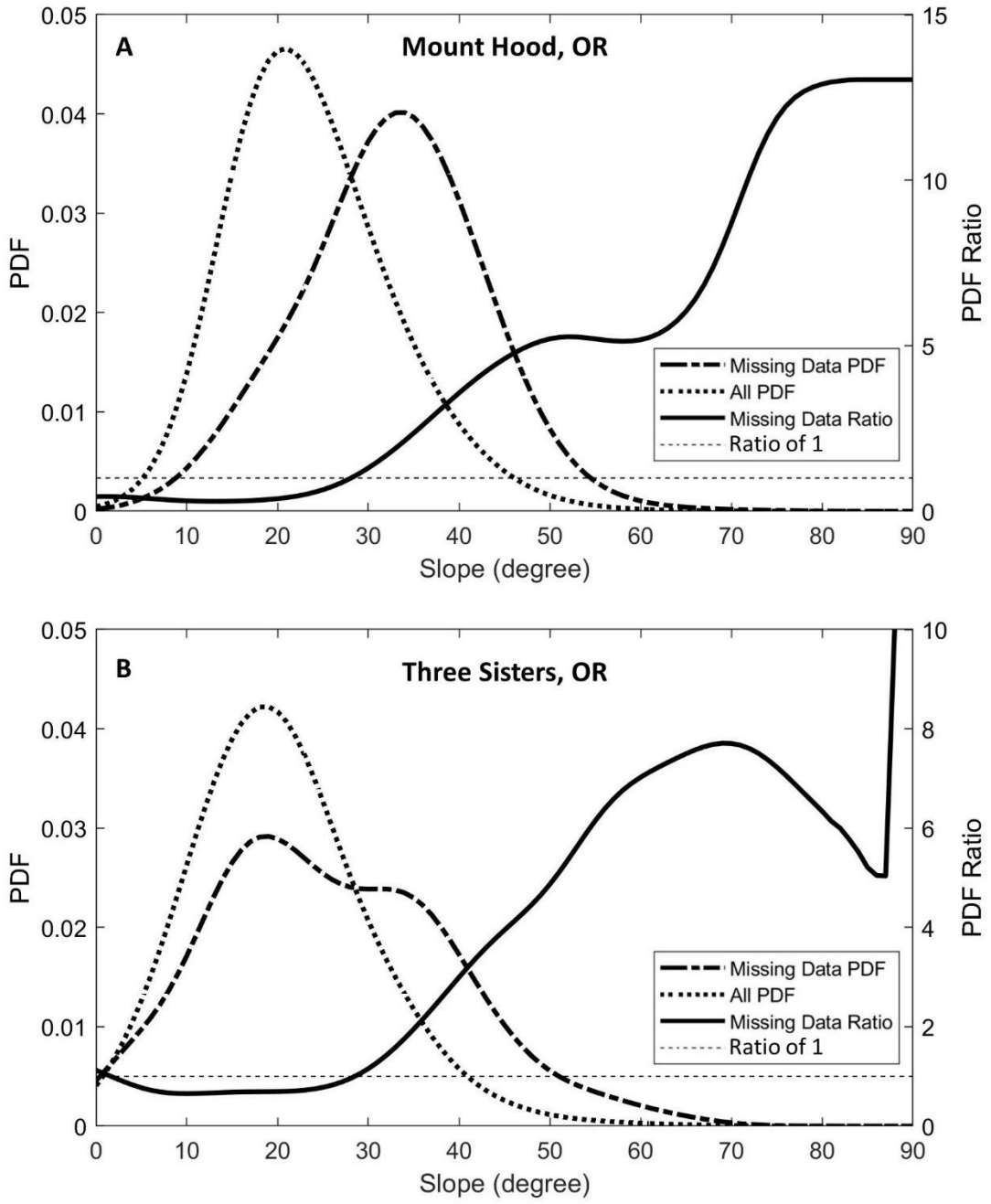

Figure B2. Plots of probability density functions (pdf) and pdf ratios of slope for all glacier and perennial snowfield (G&PS) surfaces and the missing data on G&PS surfaces for the Mount Hood, OR (A), and Three Sisters, OR (B).

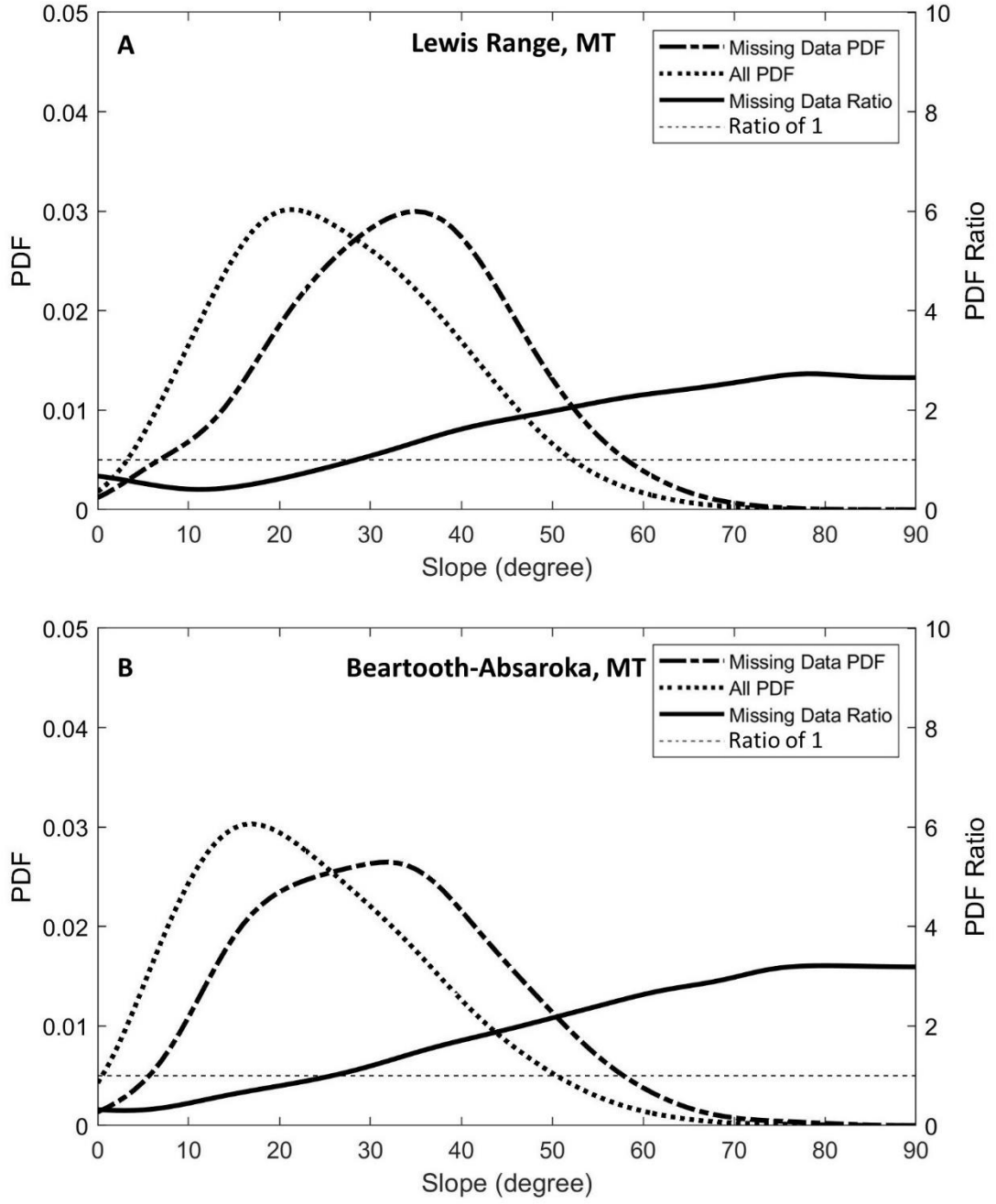

Figure B3. Plots of probability density functions (pdf) and pdf ratios of slope for all glacier and perennial snowfield (G&PS) surfaces and the missing data on G&PS surfaces for the Lewis Range, MT (A), and the Beartooth-Absaroka Range, MT (B).

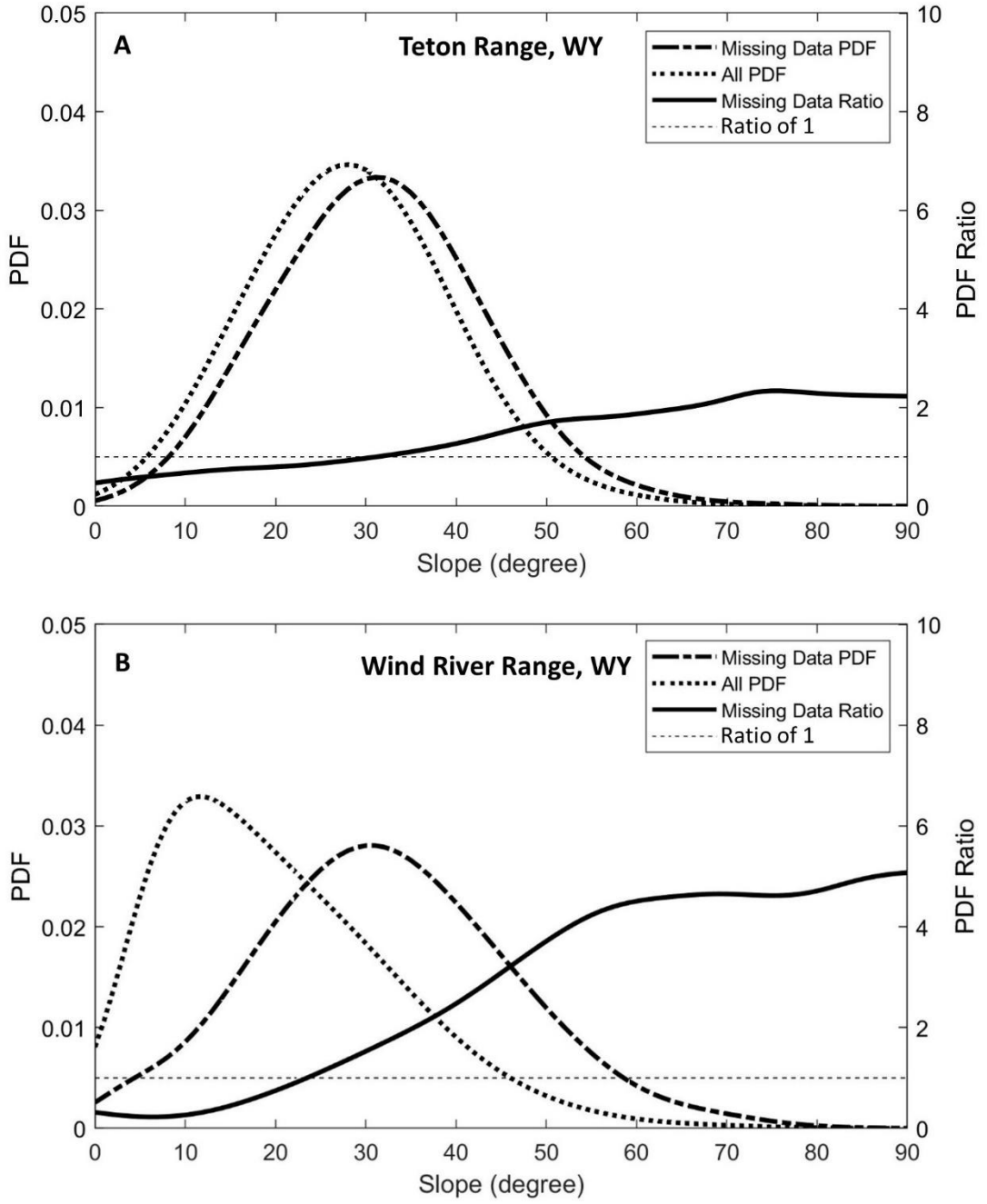

Figure B4. Plots of probability density functions (pdf) and pdf ratios of slope for all glacier and perennial snowfield (G&PS) surfaces and the missing data on G&PS surfaces for the Teton Range, WY (A), and the Wind River Range WY (B).

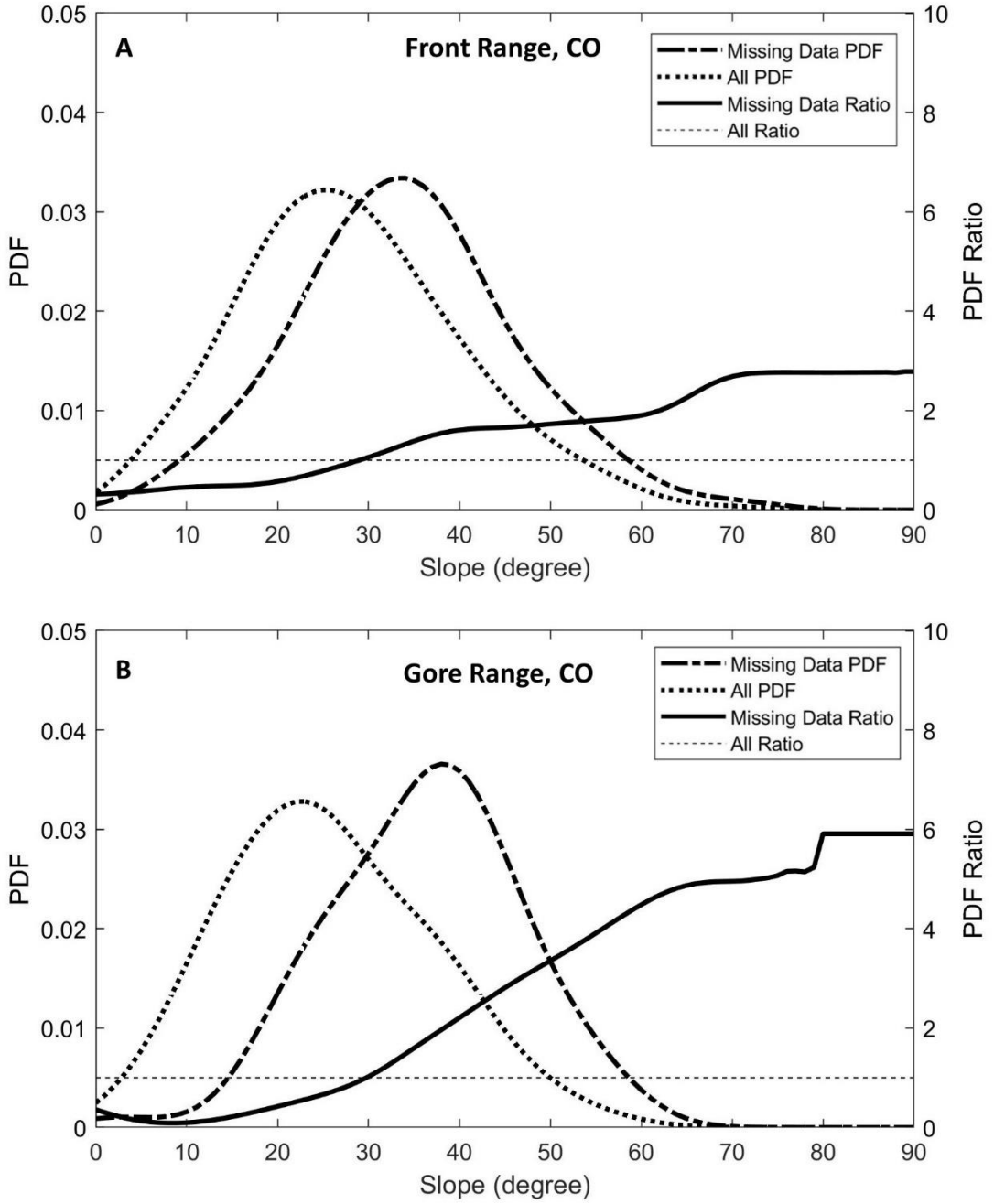

Figure B5. Plots of probability density functions (pdf) and pdf ratios of slope for all glacier and perennial snowfield (G&PS) surfaces and the missing data on G&PS surfaces for the Front Range, CO (A), and the Gore Range, CO (B).

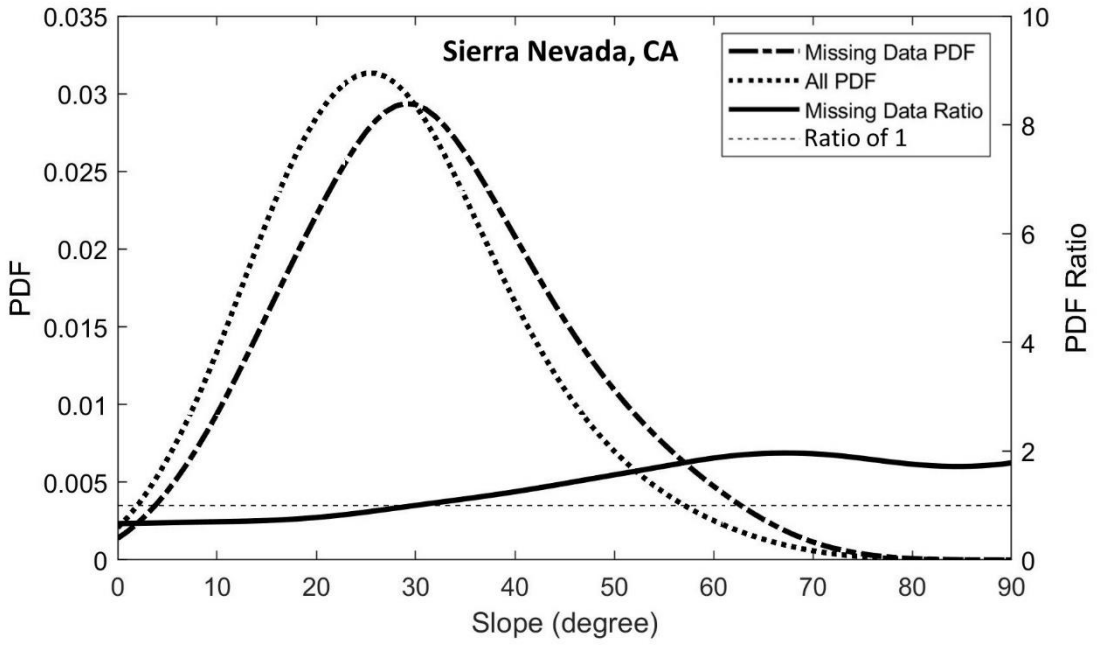

Figure B6. Plots of probability density functions (pdf) and pdf ratios of slope for all glacier and perennial snowfield (G&PS) surfaces and the missing data on G&PS surfaces for the Sierra Nevada, CA.

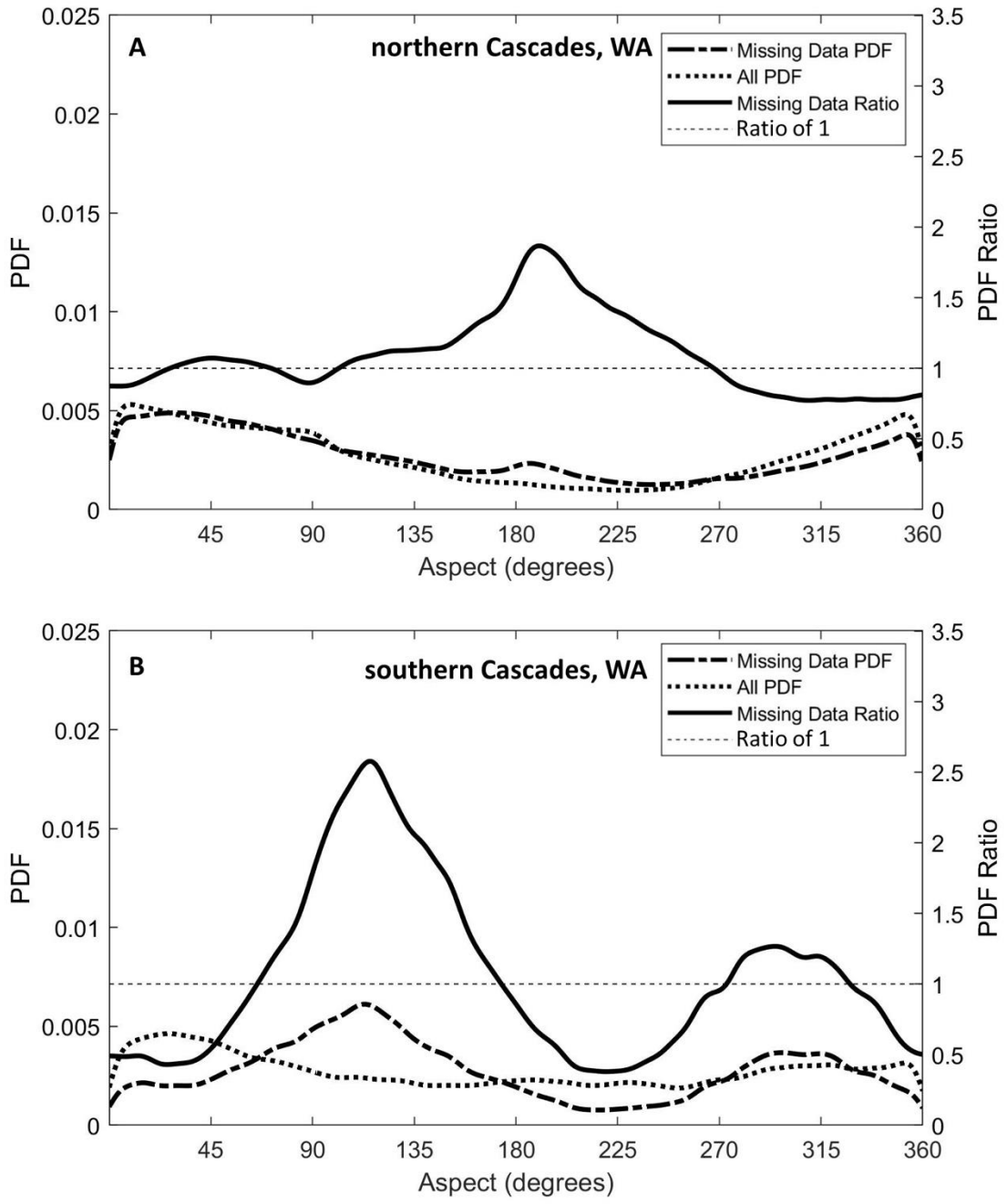

Figure B7. Plots of probability density functions (pdf) and pdf ratios of aspect for all glacier and perennial snowfield (G&PS) surfaces and the missing data on G&PS surfaces for the northern Cascades, WA (A), and the southern Cascades, WA (B).

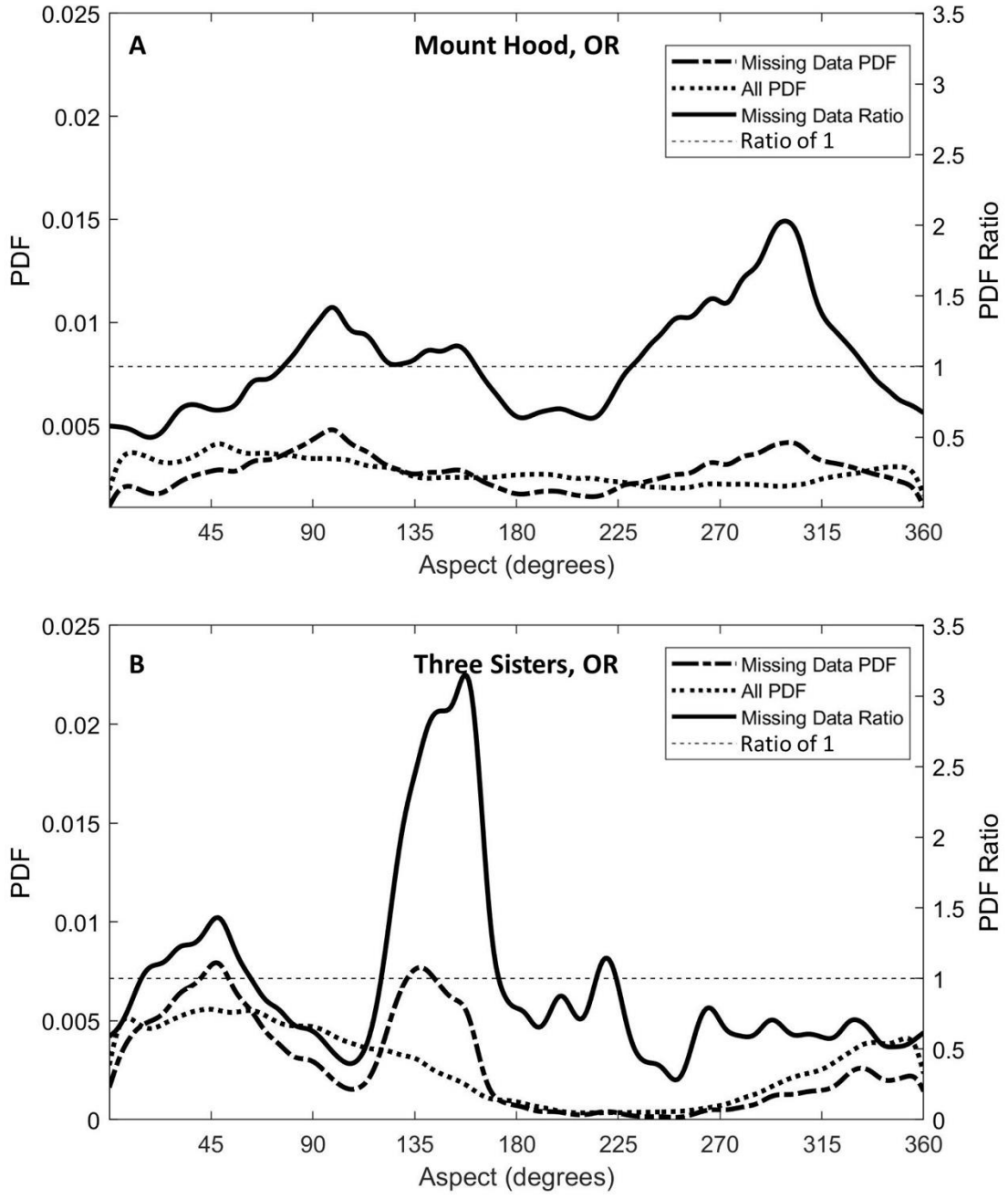

Figure B8. Plots of probability density functions (pdf) and pdf ratios of aspect for all glacier and perennial snowfield (G&PS) surfaces and the missing data on G&PS surfaces for the Mount Hood, OR (A), and Three Sisters, OR (B).

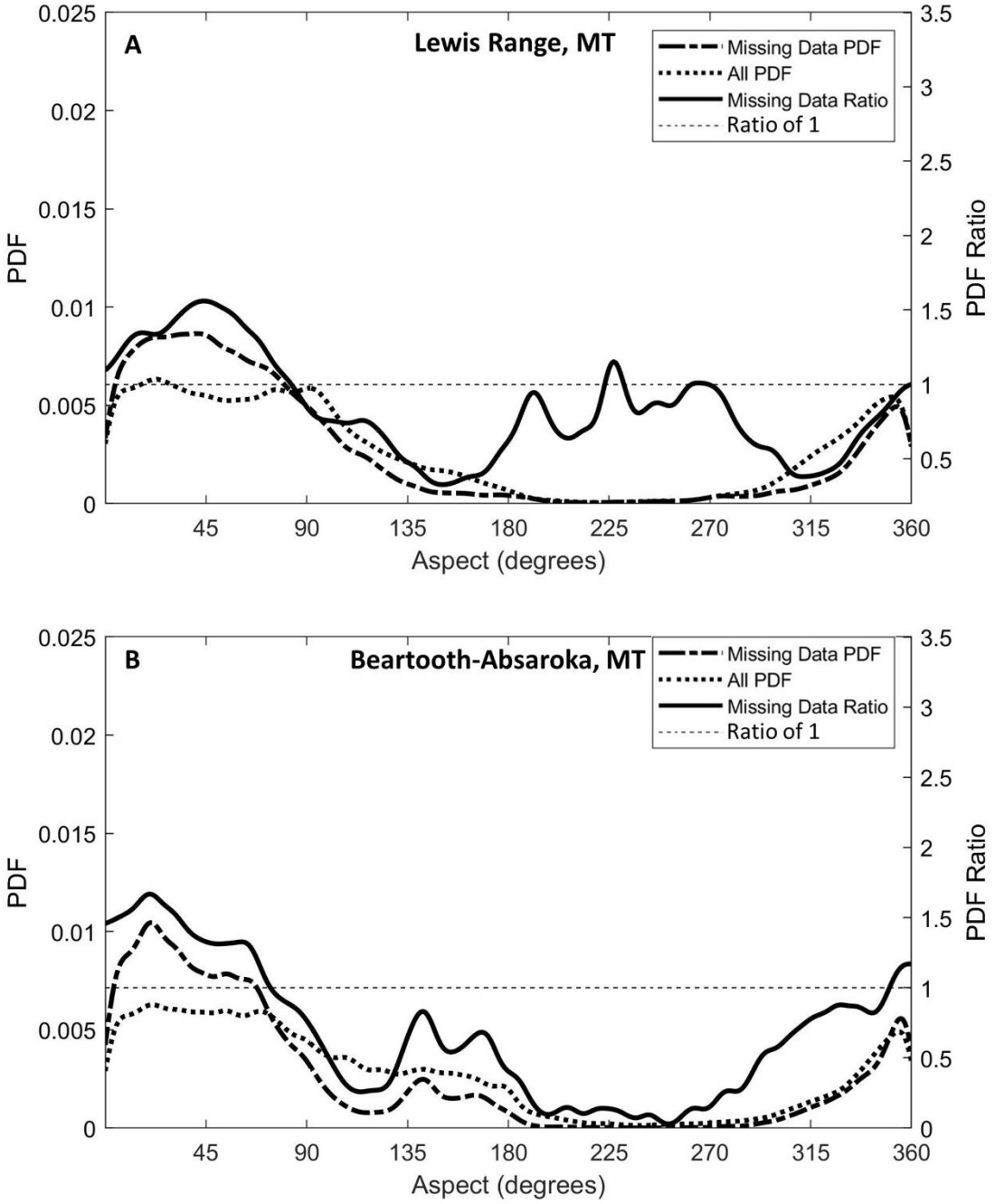

Figure B9. Plots of probability density functions (pdf) and pdf ratios of aspect for all glacier and perennial snowfield (G&PS) surfaces and the missing data on G&PS surfaces for the Lewis Range, MT (A), and Beartooth-Absaroka Range, MT (B).

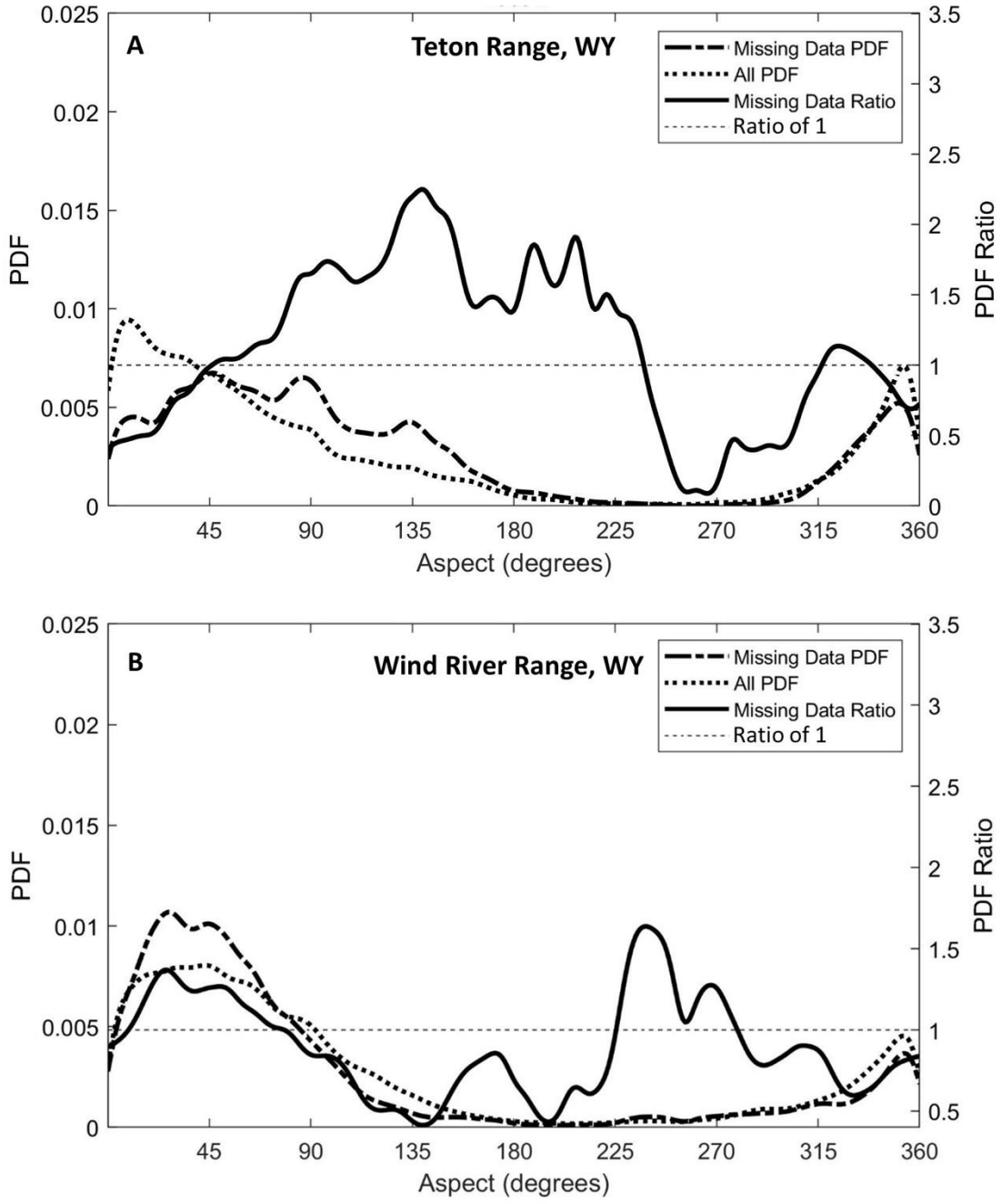

Figure B10. Plots of probability density functions (pdf) and pdf ratios of aspect for all glacier and perennial snowfield (G&PS) surfaces and the missing data on G&PS surfaces for the Teton Range, WY (A), and the Wind River Range WY (B).

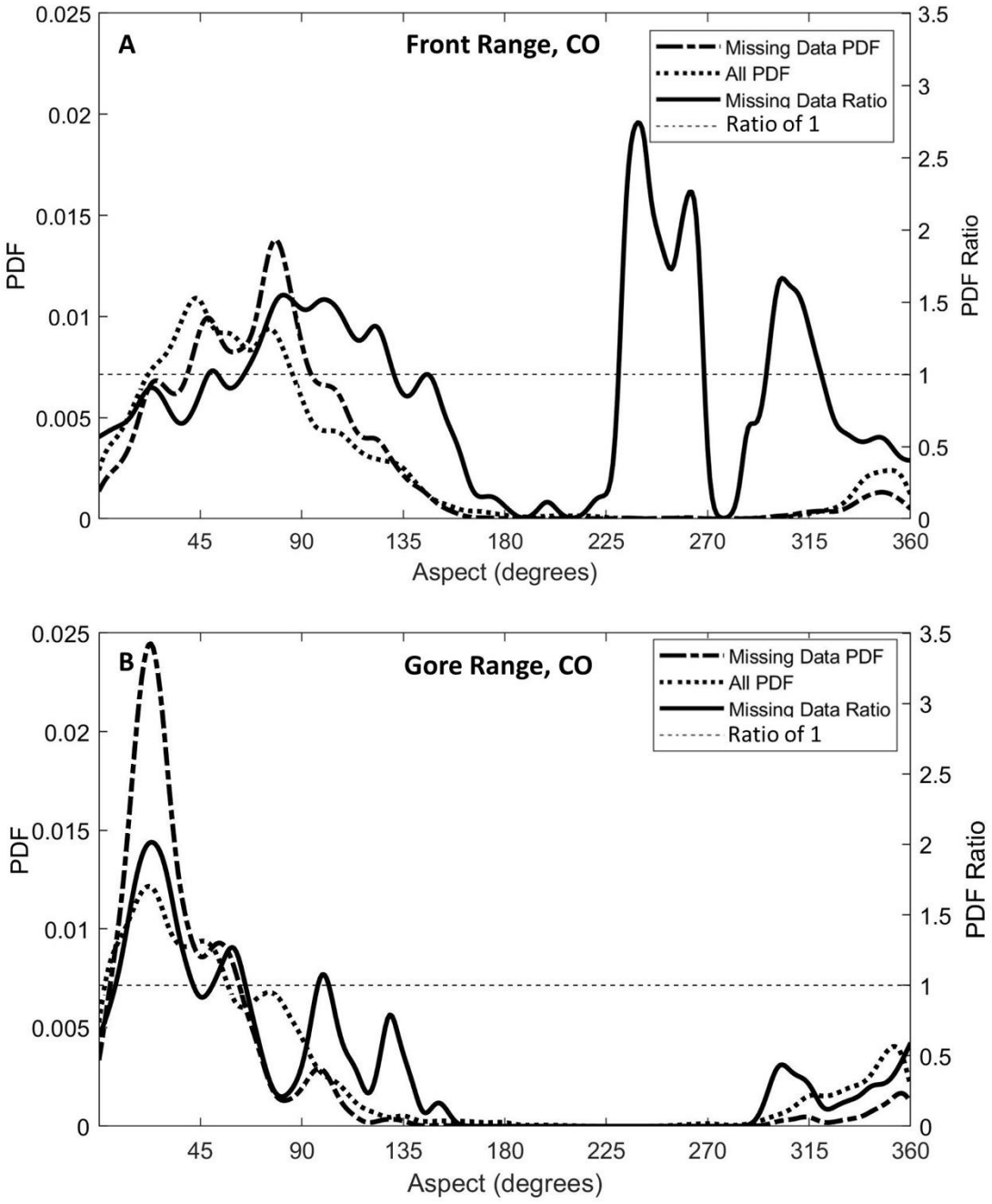

Figure B11. Plots of probability density functions (pdf) and pdf ratios of aspect for all glacier and perennial snowfield (G&PS) surfaces and the missing data on G&PS surfaces for the Front Range, CO (A), and the Gore Range, CO (B).

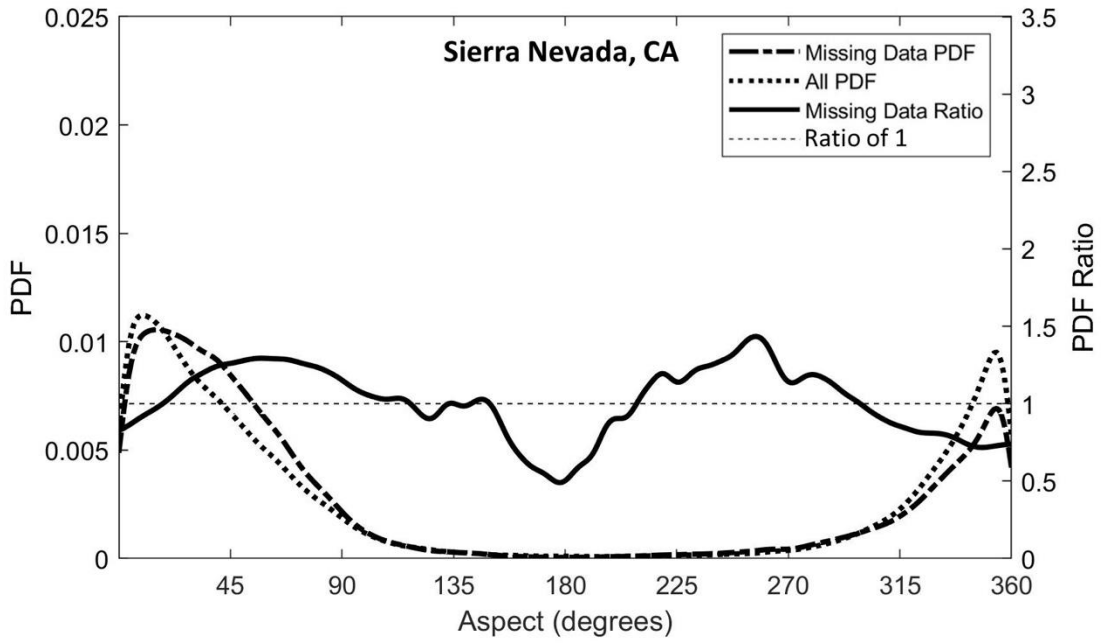

Figure B12. Plots of probability density functions (pdf) and pdf ratios of aspect for all glacier and perennial snowfield (G&PS) surfaces and the missing data on G&PS surfaces for the Sierra Nevada, CA.

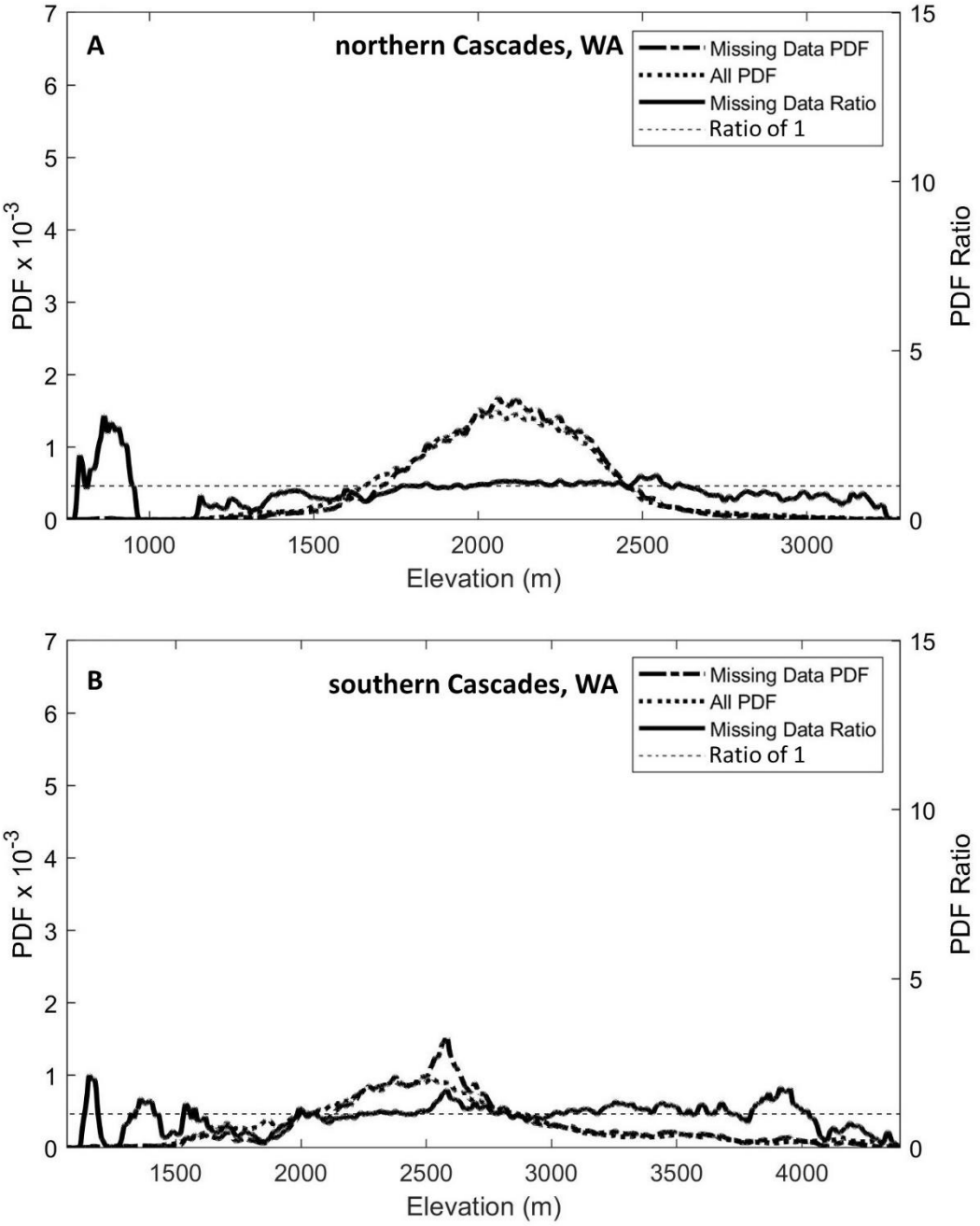

Figure B13. Plots of probability density functions (pdf) and pdf ratios of elevation for all glacier and perennial snowfield (G&PS) surfaces and the missing data on G&PS surfaces for the northern Cascades, WA (A), and the southern Cascades, WA (B).

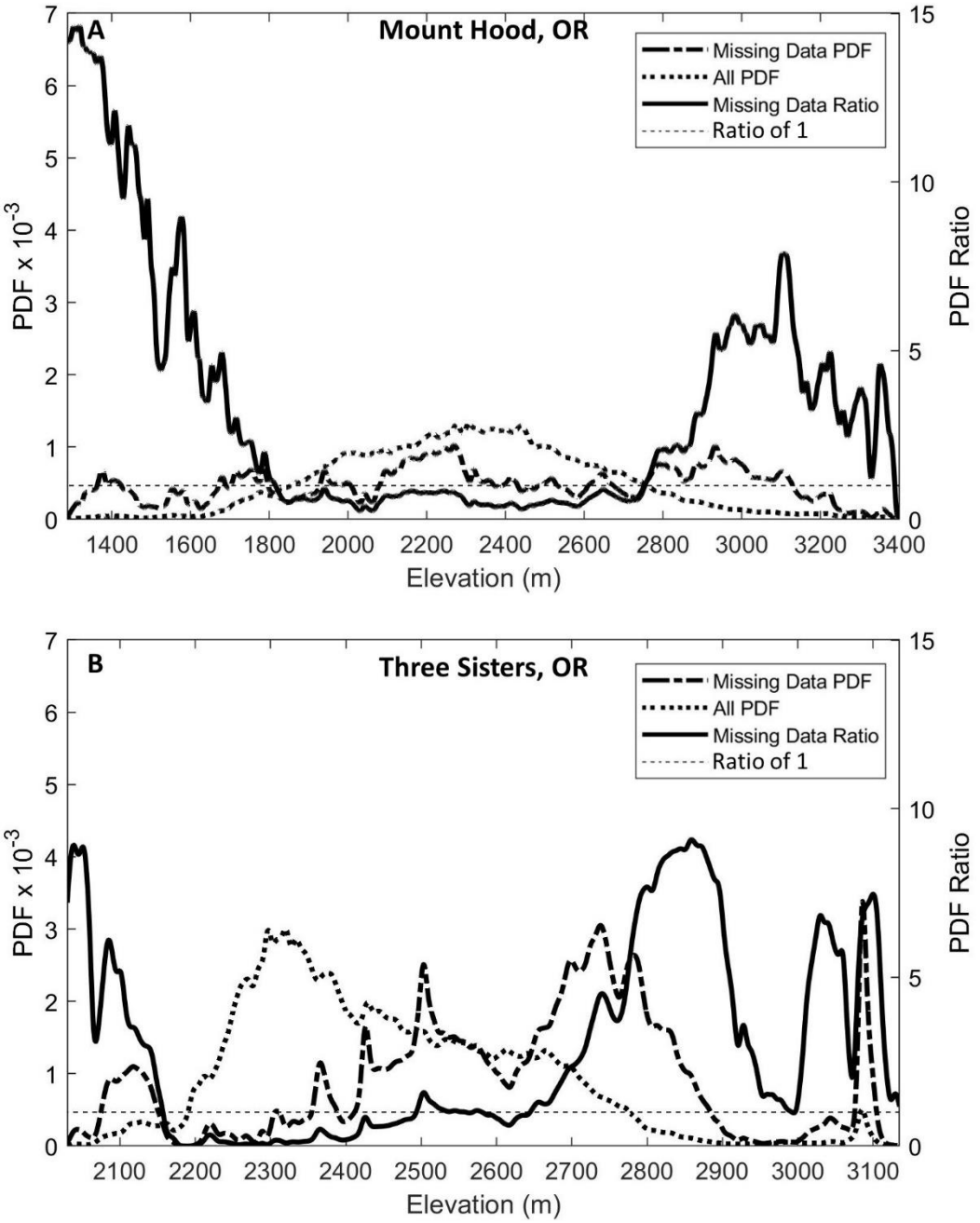

Figure B14. Plots of probability density functions (pdf) and pdf ratios of elevation for all glacier and perennial snowfield (G&PS) surfaces and the missing data on G&PS surfaces for the Mount Hood, OR (A), and Three Sisters, OR (B).

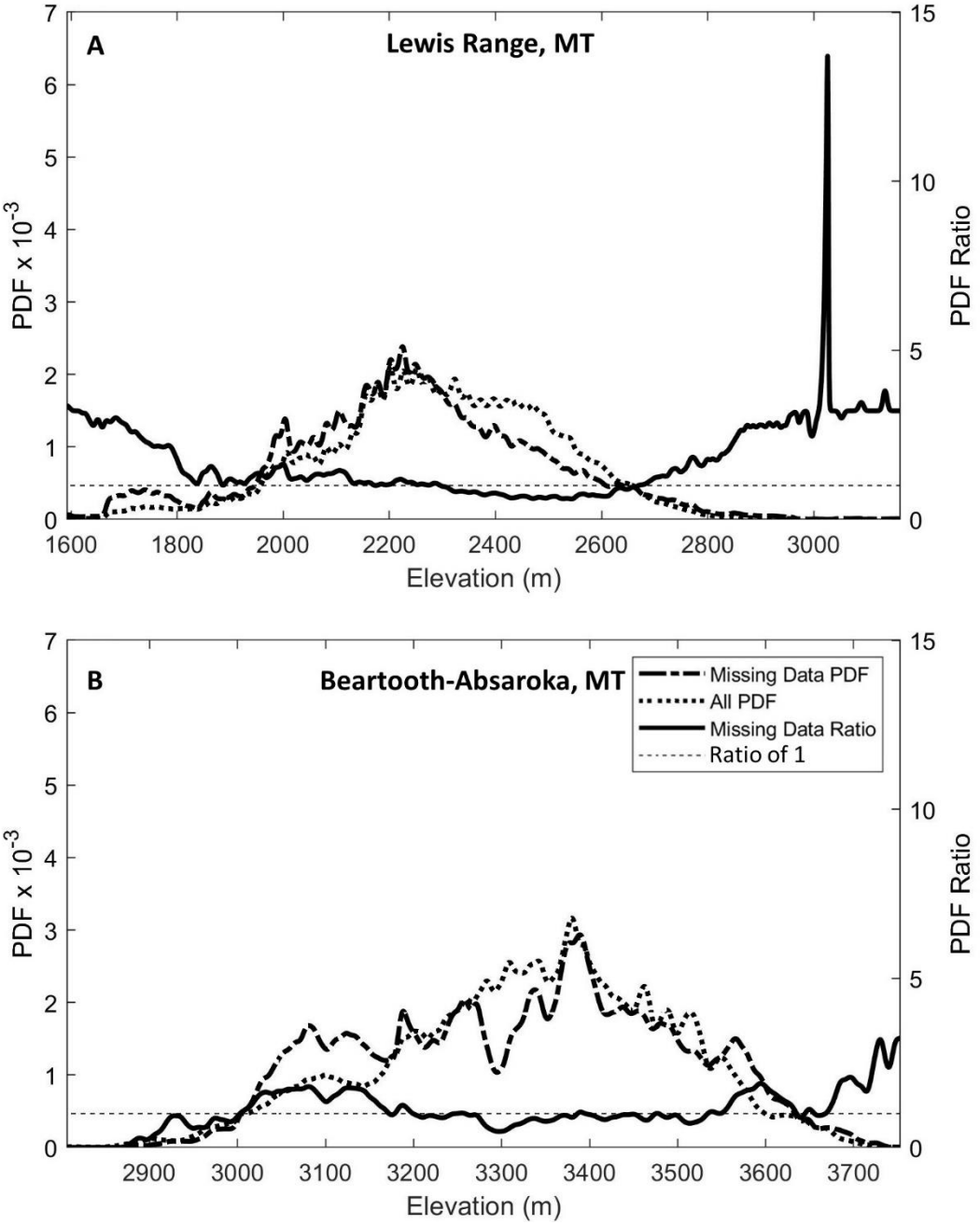

Figure B15. Plots of probability density functions (pdf) and pdf ratios of elevation for all glacier and perennial snowfield (G&PS) surfaces and the missing data on G&PS surfaces for the Lewis Range, MT (A), and Beartooth-Absaroka Range, MT (B).

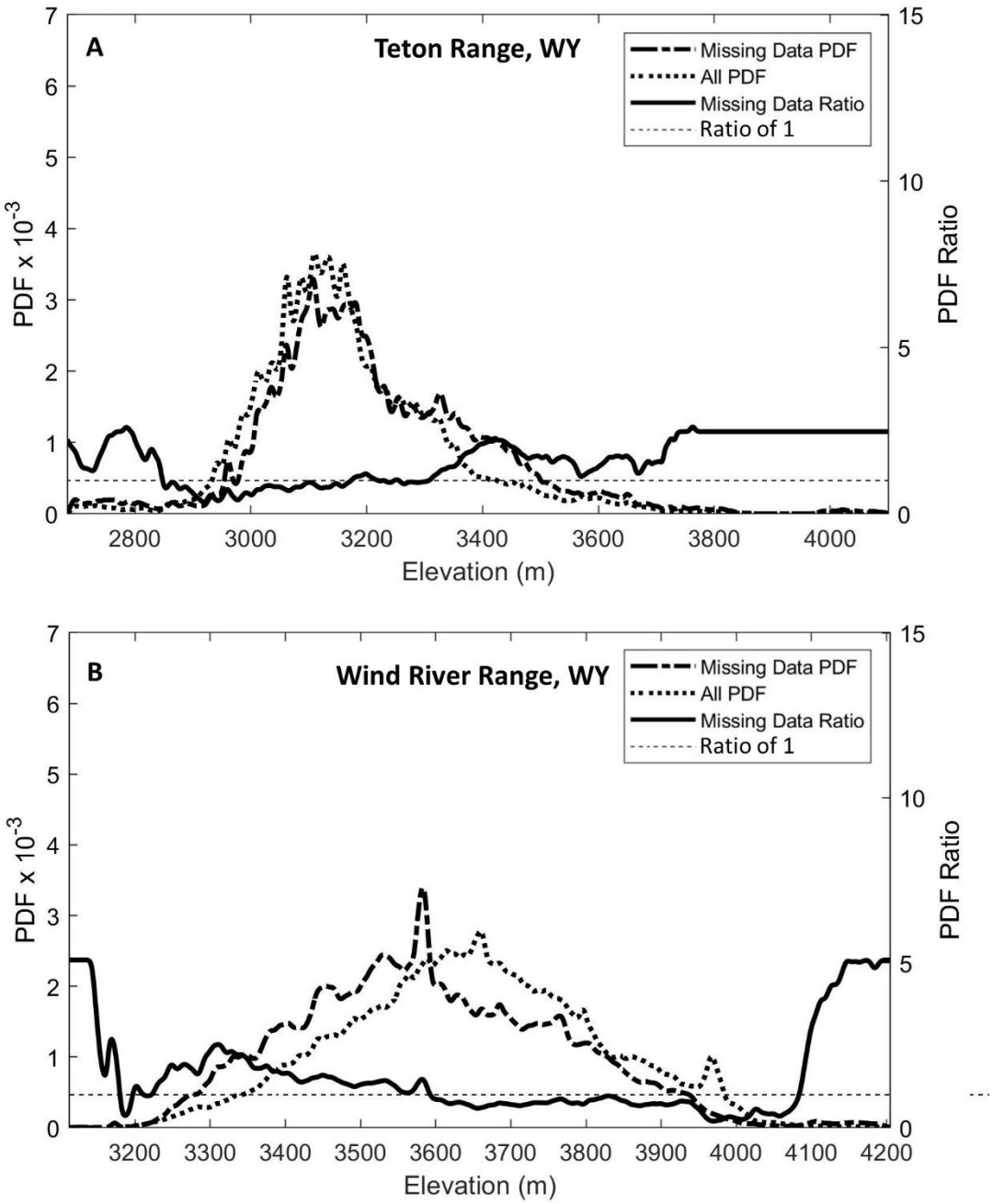

Figure B16. Plots of probability density functions (pdf) and pdf ratios of elevation for all glacier and perennial snowfield (G&PS) surfaces and the missing data on G&PS surfaces for the Grand Teton Range, WY (A), and the Wind River Range, WY (B).

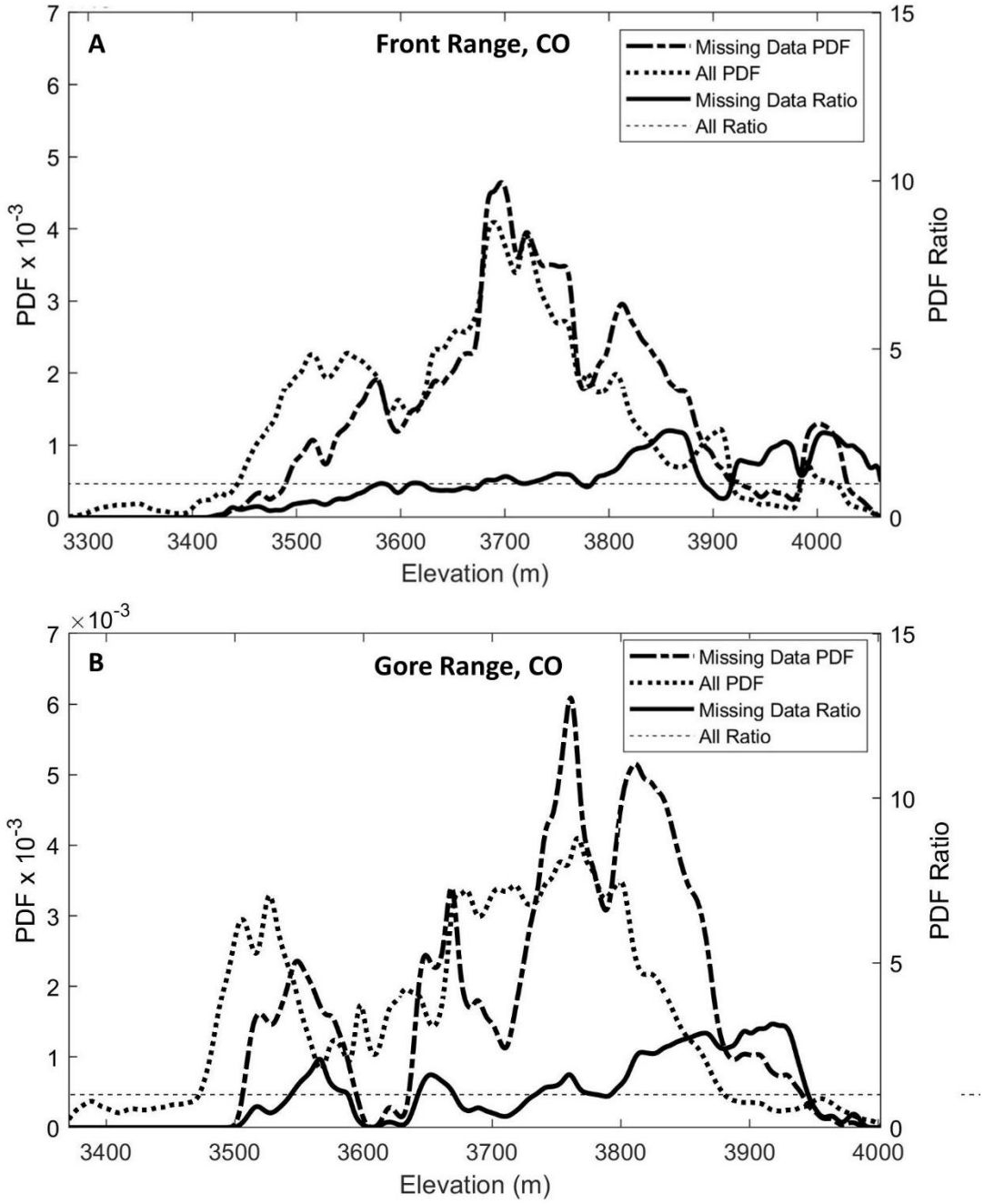

Figure B17. Plots of probability density functions (pdf) and pdf ratios of elevation for all glacier and perennial snowfield (G&PS) surfaces and the missing data on G&PS surfaces for the Front Range, CO (A), and the Gore Range, CO (B).

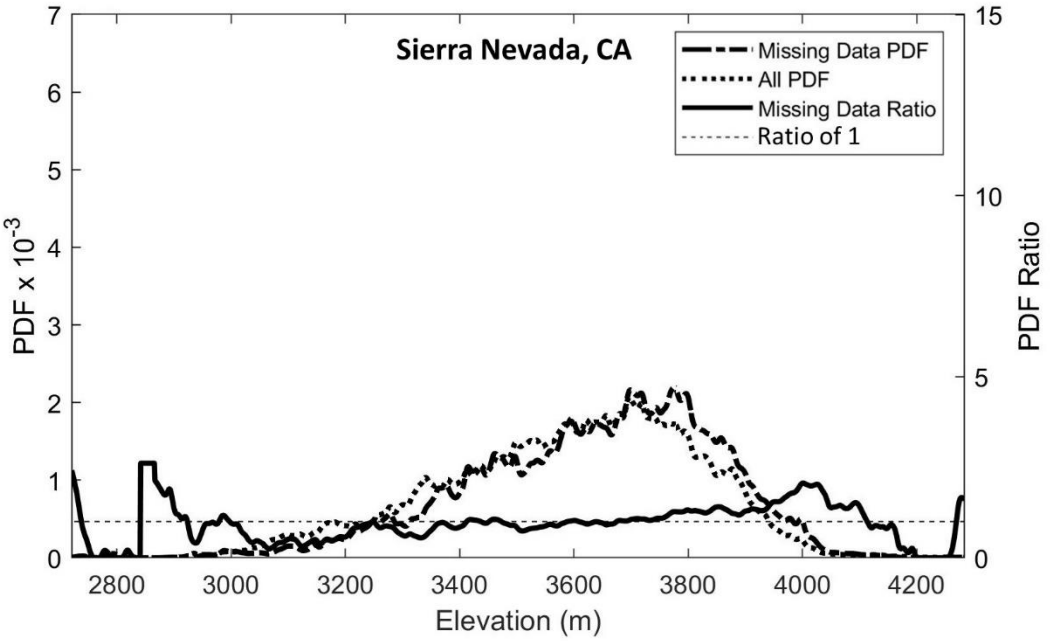

Figure B18. Plots of probability density functions (pdf) and pdf ratios of elevation for all glacier and perennial snowfield (G&PS) surfaces and the missing data on G&PS surfaces for the Sierra Nevada, CA.

Appendix C: Mount Adams Case Study

Mount Adams, WA, was used as a case study since lidar was flown 28 days prior to GLISTIN. GLISTIN was flown over Mount Adams on September 13, 2016 (Fig. B18). Two flights were flown over the mountain, with azimuths of 9.53° and 289.84°. There was an issue with the raw data of the second flight; it was not processed and was not included in the mosaicked DEM. There are 73 G&PS on Mount Adams, of which 66 had at least one pixel of coverage, and the total G&PS area covered was about 20 km^2 representing 86% of the total G&PS area. The height-precision of control zones ranged from 0.17 m to 12.59 m, with an average of 1.35 ± 1.25 m (mean ± standard deviation). For G&PS height-precision ranged from 0.16 m to 11.58 m, with a mean of 1.47 ± 1.15 m (Fig. B19). To understand GLISTIN's sensitivity to terrain, elevation differences were

binned by slope and aspect. Since the flight direction was roughly north (10°) and GLISTIN is a left looking instrument, the look aspect was towards the west. Aspects were split into two categories, aspects facing away from GLISTIN (10° to 190°, roughly west-facing) and aspects facing towards GLISTIN (190° to 360° and 0° to 10°, roughly east-facing). Lidar elevations were subtracted from GLISTIN elevations. Figure B21 shows the elevation differences grouped by slope and orientation for control zones. For aspects facing GLISTIN, the RMSE ranges from 0.96 m to 7.71 m. The RMSE for aspects facing away from GLISTIN ranges from 1.73 m to 3.79 m. As slope increases, the root mean square error increases with a drastic increase for the 60° to 70° slope bin. Aspects facing GLISTIN have a lower RMSE than aspects facing away, except for the 60° to 70° bin.

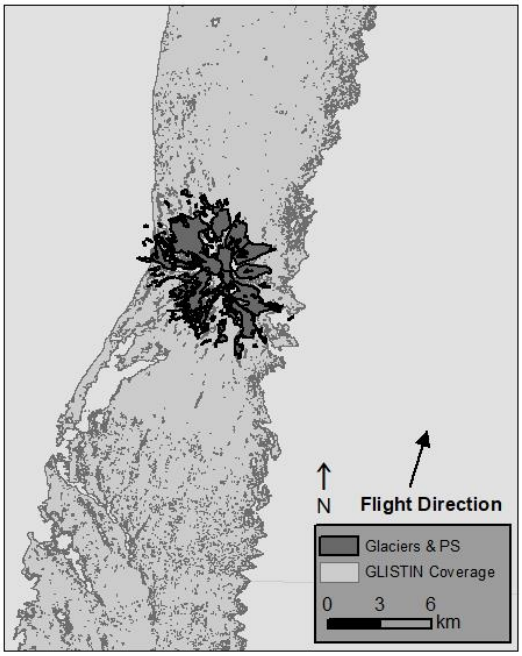

Figure C1. The flight path of GLISTIN over Mount Adams, WA. The flight direction was 10°. Dark grey outlines represent glaciers and perennial snowfields (G&PS). The light grey outline represents the GLISTIN swath.

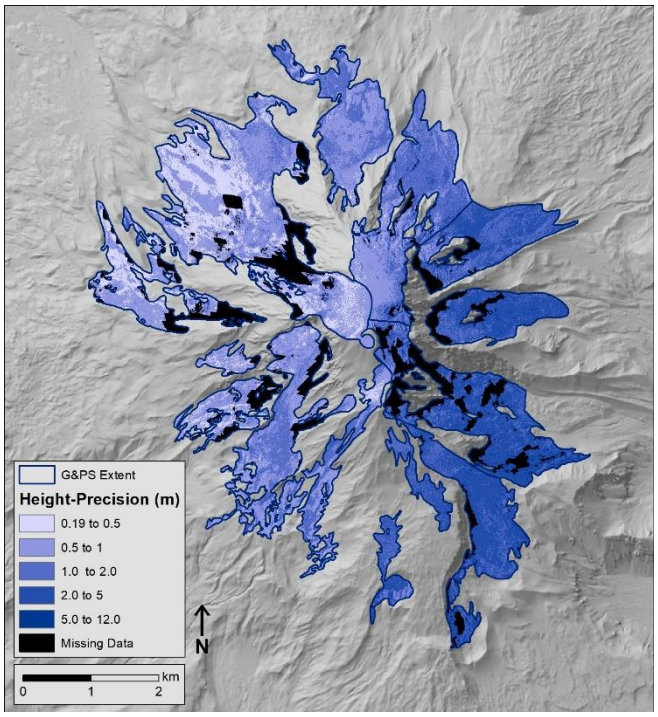

Figure C2. Height-precision of GLISTIN over Mount Adams, WA. Light purple colors indicate low height precision values, and dark colors indicate high height-precision.

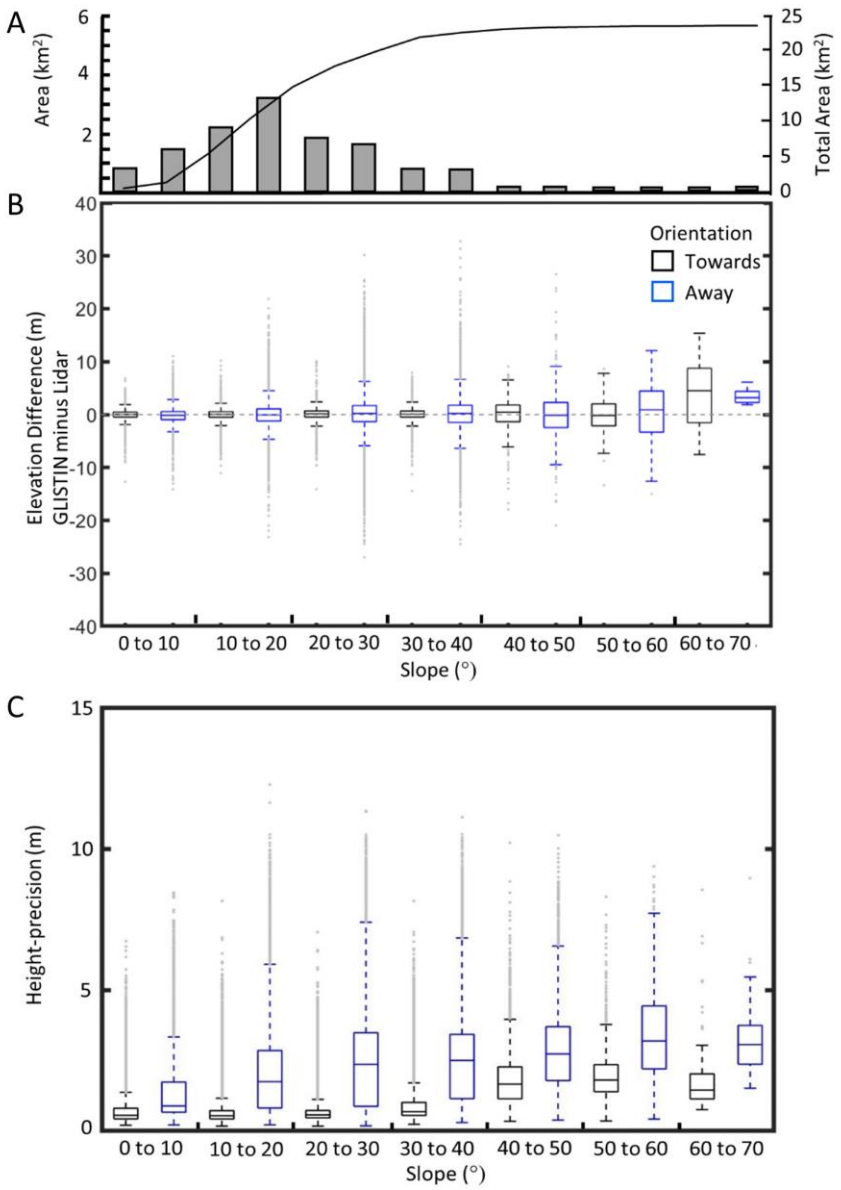

Figure C3. The elevation difference between GLISTIN and 2016 lidar for control zones, grouped by slope and orientation with respect to GLISTIN. The top of the panel shows the area per bin. The lidar elevations are subtracted from GLISTIN elevations. 'Away' refers to aspects facing away from GLISTIN (10° to 190°). 'Towards' refers to aspects facing GLISTIN (190° to 360° and 0° to 10°). Slope bins included the maximum, except for the first bin, which also includes zero. The line in the box indicates the median. The bottom and top of the boxes represent the 1st and 3rd quartile, respectively. The 'whiskers' represent the smallest and largest values not considered outliers. Light gray points indicate outliers. Values that exceed 1.5 times the interquartile below the first quartile or above the third quartile are considered outliers.

Appendix D: Volume Change by Elevation

To examine the pattern of specific volume change at all ice-covered elevations within a mountain range the specific volume change for 50 m elevation bins was calculated for the time periods 1960-2016, 1970-2016, 1975-2016, 1980-2016, and 1985-2016 with initial glacier area at each elevation (Figures 23-27). Examining G&PS together shows volume loss at most elevations. Generally, the greatest loss for G&PS was at lower elevations. Generally, volume change loss was greatest at lower elevations. Elevation bins with volume increase are due to increase in volume of perennial snowfields and not glaciers.

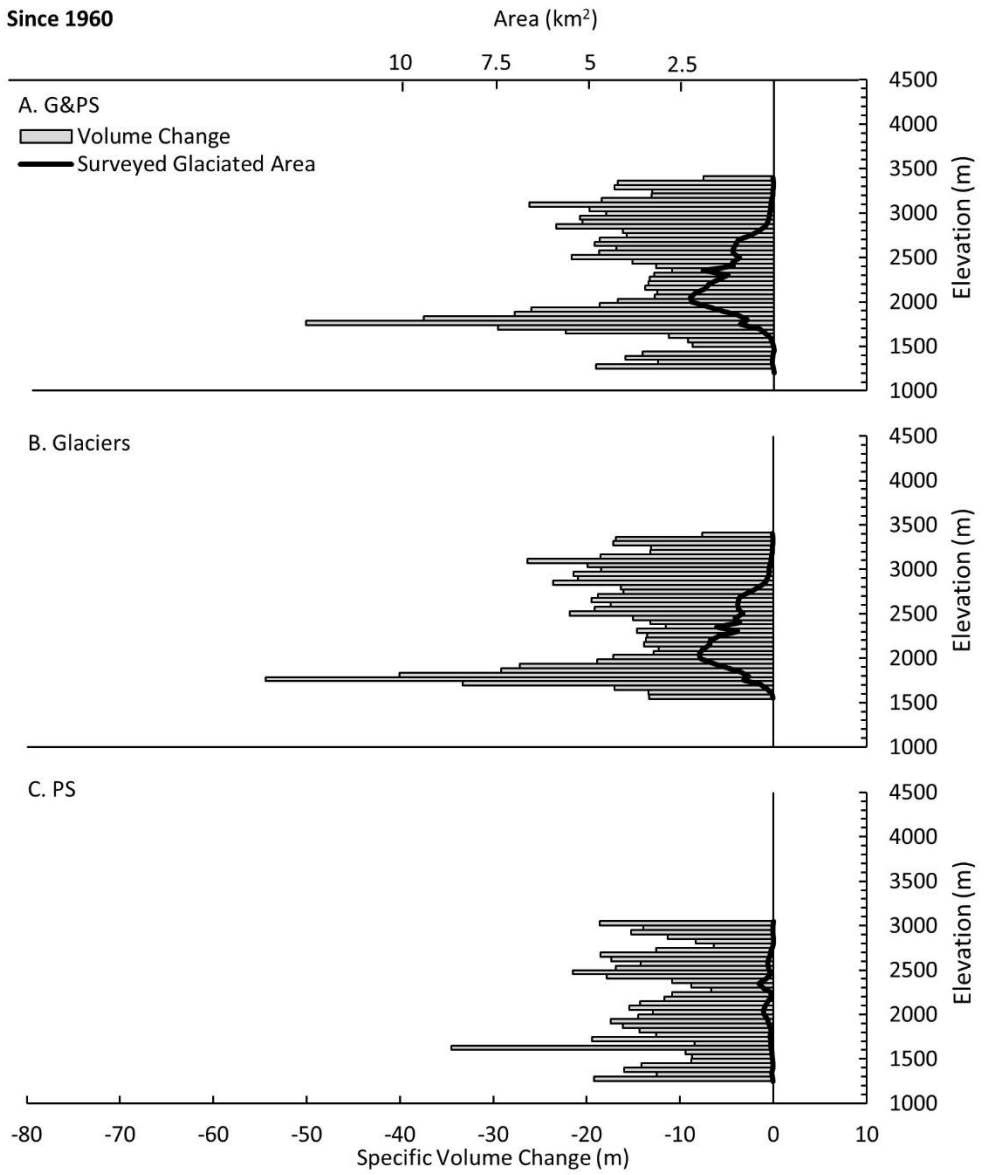

Figure D1. Specific volume change for glaciers and perennial snowfields (G&PS) as a function of elevation for the period of 1960 (1956 to 1960) to 2016. Panel A includes all G&PS panel B shows specific volume change for glaciers, and panel C shows the change of perennial snowfields. The specific volume change was calculated for each 50 m elevation bin. The value on the y-axis is the maximum elevation of that bin. The grey bars represent average specific volume change for each 50 m bin, and the black lines represent the glaciated area for each bin. Numbers indicate the region where the positive change is located. Specific volume change is the total volume change divided by total area for each elevation bin.

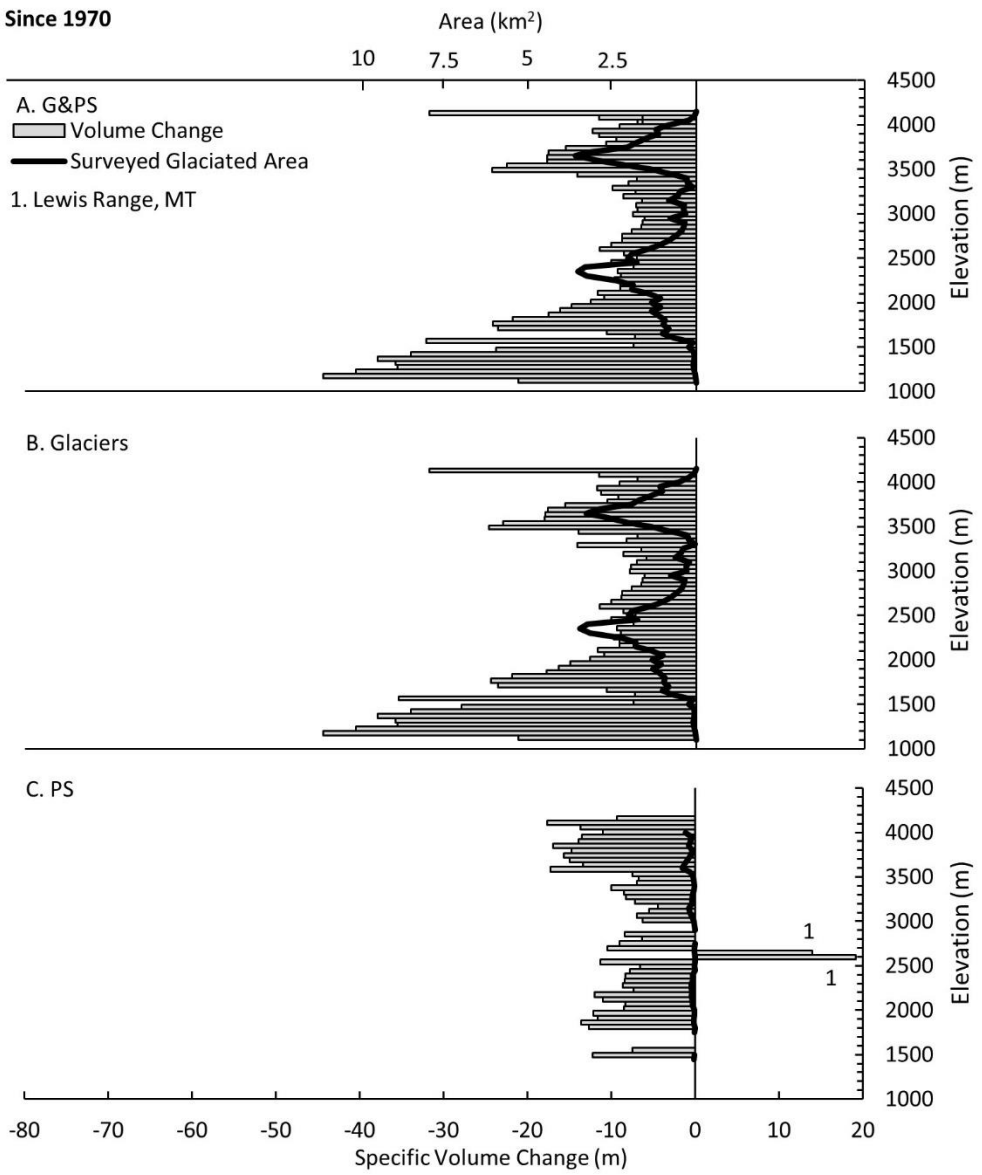

Figure D2. Specific volume change for glaciers and perennial snowfields (G&PS) as a function of elevation for the period of 1970 (1966 to 1970) to 2016. Panel A includes all G&PS panel B shows specific volume change for glaciers, and panel C shows the change of perennial snowfields. The specific volume change was calculated for each 50 m elevation bin. The value on the y-axis is the maximum elevation of that bin. The grey bars represent average specific volume change for each 50 m bin, and the black lines represent the glaciated area for each bin. Numbers indicate the region where the positive change is located. Specific volume change is the total volume change divided by total area for each elevation bin.

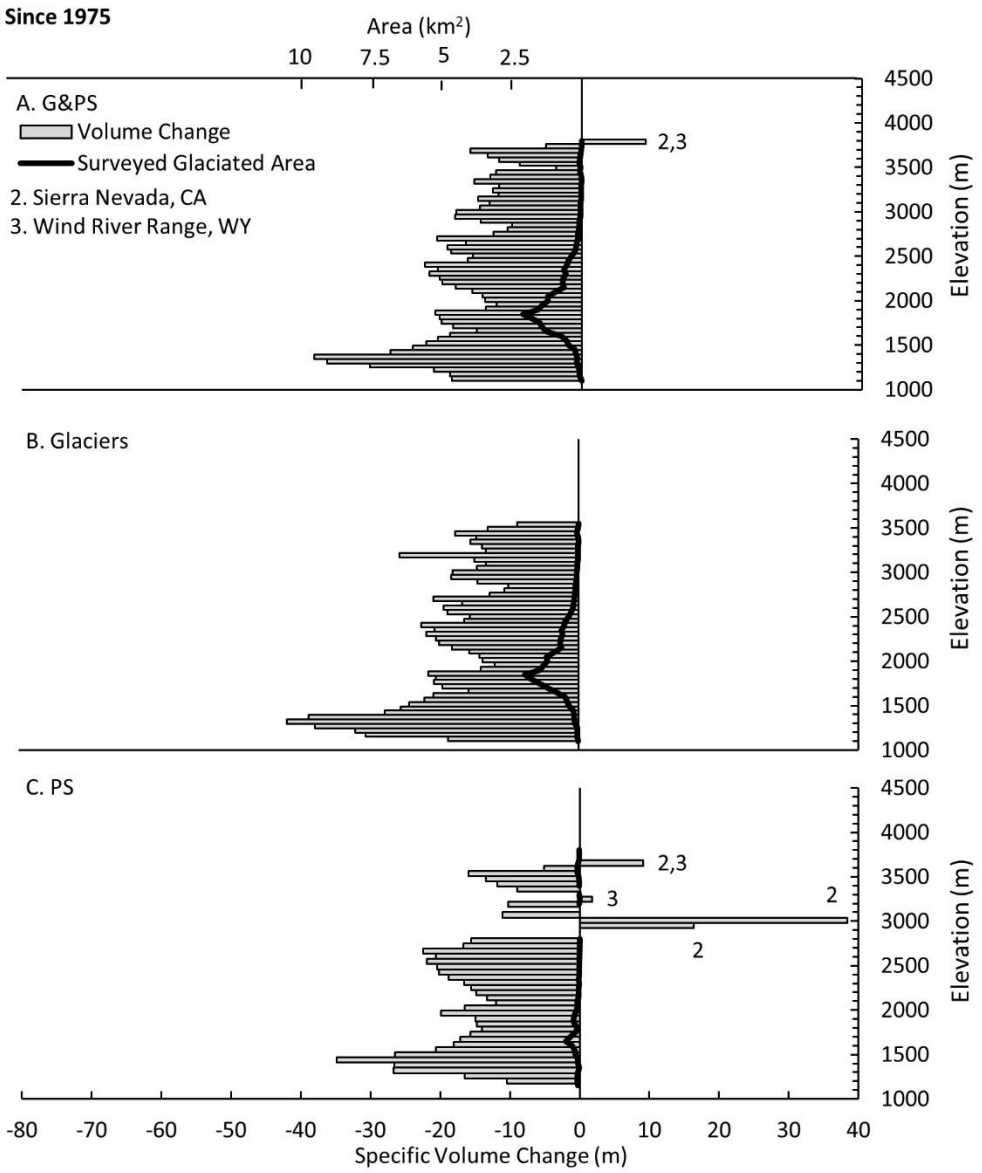

Figure D3. Specific volume change for glaciers and perennial snowfields (G&PS) as a function of elevation for the period of 1975 (1971 to 1975) to 2016. Panel A includes all G&PS panel B shows specific volume change for glaciers, and panel C shows the change of perennial snowfields. The specific volume change was calculated for each 50 m elevation bin. The value on the y-axis is the maximum elevation of that bin. The grey bars represent average specific volume change for each 50 m bin, and the black lines represent the glaciated area for each bin. Numbers indicate the region where the positive change is located. Specific volume change is the total volume change divided by total area for each elevation bin.

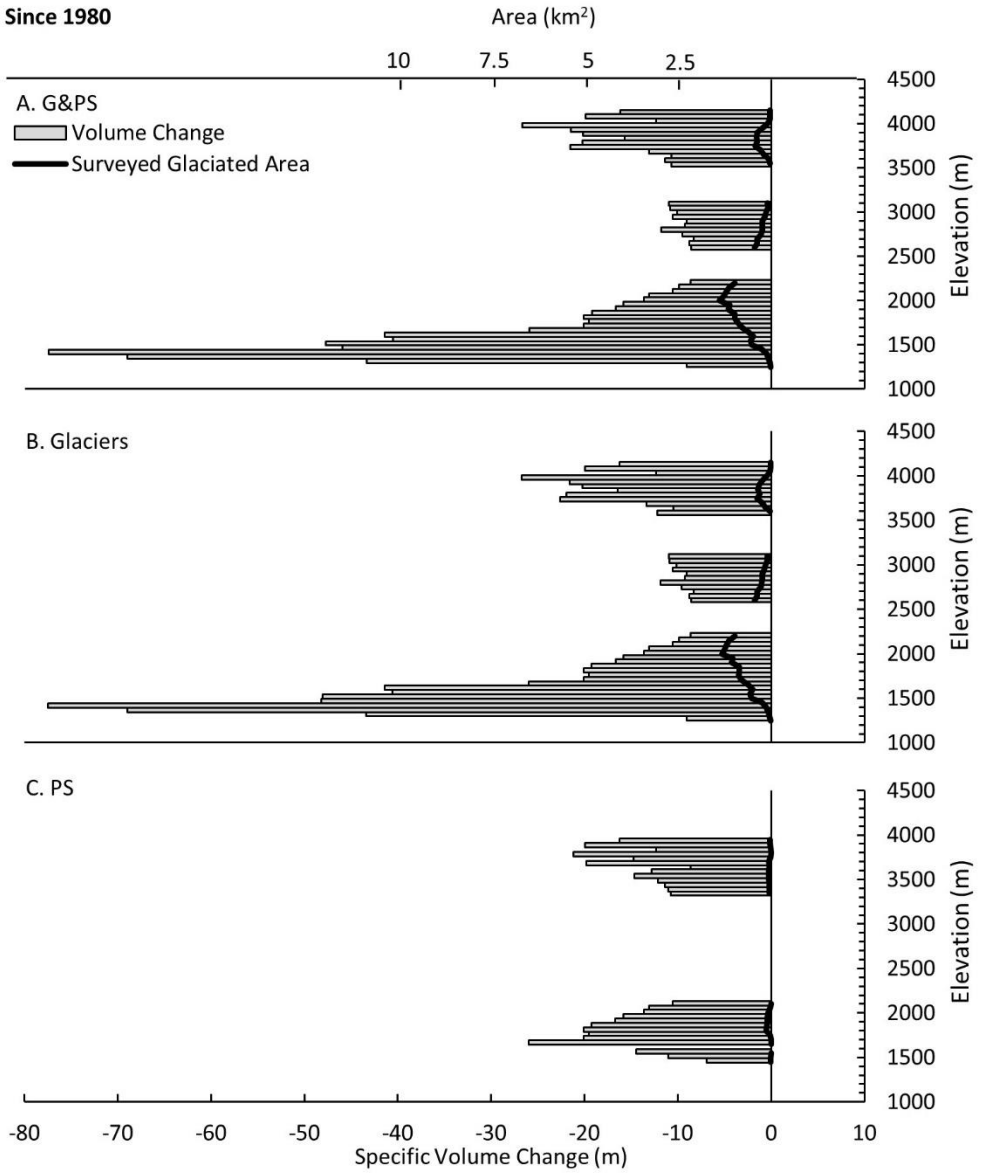

Figure D4. Specific volume change for glaciers and perennial snowfields (G&PS) as a function of elevation for the period of 1980 (1976 to 1980) to 2016. Panel A includes all G&PS panel B shows specific volume change for glaciers, and panel C shows the change of perennial snowfields. The specific volume change was calculated for each 50 m elevation bin. The value on the y-axis is the maximum elevation of that bin. The grey bars represent average specific volume change for each 50 m bin, and the black lines represent the glaciated area for each bin. Numbers indicate the region where the positive change is located. Specific volume change is the total volume change divided by total area for each elevation bin.

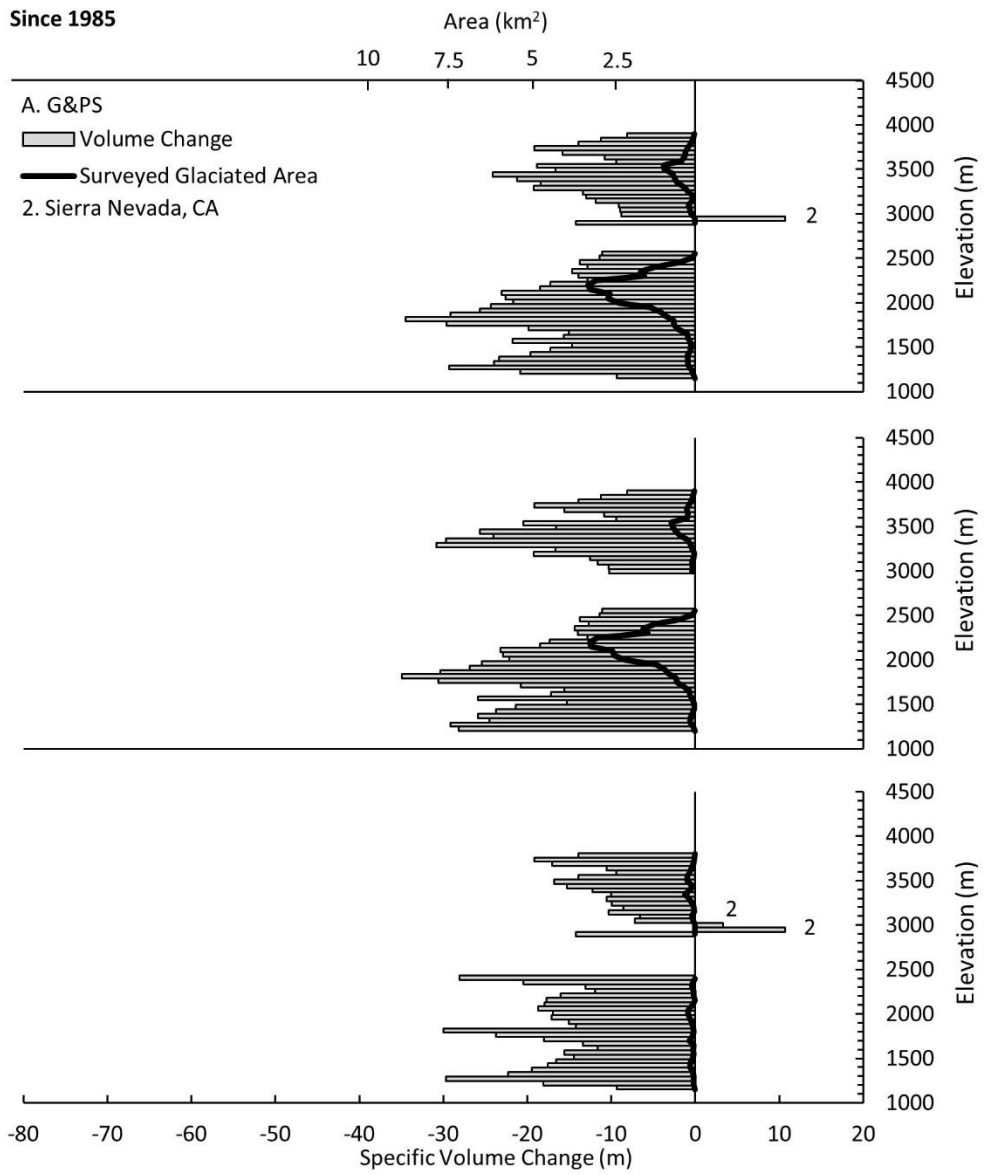

Figure D5. Specific volume change for glaciers and perennial snowfields (G&PS) as a function of elevation for the period of 1980 (1976 to 1980) to 2016. Panel A includes all G&PS panel B shows specific volume change for glaciers, and panel C shows the change of perennial snowfields. The specific volume change was calculated for each 50 m elevation bin. The value on the y-axis is the maximum elevation of that bin. The grey bars represent average specific volume change for each 50 m bin, and the black lines represent the area for each bin. Numbers indicate the region where the positive change is located. Specific volume change is the total volume change divided by total area for each elevation bin.